Environment plan
Appendix 6-2
Drill cuttings and muds dispersion modelling study (RPS)

Stromlo-1 exploration drilling program

Equinor Australia B.V.
Level 15
123 St Georges Terrace
PERTH WA 6000
Australia

November 2019

DRILL CUTTINGS AND MUDS DISPERSION MODELLING STUDY

Stromlo-1 exploration drilling program

MAQ0559J
Drill cuttings and muds dispersion modelling study
Rev 2B
30 October 2018

rpsgroup.com

Document status

Version	Purpose of document	Authored by	Reviewed by	Approved by	Review date
Rev A	Prepared for internal review	N/A	Dr Ryan Dunn		22/12/2017
Rev 0	Draft issued for client review	Dr Sasha Zigic	Dr Ryan Dunn		05/03/2018
Rev 1	Issued to client	Dr Sasha Zigic	Dr Ryan Dunn		26/09/2018
Rev 2B	Issued to client	Dr Sasha Zigic	Dr Ryan Dunn/JF	Dr Sasha Zigic	30/10/2018

Approval for issue

Dr S Zigic+		16/02/2019

This report was prepared by RPS within the terms of RPS' engagement with its client and in direct response to a scope of services. This report is supplied for the sole and specific purpose for use by RPS' client. The report does not account for any changes relating the subject matter of the report, or any legislative or regulatory changes that have occurred since the report was produced and that may affect the report. RPS does not accept any responsibility or liability for loss whatsoever to any third party caused by, related to or arising out of any use or reliance on the report.

©This report and all its appendices are protected by copyright.

Prepared by:

RPS

Dr Sasha Zigic
General Manager

Suite E1, Level 4, 140 Bundall Road
Bundall QLD 4217

T +61 7 5574 1112
E sasha.zigic@rpsgroup.com.au

Prepared for:

Equinor Australia B.V.

Level 15, 123 St Georges Terrace
Perth WA 6000

Contents

Summary **1**
Project background 1
Methods 1
Results – sediment thickness 1
Results – total suspended solids 1

1 INTRODUCTION **3**
1.1 Project background 3

2 MODELLING APPROACH **4**

3 DEVELOPMENT OF REGIONAL CURRENT DATA **5**
3.1 Tidal currents 7
3.2 Tidal model grid 7
3.3 Tidal forcing conditions 8
3.4 Validation of the tidal model 8
3.5 Ocean currents within the Great Australian Bight 13
3.6 Surface and bottom currents at Stromlo-1 13
3.7 Net water current comparison 22

4 WATER TEMPERATURE AND SALINITY **27**

5 DISPERSION MODELLING METHODS **29**
5.1 Sediment dispersion model description – MUDMAP 29
5.2 Discharge program 30
5.2.1 Discharge input data 31
5.3 Grid configuration 32
5.4 Mixing parameters 33
5.5 Minimum reporting thresholds 33

6 RESULTS **34**
6.1 Presentation of model results 34
6.2 Sediment thickness 34
6.2.1 Combined discharges for each month 34
6.2.2 Integration of model results: sediment thickness 54
6.3 Total suspended solids concentrations 56
6.3.1 Integration of model results: in-water total suspended solids concentrations 56
6.3.2 Example time-series snapshot: in-water total suspended solids concentrations 57

7 REFERENCES **59**

Tables

Table 1: Coordinates of the Stromlo-1 exploration well 3
Table 2: Statistical comparison between the observed and HYDROMAP predicted surface elevation data from 1st -31st January 2014 9
Table 3: Predicted surface and bottom current speeds for 2010 adjacent to Stromlo-1 well. Data derived by combining HYCOM ocean data and HYDROMAP tidal data from January to December (inclusive) 14
Table 4: Predicted surface and bottom current speeds for 2011 adjacent to Stromlo-1 well. Data derived by combining HYCOM ocean data and HYDROMAP tidal data from January to December (inclusive) 14
Table 5: Predicted surface and bottom current speeds for 2012 adjacent to Stromlo-1 well. Data derived by combining HYCOM ocean data and HYDROMAP tidal data from January to December (inclusive) 15

Table 6: Measured and calculated current data information 23
Table 7: Annual water temperature and salinity profiles from the closest World Ocean Atlas 2013 data point closest to the release location. Source: World Ocean Atlas (2013) 27
Table 8: Summary of the estimated volume of extracted drill cuttings and unrecoverable muds to be discharged 30
Table 9: Input data used for the drill cuttings and muds dispersion modelling 31
Table 10: Grain sizes, settling velocities and percentage distributions for the cuttings and muds 32
Table 11: Reporting thresholds for sediment thickness and TSS concentrations for the drill cuttings and muds discharge modelling 33
Table 12: Predicted maximum sediment thickness and total area of coverage of deposited cuttings and muds above the minimum reporting threshold (0.05 mm) and low exposure thresholds (1 mm). Results are based on the combined near-seabed and sea surface discharges initiated at the start of each month during 2010, 2011 and 2012 34
Table 13: Predicted minimum distance from deposited material above the minimum reporting threshold (0.05 mm) to Anna's Pimple and Murray's Mount resulting from the combined discharge of cuttings and muds from the combined near-seabed and sea surface discharges. Results are presented for model simulations initiated at the start of each month 2010, 2011 and 2012 35
Table 14: Predicted area of coverage on the sea floor and distance as a function of sediment thickness. Results are based on the collective assessment of monthly simulations (near-seabed and surface discharges) modelled under January to December 2010 – 2012 conditions 55
Table 15: Predicted maximum TSS concentration, maximum area and distance above the minimum reporting threshold (above 5 mg/L) in the upper surface waters (0–100 m). Results are based on the collective assessment of all surface discharges initiated at the start of each month during 2010, 2011 and 2012 conditions 56
Table 16: Predicted areas of exposure and maximum distances from the well to each TSS interval in the upper surface waters (0–100 m). Results are based on the collective assessment of all surface discharges initiated at the start of each month during 2010, 2011 and 2012 conditions 56

Figures

Figure 1: Location map of Stromlo-1 exploration well used as the release location in this drill cuttings and muds dispersion modelling study 3
Figure 2: Mean summer (upper image) and winter (lower image) circulation patterns over the GAB as presented by Middleton et al (2017) 6
Figure 3: Residual surface ocean current patterns during the summer conditions (data for December 2011 – February 2012 from the global ocean model; HYCOM) 6
Figure 4: Extent of the model grid used to generate the tidal currents for the study region using the HYDROMAP model. Higher resolution areas are shown by the denser mesh 7
Figure 5: Bathymetry defined within the tidal model 8
Figure 6: Location of the tide stations used in the surface elevation comparison 10
Figure 7: Comparison between predicted (blue line) and observed (red line) surface elevation variation at Albany (top), Esperance (middle) and Eucla (bottom), between 1–31 January 2014 11
Figure 8: Comparison between predicted (blue line) and observed (red line) surface elevation variation at Port Lincoln (top), Portland (middle) and Eden (bottom), between 1–31 January 2014 12
Figure 9: Predicted ocean surface currents on the 1st January 2012, summer conditions. Derived from the HYCOM ocean hindcast model. The colours of the vectors indicate current speed in m/s 13

Figure 10: Monthly surface waters current rose plots adjacent to Stromlo-1 well during 2010. The current roses were generated by combining the tidal currents and HYCOM ocean currents. The colour key shows the current speed (m/s), the compass shows the direction and the length of the wedge gives the percentage of the record for a particular speed and direction combination 16
Figure 11: Monthly surface waters current rose plots adjacent to Stromlo-1 well during 2011. The current roses were generated by combining the tidal currents and HYCOM ocean currents. The colour key shows the current speed (m/s), the compass shows the direction and the length of the wedge gives the percentage of the record for a particular speed and direction combination 17
Figure 12: Monthly surface waters current rose plots adjacent to Stromlo-1 well during 2012. The current roses were generated by combining the tidal currents and HYCOM ocean currents. The colour key shows the current speed (m/s), the compass shows the direction and the length of the wedge gives the percentage of the record for a particular speed and direction combination 18
Figure 13: Monthly bottom waters current rose plots adjacent to Stromlo-1-well during 2010. The current roses were generated by combining the tidal currents and HYCOM ocean currents. The colour key shows the current speed (m/s), the compass shows the direction and the length of the wedge gives the percentage of the record for a particular speed and direction combination 19
Figure 14: Monthly bottom waters current rose plots adjacent to Stromlo-1 during 2011. The current roses were generated by combining the tidal currents and HYCOM ocean currents. The colour key shows the current speed (m/s), the compass shows the direction and the length of the wedge gives the percentage of the record for a particular speed and direction combination 20
Figure 15: Monthly bottom waters current rose plots adjacent to Stromlo-1 during 2012. The current roses were generated by combining the tidal currents and HYCOM ocean currents. The colour key shows the current speed (m/s), the compass shows the direction and the length of the wedge gives the percentage of the record for a particular speed and direction combination 21
Figure 16: Current measurement location in relation to the Stromlo-1 well site 22
Figure 17: Modelled (left) and measured (right) current roses for depth layer of 30 m at 340 28' 30''S, 1300 42' 5''E. Source of measured data: RPS MetOcean (2013) 23
Figure 18: Modelled (left) and measured (right) current roses for depth layer of 50 m at 340 28' 30'' S, 1300 42' 5'' E. Source of measured data: RPS MetOcean (2013)....24
Figure 19: Modelled (left) and measured (right) current roses for depth layer of 70 m at 340 28' 30'' S, 1300 42' 5'' E. Source of measured data: RPS MetOcean (2013)....24
Figure 20: Modelled (left) and measured (right) current roses for depth layer of 200 m at 340 28' 30'' S, 1300 42' 5'' E. Source of measured data: RPS MetOcean (2013)....25
Figure 21: Modelled (left) and measured (right) current roses for depth layer of 300 m at 340 28' 30'' S, 1300 42' 5'' E. Source of measured data: RPS MetOcean (2013)....25
Figure 22: Modelled (left) and measured (right) current roses for depth layer of 1000 m at 340 28' 30'' S, 1300 42' 5'' E. Source of measured data: RPS MetOcean (2013) 26
Figure 23: Monthly temperature (blue) and salinity (green) profiles from the closest World Ocean Atlas 2013 data point closest to the release location. Source: World Ocean Atlas (2013)....28
Figure 24: Conceptual diagram showing the general behaviour of cuttings and muds following the discharge to the ocean (Neff, 2005) and the idealised representation of the three discharge phases 30
Figure 25: Predicted coverage and sediment thickness from the discharge of drill cuttings and unrecoverable drilling muds on the sea floor if the operation commenced 1st January 2010 36

Figure 26: Predicted coverage and sediment thickness from the discharge of drill cuttings and unrecoverable drilling muds on the sea floor if the operation commenced 1st January 2011 36
Figure 27: Predicted coverage and sediment thickness from the discharge of drill cuttings and unrecoverable drilling muds on the sea floor if the operation commenced 1st January 2012 37
Figure 28: Predicted coverage and sediment thickness from the discharge of drill cuttings and unrecoverable drilling muds on the sea floor if the operation commenced 1st February 2010 37
Figure 29: Predicted coverage and sediment thickness from the discharge of drill cuttings and unrecoverable drilling muds on the sea floor if the operation commenced 1st February 2011 38
Figure 30: Predicted coverage and sediment thickness from the discharge of drill cuttings and unrecoverable drilling muds on the sea floor if the operation commenced 1st February 2012 38
Figure 31: Predicted coverage and sediment thickness from the discharge of drill cuttings and unrecoverable drilling muds on the sea floor if the operation commenced 1st March 2010....39
Figure 32: Predicted coverage and sediment thickness from the discharge of drill cuttings and unrecoverable drilling muds on the sea floor if the operation commenced 1st March 2011....39
Figure 33: Predicted coverage and sediment thickness from the discharge of drill cuttings and unrecoverable drilling muds on the sea floor if the operation commenced 1st March 2012....40
Figure 34: Predicted coverage and sediment thickness from the discharge of drill cuttings and unrecoverable drilling muds on the sea floor if the operation commenced 1st April 2010 40
Figure 35: Predicted coverage and sediment thickness from the discharge of drill cuttings and unrecoverable drilling muds on the sea floor if the operation commenced 1st April 2011 41
Figure 36: Predicted coverage and sediment thickness from the discharge of drill cuttings and unrecoverable drilling muds on the sea floor if the operation commenced 1st April 2012 41
Figure 37: Predicted coverage and sediment thickness from the discharge of drill cuttings and unrecoverable drilling muds on the sea floor if the operation commenced 1st May 2010....42
Figure 38: Predicted coverage and sediment thickness from the discharge of drill cuttings and unrecoverable drilling muds on the sea floor if the operation commenced 1st May 2011....42
Figure 39: Predicted coverage and sediment thickness from the discharge of drill cuttings and unrecoverable drilling muds on the sea floor if the operation commenced 1st May 2012....43
Figure 40: Predicted coverage and sediment thickness from the discharge of drill cuttings and unrecoverable drilling muds on the sea floor if the operation commenced 1st June 2010....43
Figure 41: Predicted coverage and sediment thickness from the discharge of drill cuttings and unrecoverable drilling muds on the sea floor if the operation commenced 1st June 2011....44
Figure 42: Predicted coverage and sediment thickness from the discharge of drill cuttings and unrecoverable drilling muds on the sea floor if the operation commenced 1st June 2012....44
Figure 43: Predicted coverage and sediment thickness from the discharge of drill cuttings and unrecoverable drilling muds on the sea floor if the operation commenced 1st July 2010 45
Figure 44: Predicted coverage and sediment thickness from the discharge of drill cuttings and unrecoverable drilling muds on the sea floor if the operation commenced 1st July 2011 45
Figure 45: Predicted coverage and sediment thickness from the discharge of drill cuttings and unrecoverable drilling muds on the sea floor if the operation commenced 1st July 2012 46
Figure 46: Predicted coverage and sediment thickness from the discharge of drill cuttings and unrecoverable drilling muds on the sea floor if the operation commenced 1st August 2010 46
Figure 47: Predicted coverage and sediment thickness from the discharge of drill cuttings and unrecoverable drilling muds on the sea floor if the operation commenced 1st August 2011 47
Figure 48: Predicted coverage and sediment thickness from the discharge of drill cuttings and unrecoverable drilling muds on the sea floor if the operation commenced 1st August 2012 47

Figure 49: Predicted coverage and sediment thickness from the discharge of drill cuttings and unrecoverable drilling muds on the sea floor if the operation commenced 1st September 2010 48
Figure 50: Predicted coverage and sediment thickness from the discharge of drill cuttings and unrecoverable drilling muds on the sea floor if the operation commenced 1st September 2011 48
Figure 51: Predicted coverage and sediment thickness from the discharge of drill cuttings and unrecoverable drilling muds on the sea floor if the operation commenced 1st September 2012 49
Figure 52: Predicted coverage and sediment thickness from the discharge of drill cuttings and unrecoverable drilling muds on the sea floor if the operation commenced 1st October 2010 49
Figure 53: Predicted coverage and sediment thickness from the discharge of drill cuttings and unrecoverable drilling muds on the sea floor if the operation commenced 1st October 2011 50
Figure 54: Predicted coverage and sediment thickness from the discharge of drill cuttings and unrecoverable drilling muds on the sea floor if the operation commenced 1st October 2012 50
Figure 55: Predicted coverage and sediment thickness from the discharge of drill cuttings and unrecoverable drilling muds on the sea floor if the operation commenced 1st November 2010 51
Figure 56: Predicted coverage and sediment thickness from the discharge of drill cuttings and unrecoverable drilling muds on the sea floor if the operation commenced 1st November 2011 51
Figure 57: Predicted coverage and sediment thickness from the discharge of drill cuttings and unrecoverable drilling muds on the sea floor if the operation commenced 1st November 2012 52
Figure 58: Predicted coverage and sediment thickness from the discharge of drill cuttings and unrecoverable drilling muds on the sea floor if the operation commenced 1st December 2010 52
Figure 59: Predicted coverage and sediment thickness from the discharge of drill cuttings and unrecoverable drilling muds on the sea floor if the operation commenced 1st December 2011 53
Figure 60: Predicted coverage and sediment thickness from the discharge of drill cuttings and unrecoverable drilling muds on the sea floor if the operation commenced 1st December 2012 53
Figure 61: Cross-sectional view of the predicted sediment thickness on the sea floor along the north-south axis (upper image) and east-west axis (lower image). Results are based on the combined near-seabed and sea surface discharge of drill cuttings and unrecoverable muds commencing May 2012. Note the vertical scale is exaggerated 54
Figure 62: Predicted maximum thickness at each grid cell from all 36 monthly simulations (combined near-seabed and surface discharges) used to define the area of greatest extent from the discharge of cuttings and unrecoverable muds 55
Figure 63: Predicted maximum instantaneous TSS concentrations in each grid cell based on the collective assessment of all monthly surface discharges in the upper surface waters (0–100 m). Results are presented for model simulations initiated at the start of each month during 2010, 2011 and 2012 conditions 57
Figure 64: Example time-series snapshots of the maximum predicted TSS concentrations, at 3 hourly intervals, resulting from the surface discharge of drill cuttings and drilling muds commencing on the 12th April 2010. Note figure insets displays depth profiles through the water column across transect A to B in each figure 58

SUMMARY

Project background

Equinor Australia B.V. is planning to drill the Stromlo-1 exploration well in the Ceduna Sub-basin permit EPP39. The well is to be drilled in five sections, or well intervals. Cuttings and adhered muds from two surface well intervals (conductor and surface hole) will be returned directly to the seabed during the riserless drilling. Whilst cuttings and adhered drilling muds from the lower three intervals (intermediate holes and bottom hole) will be brought to the platform through the riser for treatment through solids control equipment and discharged overboard at the sea surface.

To support the environmental management and impact assessment process, RPS was commissioned to undertake a dispersion modelling study, with the primary objective being to quantify the potential sediment thickness and Total Suspended Solids (TSS) concentrations from the cuttings and unrecoverable muds discharges during the planned drilling activity. In addition, the likelihood of contact from deposited cuttings and muds to the two closest seamounts, Anna's Pimple (20.9 km north-northeast of Stromlo-1) and Murray's Mount (24.6 km north of Stromlo-1), was investigated. The report presents the potential area that may be influenced based on a monthly and annual dispersion modelling.

Methods

The modelling study was carried out in several stages. Firstly, three-dimensional currents that include the combined influence of ocean and tidal currents were generated. Secondly, the current data and the cuttings discharge characteristics were input into the three-dimensional sediment dispersion model, MUDMAP. Thirdly, the movement and initial settlement of cuttings and adhered muds were predicted for the near-seabed and surface discharges, initiated at the start of each month during 2010, 2011 and 2012 conditions (i.e. total of 36 monthly simulations). The results from all monthly simulations were combined to delineate the greatest area that may be influenced by the discharge of drill cuttings and muds at any time of year.

A thickness of 0.05 mm was the lowest modelled level of accumulated sediment thickness. Thresholds of 1-10 mm and above 10 mm were used to define low and high exposure levels (biological effect), respectively. The minimum reporting threshold for TSS was 5 mg/L and a threshold range of 10-1830 mg/L and above 1830 mg/L were used to define low and high exposure, respectively.

Results – sediment thickness

The maximum thickness on the sea floor (height of cuttings mound) for a given month, ranged between 1690 mm and 4036 mm, which was localised and generally occurred within 50 m from the release location. The area of coverage above the minimum reporting threshold of 0.05 mm was between 3.13 km^2 and 3.87 km^2.

No deposition was predicted to occur at, or in the vicinity of, either Anna's Pimple or Murray's Mount (closest seamounts) under any month modelled during the 2010, 2011 and 2012 conditions. The minimum distance from the deposited material above the minimum reporting threshold to Anna's Pimple and Murray's Mount was 16.0 km and 19.9 km, respectively.

The model results for all simulations (January 2010 to December 2012) were integrated to provide a collective assessment. Based on this collective assessment the total area of coverage on the sea floor above the minimum reporting threshold was 24.62 km^2, which was predicted to occur up to a maximum distance of 5.65 km from the well. In comparison, the area of coverage based on the low (1-10 mm) and high (>10 mm) exposure thresholds was 1.78 km^2 and 0.17 km^2, respectively equating to 7% and 1% of the total area of coverage, respectively. The maximum distance from the well where seabed deposition exceeded the low (1-10 mm) and high (>10 mm) effects thresholds, was 2.34 km and 0.7 km, respectively.

Results – total suspended solids

The maximum instantaneous TSS concentration was 1857 mg/L, which occurred within the immediate vicinity of the discharge outlet (<10 m). The results for all surface discharge simulations were also integrated (January 2010 to December 2012) for a collective assessment. This assessment demonstrated the area of

exposure above the minimum reporting threshold (5 mg/L) was 4.32 km^2. Additionally, the maximum distance from the release location to the minimum reporting TSS concentration threshold of 5 mg/L was 3.92 km, occurring north-east of the release location. TSS concentrations greater than 10 mg/L and 1830 mg/L extended maximum distances of 2.08 km and 0.01 km from the release location, respectively.

1 INTRODUCTION

1.1 Project background

Equinor Australia (formerly Statoil) is the sole titleholder of exploration permit EPP39 which is in the Ceduna Sub-basin, off southern Australia and plan to drill the Stromlo-1 exploration well in 2239 m of water within the permit area (see Table 1 and Figure 1). To support environmental planning procedures, RPS was commissioned to undertake a detailed drill cuttings and unrecoverable drilling muds dispersion modelling study.

The primary objective of the study was to quantify the potential sediment thickness and Total Suspended Solids (TSS) concentrations from the cuttings and unrecoverable muds discharged during the proposed drilling operation. In addition, the likelihood of contact from deposited cuttings and muds to the nearby features, Anna's Pimple (20.9 km north-northeast of Stromlo-1) and Murray's Mount (24.6 km north of Stromlo-1) was also investigated. Although, the drilling campaign will occur between October and May, this report presents the results if the drilling operation was to start on the 1st day of each calendar month. This allows better assessment of the full range of variation over the year.

Table 1: Coordinates of the Stromlo-1 exploration well

Name	Latitude	Longitude	Water dept (m)
Stromlo-1	34o 56' 21.47'' S	130o 39' 44.61'' E	2239

The WGS84 Geographic projection is used throughout the report.

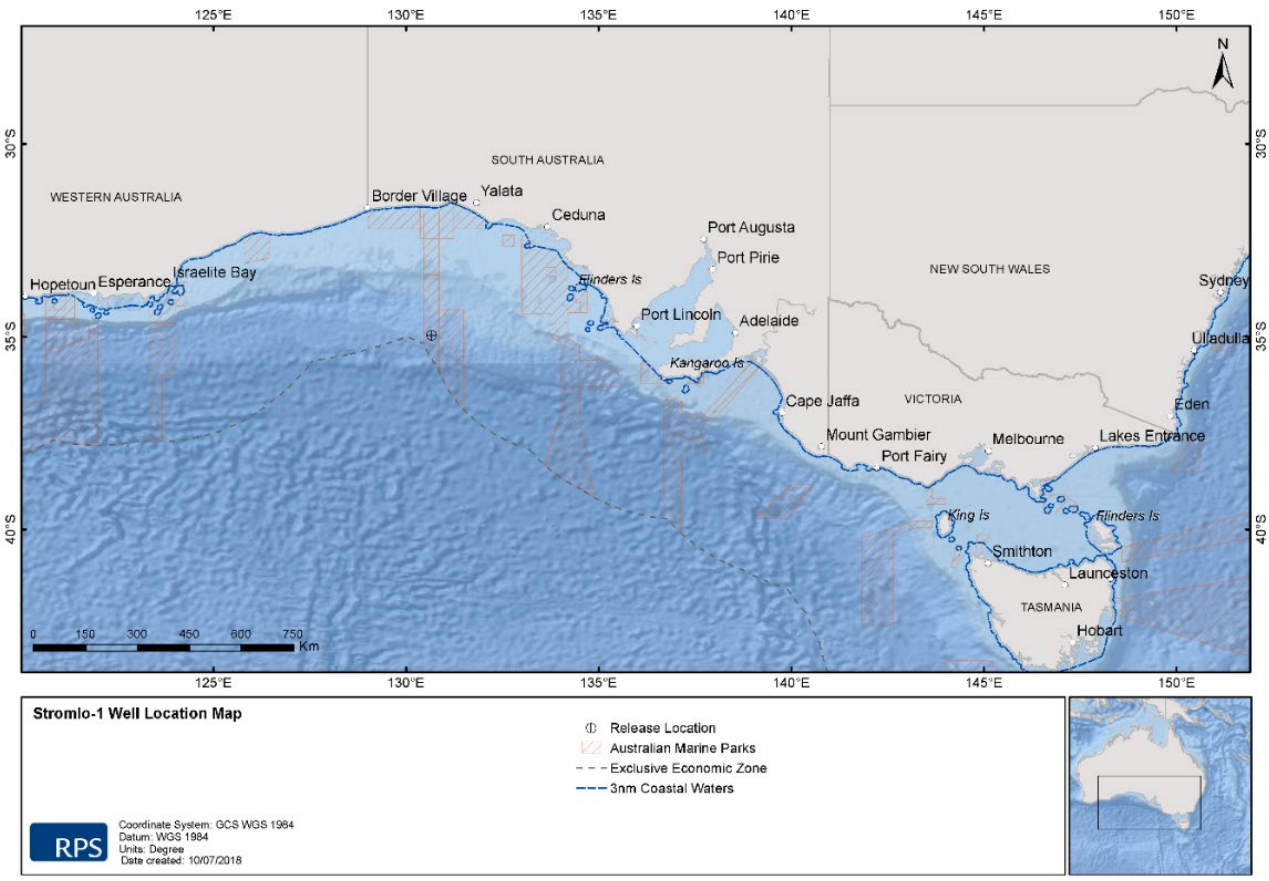

Figure 1: Location map of Stromlo-1 exploration well used as the release location in this drill cuttings and muds dispersion modelling study

2 MODELLING APPROACH

The modelling included the following components:

1. Generating three-dimensional (3D) spatially varying current data surrounding the proposed exploration site, for a three year (2010–2012) hindcast period. The current data set included the combined influence of drift and tidal currents and was suitably long to be indicative of interannual variability in ocean currents.

2. Entering the current data and drill cuttings/muds discharge characteristics into the three-dimensional sediment dispersion model, MUDMAP, to predict the movement and initial settlement of the discharged drill cuttings and unrecoverable muds commencing on the 1st of each calendar month within the three-year hind cast period of currents (i.e. 36 simulation periods).

3. Analysing and reporting the potential sediment thickness above the minimum reporting thresholds of 0.05 mm based on monthly simulations.

4. Integrating the monthly simulations to define the area of greatest extent that may be influenced by sediment thickness and TSS concentrations above the minimum reporting thresholds of 0.05 mm and 5 mg/L, respectively.

3 DEVELOPMENT OF REGIONAL CURRENT DATA

The Great Australian Bight (GAB) is a large, open body of water located offshore the southern shelf of the Australian continent and forms part of the South-eastern Indian Ocean. General circulation features of the GAB have been described by Middleton & Bye (2007) with further refinement by Middleton et. al. (2017).

Oceanographic processes in the GAB are strongly influenced by frequent gales and heavy seas in addition to a moderate to high wave energy along regional coastlines. The varied geography and bathymetry of the region, in addition to the forcing of the south-eastern Indian Ocean and local meteorology lead to complex shelf and slope circulation patterns (Middleton and Bye 2007). Several important currents interact and influence the region, contributing to the great complexity of its oceanography:

- Leeuwin Current – This shelf current originates from the warm waters of the Indian Ocean, flowing south along the continental shelf of Western Australia. The warm waters travel east through the GAB intensifying during winter months, when current velocities are highest (Rochford 1986). The current creates both upwelling or downwelling eddies but these are relatively weak (Middleton et. al. 2017).

- South Australian Current – An eastward extension of the Leeuwin Current that originates over the eastern side of the GAB, westward of Spencers Gulf, and flows eastward through Bass Strait.

- Flinders Current – This subsurface current originates in the waters off the west coast of Tasmania and flows westward through the GAB where it forms part of the Leeuwin undercurrent (a subsea counter-current). The magnitude of this current is affected by seasonally-varying winds, oceanic transport and associated shelf-slope currents (Middleton and Bye, 2007).

The mean pattern of near-surface circulation along the coastline in summer, calculated over the longer term (months to years) occurs as relatively weak (< 0.05 m/s) currents directed westward (Figure 2). The residual current switches to eastward further offshore over depths less than 200 m (Middleton et. al. 2017). The eastward migration of the Leeuwin Current with the South Australian Current forms a barrier current migrating eastward, centred around the 200 m isobar. Residual circulation over deeper waters features a series of gyres that add complexity to the circulation patterns. When analysed over the longer term (months to years), the residual flows of these eddies are anti-cyclonic (i.e. counter-clockwise in the southern hemisphere; Middleton et. al. 2017). Residual currents during summer are weaker than during the winter, which has been partially attributed to the relative strength of the Leeuwin Current (Middleton et. al. 2017).

Figure 3 presents the residual (averaged) surface ocean current patterns calculated during one past summer period (December 2011 – February 2012; source: HYCOM global ocean model) which reveals a complex set of interacting eddies over the offshore waters.

A composite modelled ocean current data product was derived by combining predictions of mesoscale circulation currents, available at daily resolution from HYCOM global ocean models, with predictions of the hourly tidal currents generated by the RPS HYDROMAP model. By combining a drift current model with a tidal model, the influences of inter-annual and seasonal drift patterns, and the more regular variations in tide, were included.

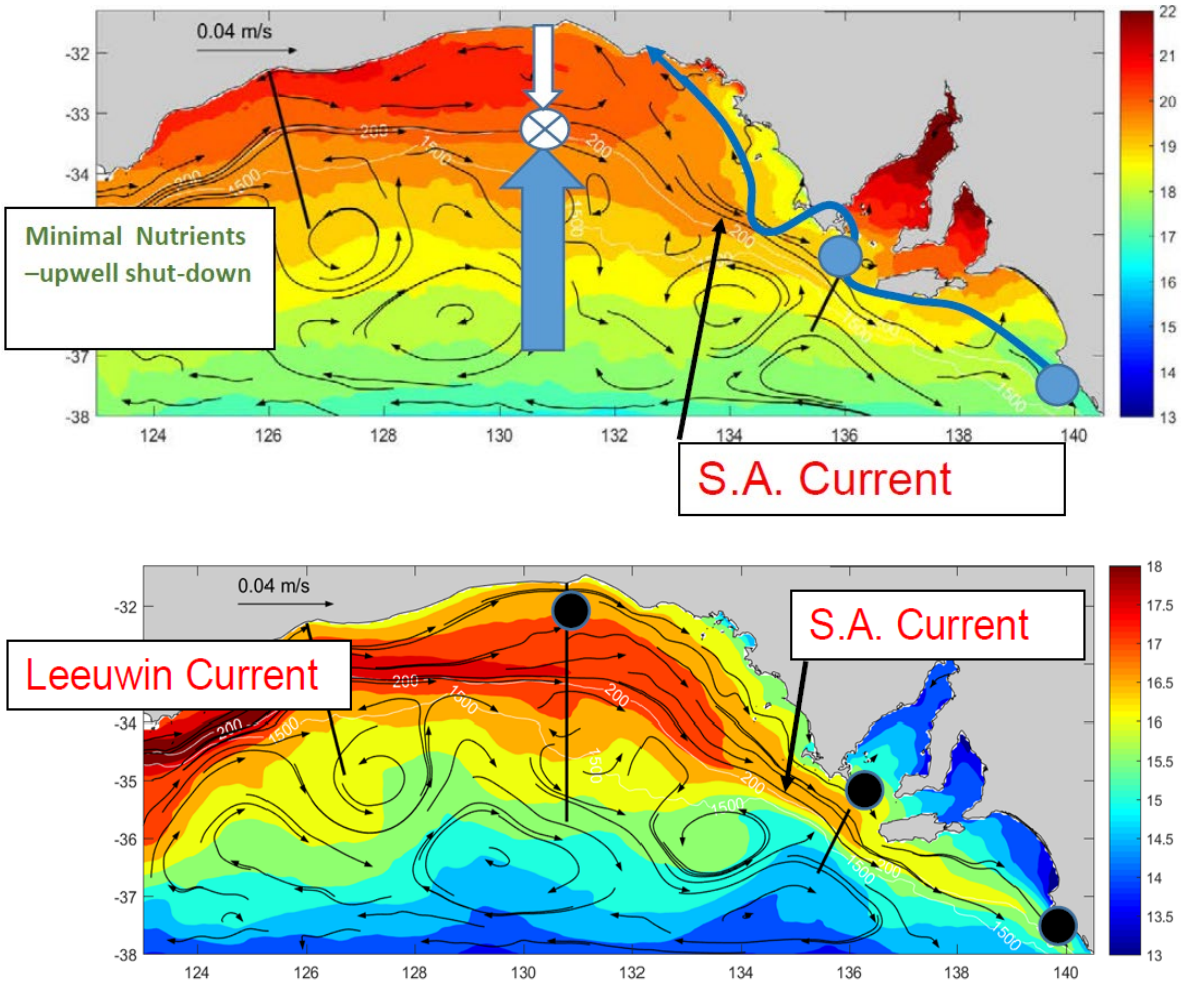

Figure 2: **Mean summer (upper image) and winter (lower image) circulation patterns over the GAB as presented by Middleton et al (2017)**

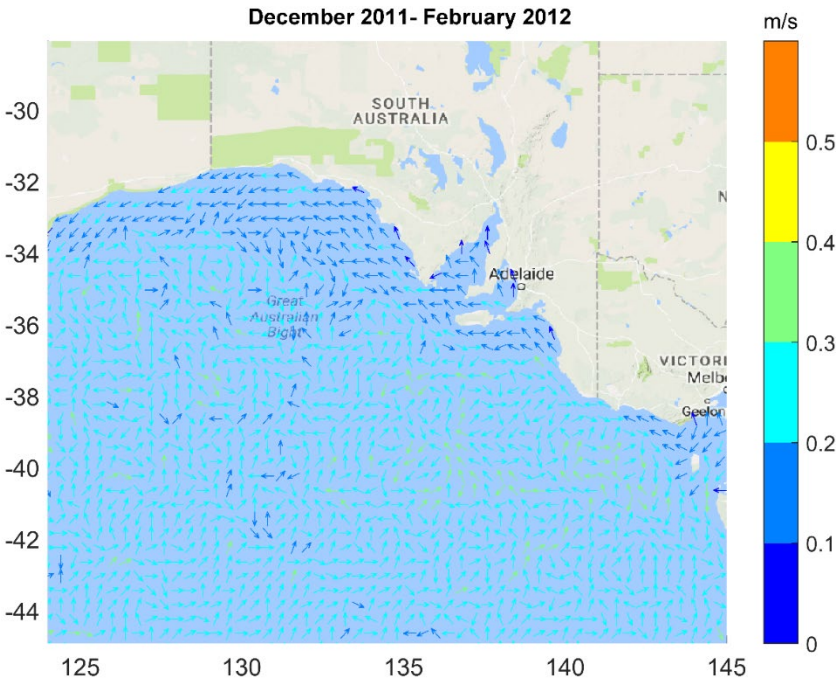

Figure 3: **Residual surface ocean current patterns during the summer conditions (data for December 2011 – February 2012 from the global ocean model; HYCOM)**

3.1 Tidal currents

The effects of tides were generated using RPS' advanced ocean/coastal model, HYDROMAP. The HYDROMAP model has been thoroughly tested and verified through field measurements throughout the world over 30 years (Isaji and Spaulding, 1984; Isaji et al., 2001; Zigic et al., 2003). In fact, HYDROMAP tidal current data has been used as input to forecast (in the future) and hindcast (in the past) oil spills in Australian waters and forms part of the Australian National Oil Spill Emergency Response System operated by AMSA (Australian Maritime Safety Authority).

HYDROMAP employs a sophisticated sub-gridding strategy, which supports up to six levels of spatial resolution, halving the grid cell size as each level of resolution is employed. The sub-gridding allows for higher resolution of currents within areas of greater bathymetric and coastline complexity, and/or of particular interest to a study.

The numerical solution methodology follows that of Davies, 1977a, 1977b with further developments for model efficiency by Owen (1980) and Gordon (1982). A more detailed presentation of the model can be found in Isaji and Spaulding (1984) and Isaji et al. (2001). Forcing of the model when used as a tide-only model is provided at the open boundaries of the model domain by spatially-varying data describing the amplitude and phase of the major tidal constituents. Tidal constituent data is extracted from the TOPEX/ POSIEDON tidal database generated from satellite-borne altimeter observations.

3.2 Tidal model grid

The resolution of the tidal model grid was varied from 500 m in shallow and coastal regions up to 8 km for offshore, or deep waters. The finer grid cells were used to more accurately resolve flows along the coastline, around islands and over regions with more complex bathymetry. Figure 4 shows the extent of the tidal model grid that was applied for the region. The regional coverage of the tidal model was set to match the domain of the ocean model that was incorporated for the study, extending eastward and westward to encompass the south-east and south-west coasts of the Australian mainland and southward beyond Tasmania.

A bathymetric grid was developed for this region from multiple data sources, including 250 m resolution bathymetric data developed by Geoscience Australia and digitisation of navigational charts (Figure 5).

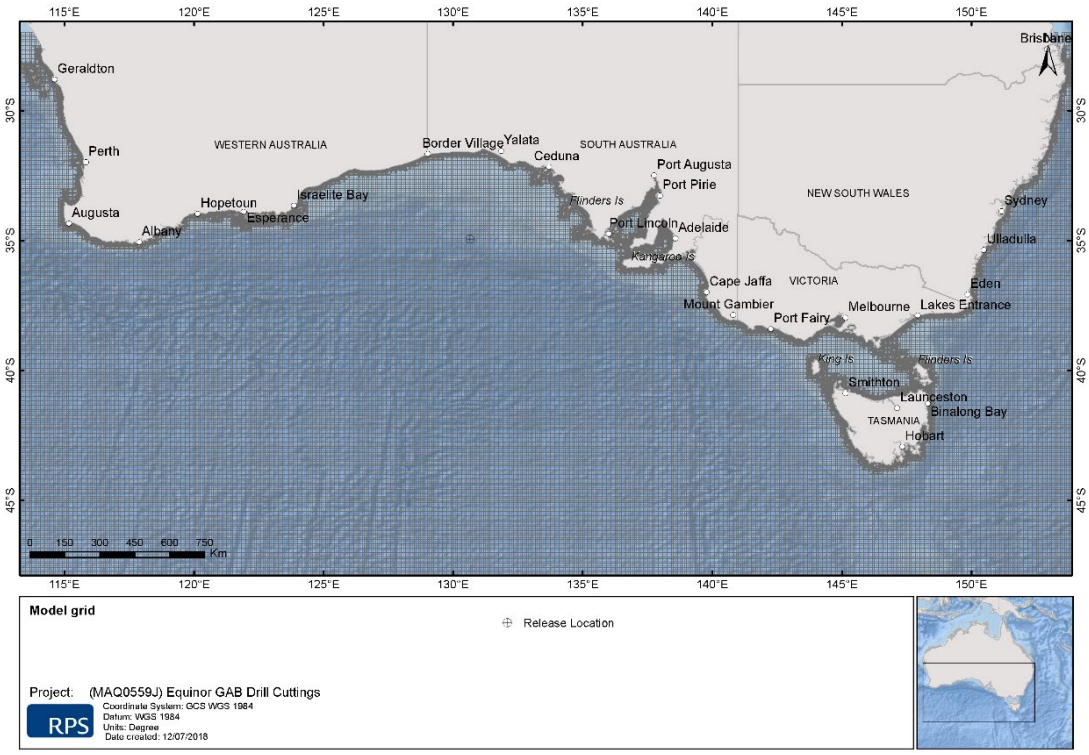

Figure 4: Extent of the model grid used to generate the tidal currents for the study region using the HYDROMAP model. Higher resolution areas are shown by the denser mesh

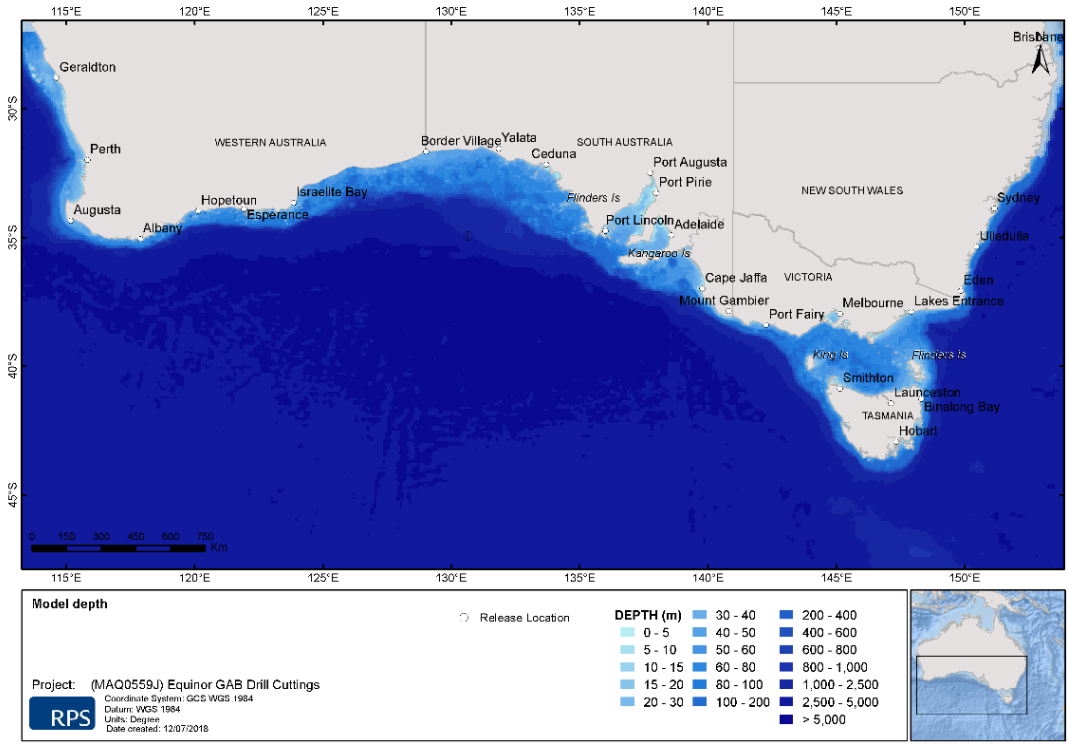

Figure 5: Bathymetry defined within the tidal model

3.3 Tidal forcing conditions

Tidal forcing along the boundary of the tidal model was obtained from satellite measured altimetry data (TOPEX/Poseidon 7.2). The altimeter derived data provided estimates of the eight dominant tidal constituents at a horizontal scale of approximately 0.25 degrees. The eight major tidal constituents used were K2, S2, m^2, N2, K1, P1, O1 and Q1. Local spatial variation in the tidal amplitude and phase of these 8 constituents along the open boundaries was calculated by spatial interpolation from the grid scale of the TOPEX/Poseidon data to the grid scale of the open boundaries. Hydromap calculates local heights along the open boundaries, at each time step in the model to derive the slope in the water surface, which is applied to calculate the propagation of individual tidal waves. Net water levels are constituted at each time step from these tidal waves.

The Topex-Poseidon satellite data has a resolution of 0.25 degrees globally and is produced and quality controlled by NASA (National Aeronautics and Space Administration). The TOPEX and Poseidon satellites were equipped with two highly accurate altimeters, capable of taking sea level measurements at resolutions of ± 5 cm. Collectively, these satellites carried out 62,000 orbits of the planet (1992–2005). The Topex-Poseidon tidal data has been widely used and scrutinised by the oceanographic community (e.g. Andersen, 1995; Ludicone et al., 1998; Matsumoto et al., 2000; Kostianoy et al., 2003; Yaremchuk and Tangdong, 2004; Qiu and Chen 2010). As such the TOPEX/Poseidon tidal data is considered suitably accurate for calculation of tidal currents for this study.

3.4 Validation of the tidal model

To ensure that tidal predictions were accurate, predicted surface elevations were first compared graphically to observed data at six locations within the domain (Table 2 and Figure 6).

Figure 7 and Figure 8 show a comparison between the predicted and observed surface elevations for each of the six locations between the 1st and the 31st January 2014. As shown on the graphs, the HYDROMAP model accurately reproduced the phase and amplitudes of the sea surface elevation fluctuations attributable to astronomical tides throughout the spring and neap tidal cycles.

Measured and predicted tidal predictions for the six tide stations were also compared statistically applying the Mean Absolute Error (MAE) (Willmott, 1982, Willmott and Matsuura, 2005) and the Index of Agreement (IOA) (Willmott, 1981).

The MAE is simply the average discrepancy between each of the model-predicted (P) and observed (O) value, where the differences are expressed as absolute values. The MAE is a more natural measure of the average error (Willmott and Matsuura, 2005) and more readily understood.

$$MAE = N^{-1}\sum_{i=1}^{N}|P_i - O_i|$$

A low MAE indicates better fit between the predicted and observed data. One limitation of the MAE, for data that fluctuates (as per tidal levels) is that a small discrepancy in the phase of the data being compared will yield an apparently large error. Phase errors would not have any significance for the application of the predicted data in this study because spill times are randomised (i.e. not analysed for release at specific times).

The Index of Agreement (IOA) provides a standardised comparison that identifies additive and proportional differences in the means and variances between predicted and observed values:

$$IOA = 1 - \frac{\sum|X_{model} - X_{obs}|^2}{\sum(|X_{model} - \overline{X_{obs}}| + |X_{obs} - \overline{X_{obs}}|)^2}$$

Where: X represents the variable being compared and $\overline{X_{obs}}$ is the time mean of the observed values. A perfect agreement would exist between the predictions and observations if the index gives an agreement value of 1 and complete disagreement will produce an index measure of 0 (Wilmott, 1981). Willmott et al. (1985) also suggests that values meaningfully larger than 0.5 represent good model performance.

MAE values calculated for the nine stations were low and approaching 0 indicative of good fit of both the phase and amplitude of the predictions. MAE values indicated discrepancies of between 5 cm to 11 cm among the sites (Table 2). Given that observed water levels are subject to other phenomenon than astronomical tides, this comparison indicates robust calculation for tidal propagation over the region. The IOA values calculated from the comparison ranged between 0.95 to 0.99 across the 6 sites, approaching the ideal fit of 1, also indicative of robust model performance. No spatial trends in error indexes are presented, providing evidence that tidal predictions can be relied on away from the observation sites.

Table 2: Statistical comparison between the observed and HYDROMAP predicted surface elevation data from 1st -31st January 2014

Tide station	Ioa	Mae (m)
Albany	0.98	0.07
Esperance	0.98	0.06
Eucla	0.96	0.08
Port Lincoln	0.95	0.11
Portland	0.97	0.07
Eden	0.99	0.05
Average	**0.97**	**0.07**

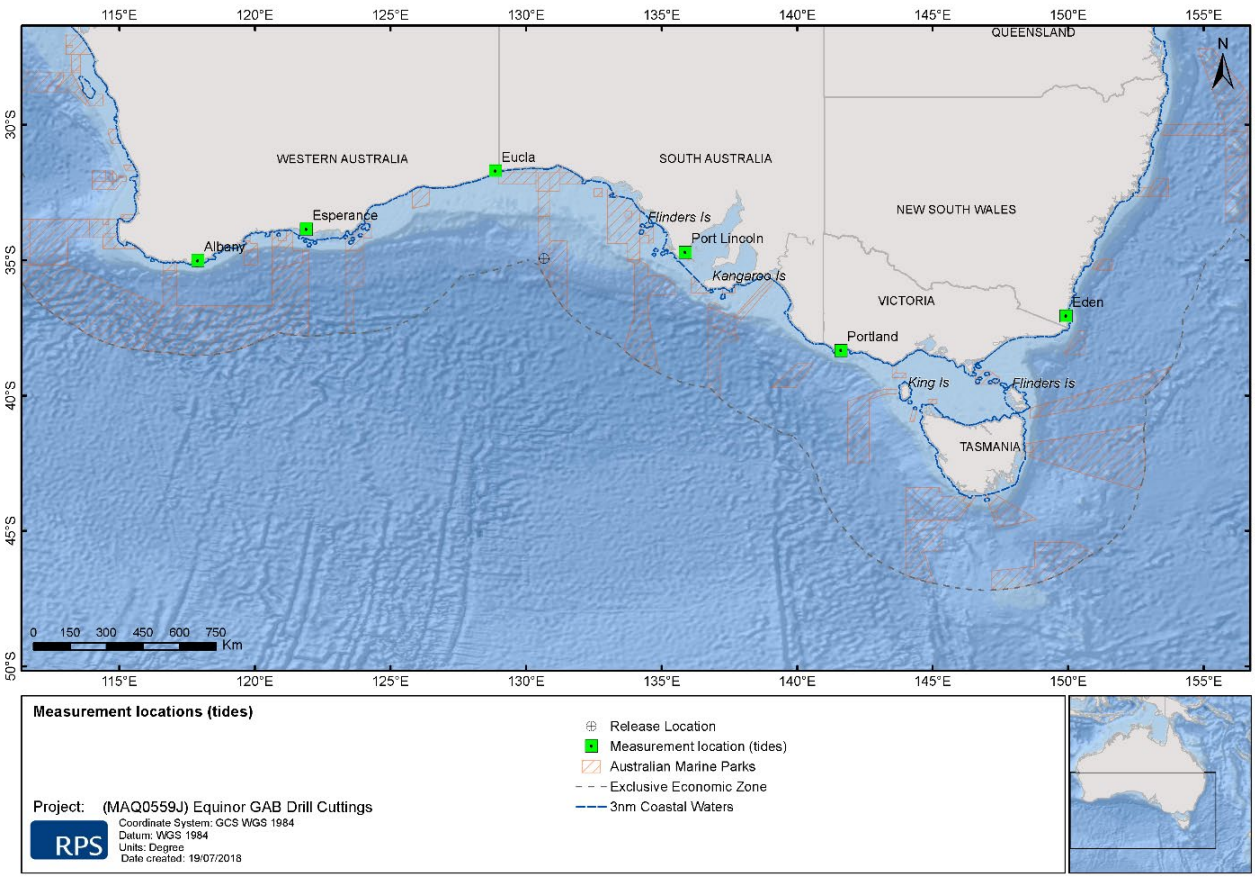

Figure 6: Location of the tide stations used in the surface elevation comparison

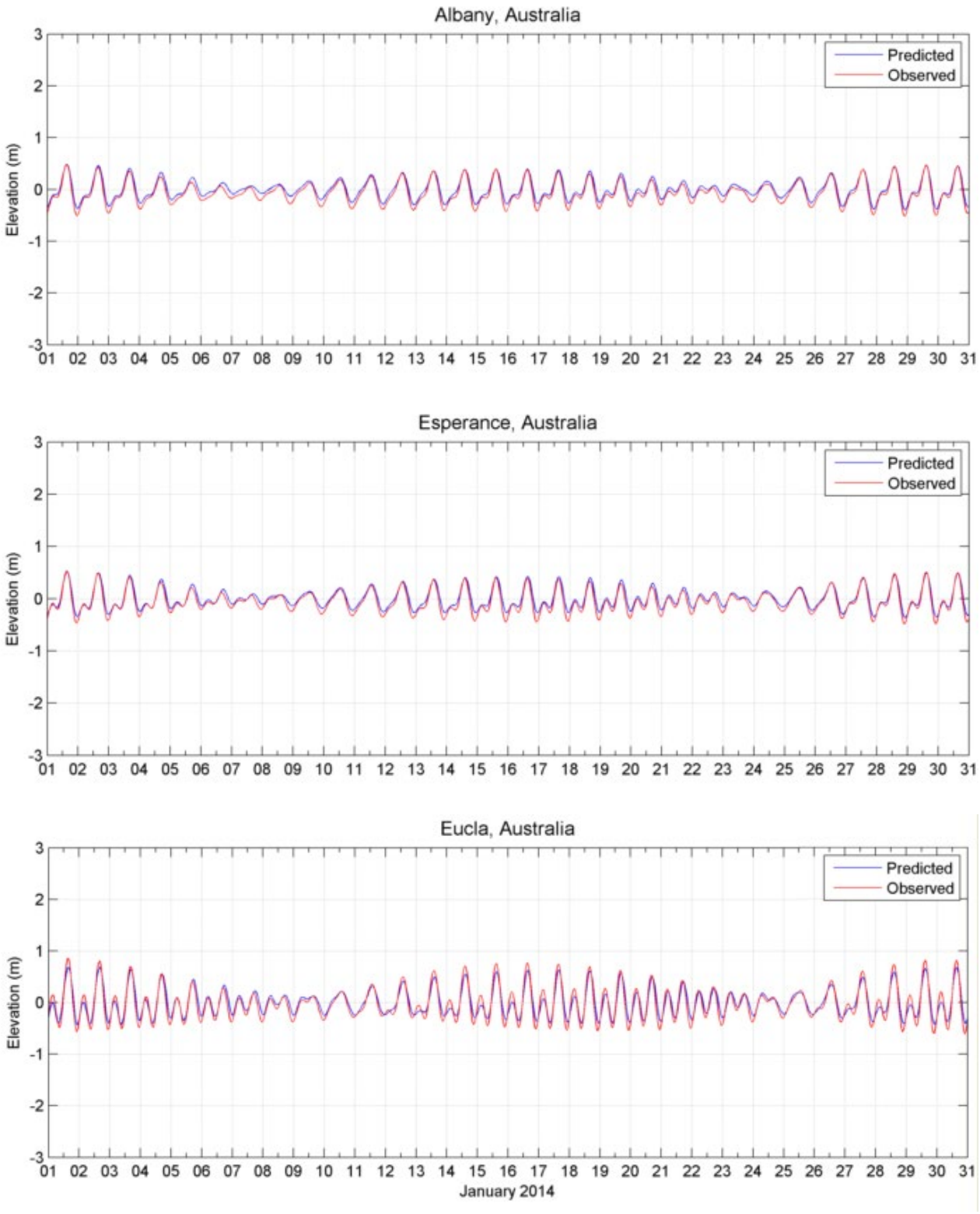

Figure 7: Comparison between predicted (blue line) and observed (red line) surface elevation variation at Albany (top), Esperance (middle) and Eucla (bottom), between 1–31 January 2014

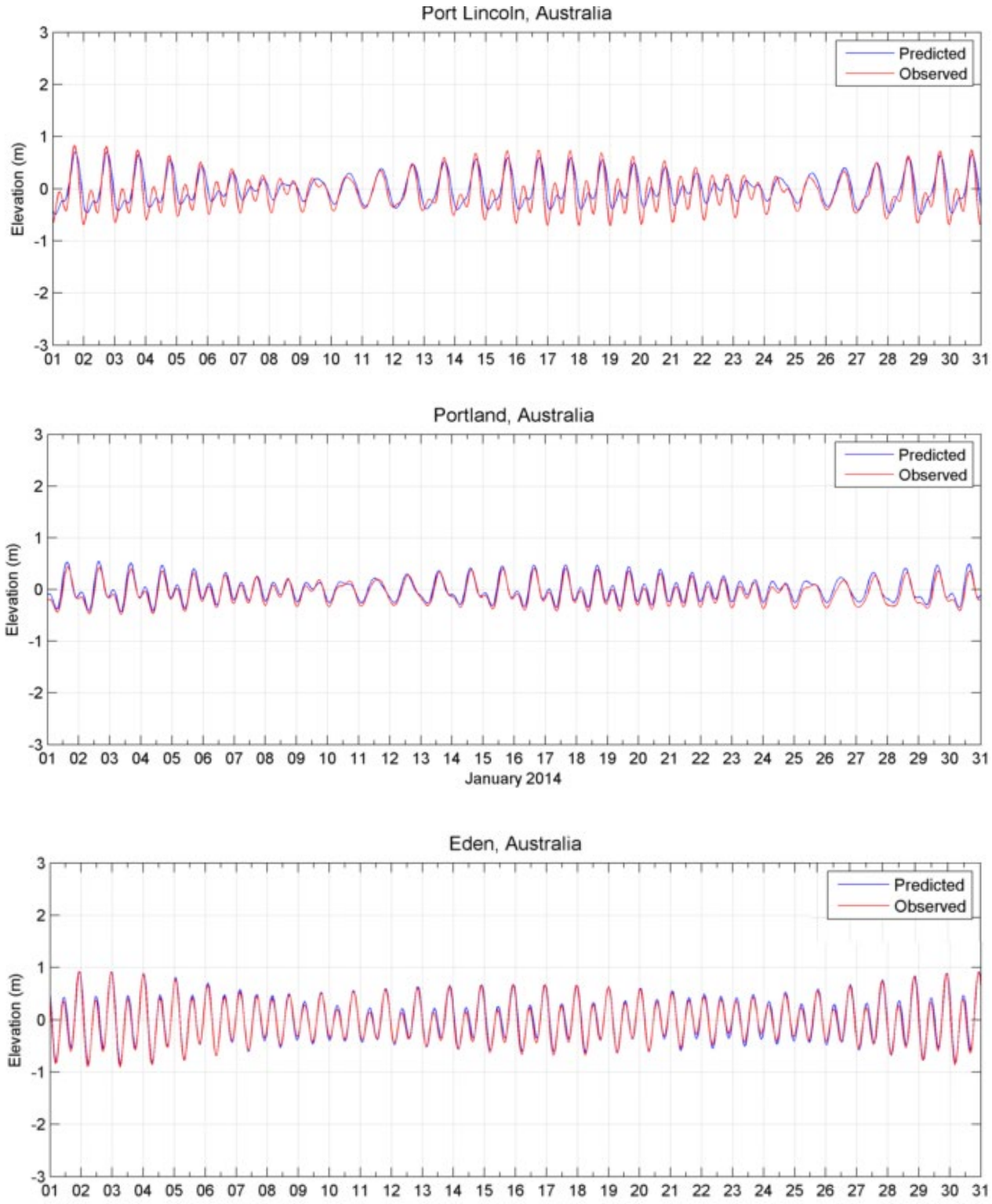

Figure 8: Comparison between predicted (blue line) and observed (red line) surface elevation variation at Port Lincoln (top), Portland (middle) and Eden (bottom), between 1–31 January 2014

3.5 Ocean currents within the Great Australian Bight

Three-dimensional (3D) ocean current data from 2010 to 2012 (inclusive) was obtained from the Hybrid Coordinate Ocean Model (HYCOM; Chassignet et al., 2007), which is operated by the HYCOM Consortium, sponsored by the Global Ocean Data Assimilation Experiment (GODAE). HYCOM is a three-dimensional ocean model that assimilates actual observations of sea surface height, sea surface temperature and in-situ temperature and salinity measurements (Chassignet, et al., 2009). The HYCOM predictions for drift currents are produced at a horizontal spatial resolution of approximately 8.25 km (1/12th of a degree) over the region, at a frequency of once per day. The model is self-validated meaning that the model automatically self-calibrates and corrects with in-situ and satellite observations. The automatic calibration and quality control of the datasets from HYCOM makes these datasets more reliable than uncalibrated forecast data.

The complexity of the ocean current flows over the region that is calculated by the HYCOM model data is revealed by an example plot representing 1 single day (1st January 2012, see Figure 9). Arrows point in the direction of flow and the speed of the current is represented by the scale and colour of the arrows. Because these data are presented at daily steps, the HYCOM data does not represent tidal variations, which fluctuate over shorter time-scales.

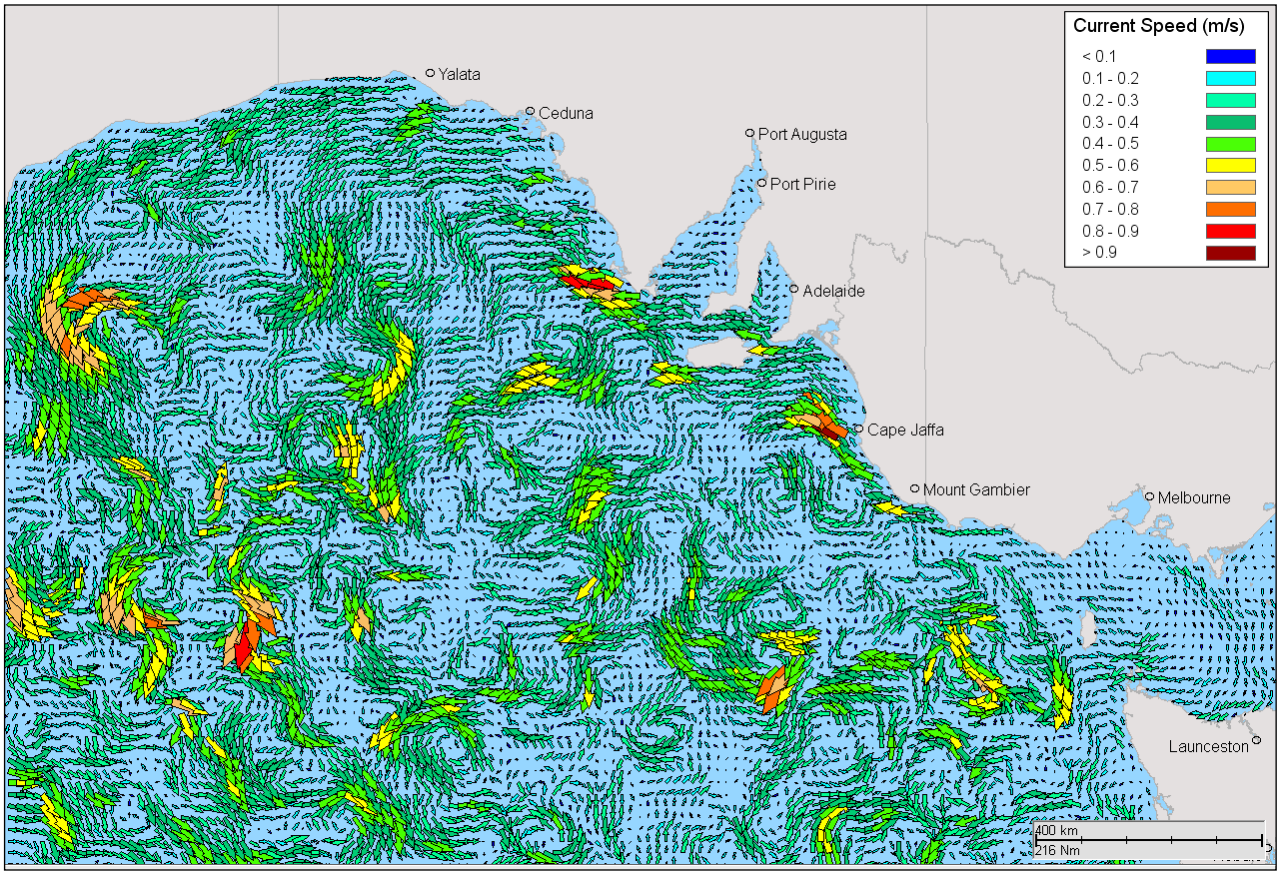

Figure 9: Predicted ocean surface currents on the 1st January 2012, summer conditions. Derived from the HYCOM ocean hindcast model. The colours of the vectors indicate current speed in m/s

3.6 Surface and bottom currents at Stromlo-1

The average and maximum surface and bottom combined current speeds (tides plus ocean currents) at Stromlo-1 for each year (2010, 2011 and 2012) and month are presented in Table 3 to Table 5. The average and maximum surface currents speeds were greater (i.e. faster) compared to the bottom currents. The maximum surface current speeds ranged from 0.32 m/s to 0.88 m/s during December 2011 and August 2011, respectively, compared to 0.05 m/s (February 2010) and 0.11 m/s (August and September 2011) for the bottom currents. The average monthly surface current speeds ranged between 0.12 m/s and 0.43 m/s, whilst the average monthly bottom current speeds ranged between 0.02 m/s and 0.05 m/s.

Figure 10 to Figure 12 and Figure 13 to Figure 15 show the surface and bottom current rose plots for each month for 2010–2012 adjacent to the Stromlo-1 well. Note the convention for defining current direction is the direction the current flows towards, which is used to reference current direction throughout this report. Each branch of the rose represents the currents flowing to that direction, with north to the top of the diagram. The rose branches are each divided into segments of different colour according to speed intervals, which represent current speeds within the monthly dataset. The length of each coloured segment (indicative of speeds) is relative to the proportion of time the currents flow to the corresponding direction.

Table 3: Predicted surface and bottom current speeds for 2010 adjacent to Stromlo-1 well. Data derived by combining HYCOM ocean data and HYDROMAP tidal data from January to December (inclusive)

Month	Surface currents		Bottom currents	
	Mean current speed (m/s)	Maximum current speed (m/s)	Mean current speed (m/s)	Maximum current speed (m/s)
January	0.19	0.50	0.03	0.06
February	0.20	0.54	0.02	0.05
March	0.19	0.44	0.05	0.09
April	0.21	0.41	0.02	0.05
May	0.23	0.60	0.02	0.06
June	0.20	0.39	0.03	0.07
July	0.12	0.36	0.04	0.10
August	0.17	0.44	0.04	0.09
September	0.33	0.72	0.03	0.08
October	0.38	0.65	0.02	0.06
November	0.16	0.46	0.02	0.05
December	0.17	0.47	0.02	0.07
Minimum	**0.12**	**0.36**	**0.02**	**0.05**
Maximum	**0.38**	**0.72**	**0.05**	**0.10**

Table 4: Predicted surface and bottom current speeds for 2011 adjacent to Stromlo-1 well. Data derived by combining HYCOM ocean data and HYDROMAP tidal data from January to December (inclusive)

Month	Surface currents		Bottom currents	
	Mean current speed (m/s)	Maximum current speed (m/s)	Mean current speed (m/s)	Maximum current speed (m/s)
January	0.18	0.41	0.03	0.06
February	0.18	0.38	0.02	0.07
March	0.15	0.34	0.03	0.07
April	0.16	0.47	0.02	0.07
May	0.16	0.47	0.02	0.07
June	0.20	0.45	0.03	0.08
July	0.32	0.66	0.03	0.08
August	0.43	0.88	0.03	0.10
September	0.21	0.53	0.04	0.09
October	0.29	0.52	0.03	0.07
November	0.21	0.50	0.03	0.06
December	0.15	0.32	0.03	0.07
Minimum	**0.15**	**0.32**	**0.02**	**0.06**
Maximum	**0.43**	**0.88**	**0.04**	**0.10**

Table 5: Predicted surface and bottom current speeds for 2012 adjacent to Stromlo-1 well. Data derived by combining HYCOM ocean data and HYDROMAP tidal data from January to December (inclusive)

Month	Surface currents		Bottom currents	
	Mean current speed (m/s)	Maximum current speed (m/s)	Mean current speed (m/s)	Maximum current speed (m/s)
January	0.17	0.49	0.02	0.06
February	0.21	0.40	0.03	0.07
March	0.18	0.40	0.02	0.06
April	0.24	0.47	0.03	0.10
May	0.21	0.58	0.03	0.07
June	0.15	0.33	0.04	0.10
July	0.19	0.45	0.03	0.09
August	0.20	0.58	0.03	0.11
September	0.35	0.82	0.03	0.11
October	0.20	0.55	0.03	0.07
November	0.22	0.54	0.03	0.08
December	0.17	0.43	0.03	0.06
Minimum	**0.15**	**0.33**	**0.02**	**0.06**
Maximum	**0.35**	**0.82**	**0.04**	**0.11**

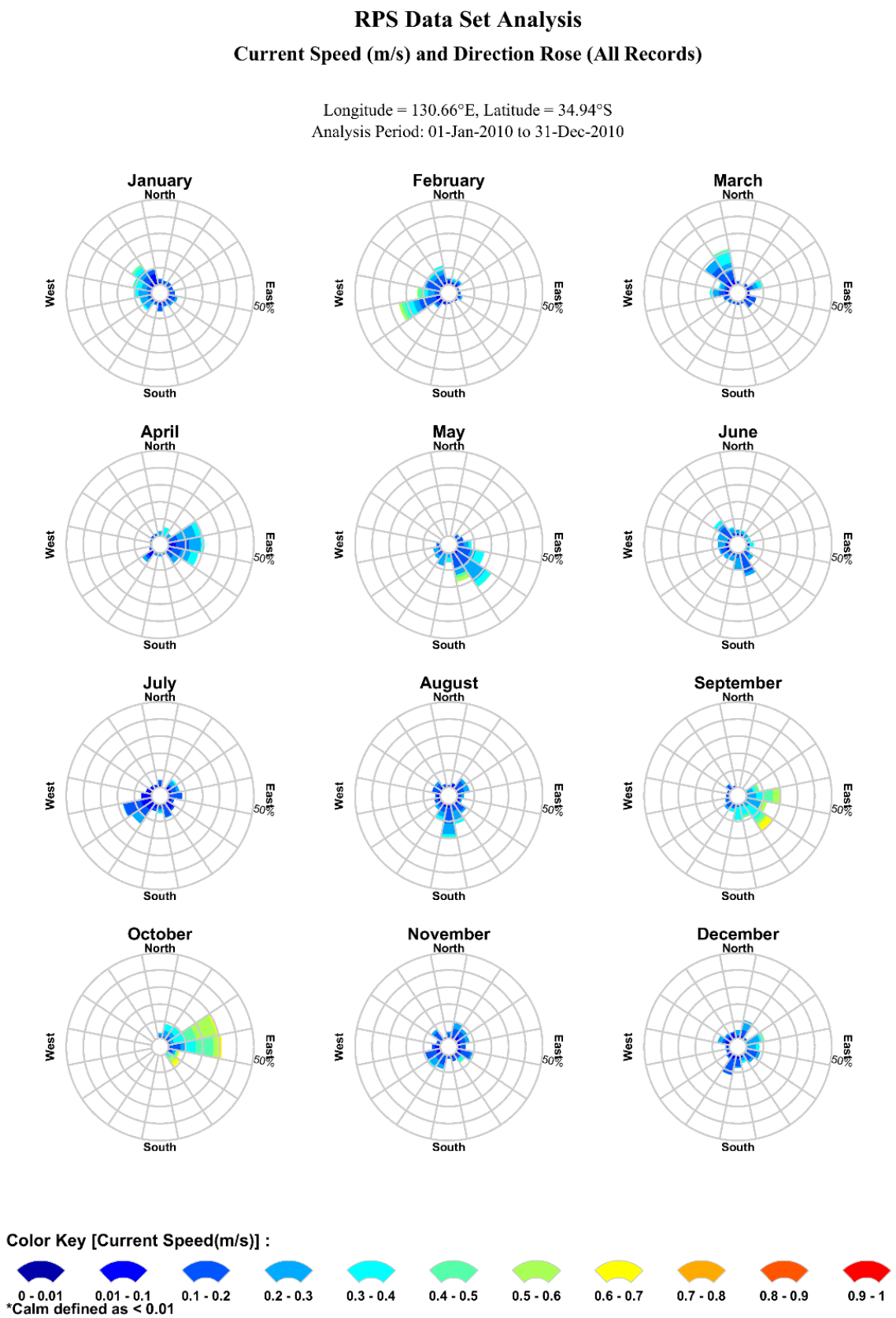

Figure 10: Monthly surface waters current rose plots adjacent to Stromlo-1 well during 2010. The current roses were generated by combining the tidal currents and HYCOM ocean currents. The colour key shows the current speed (m/s), the compass shows the direction and the length of the wedge gives the percentage of the record for a particular speed and direction combination

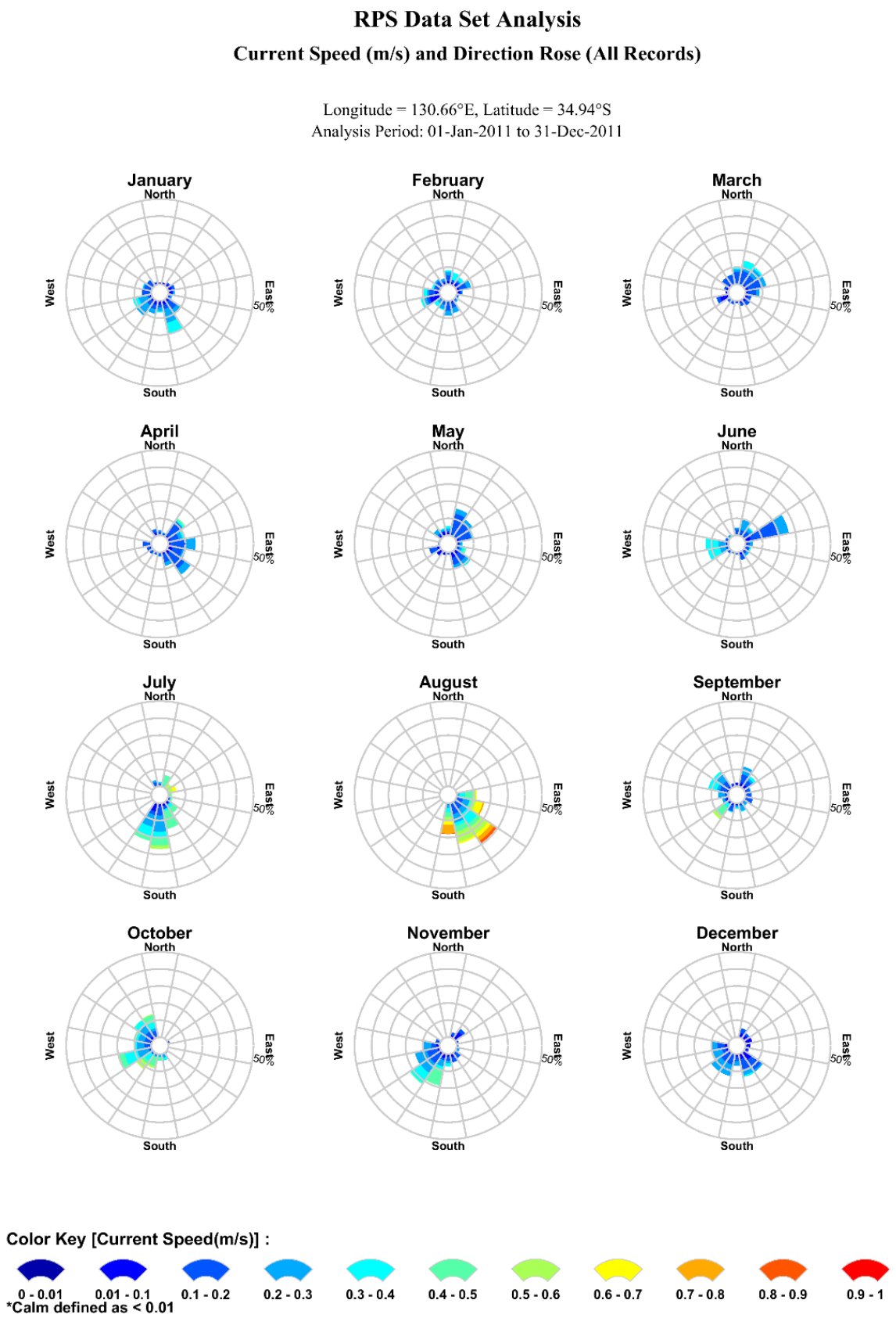

Figure 11: Monthly surface waters current rose plots adjacent to Stromlo-1 well during 2011. The current roses were generated by combining the tidal currents and HYCOM ocean currents. The colour key shows the current speed (m/s), the compass shows the direction and the length of the wedge gives the percentage of the record for a particular speed and direction combination

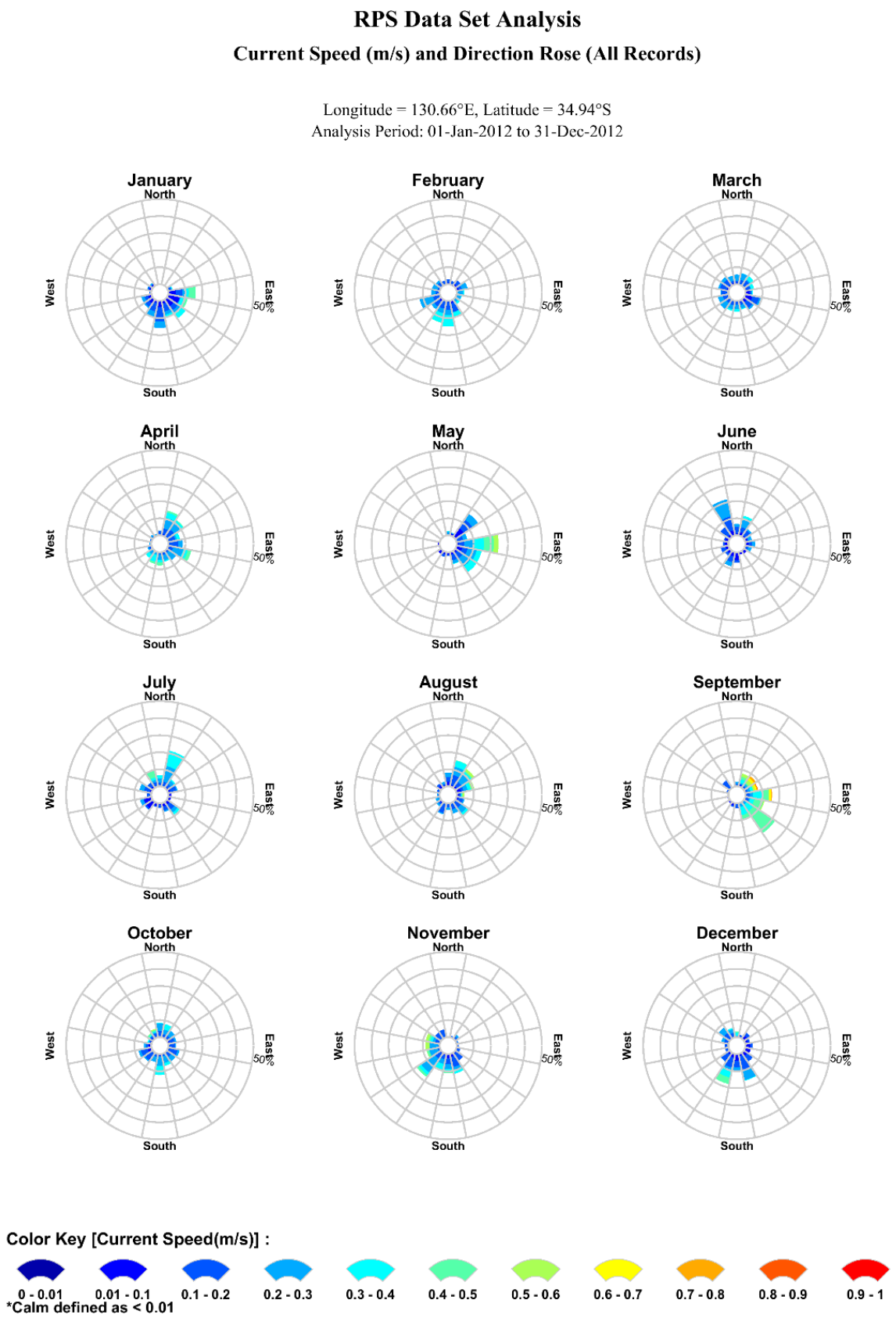

Figure 12: Monthly surface waters current rose plots adjacent to Stromlo-1 well during 2012. The current roses were generated by combining the tidal currents and HYCOM ocean currents. The colour key shows the current speed (m/s), the compass shows the direction and the length of the wedge gives the percentage of the record for a particular speed and direction combination

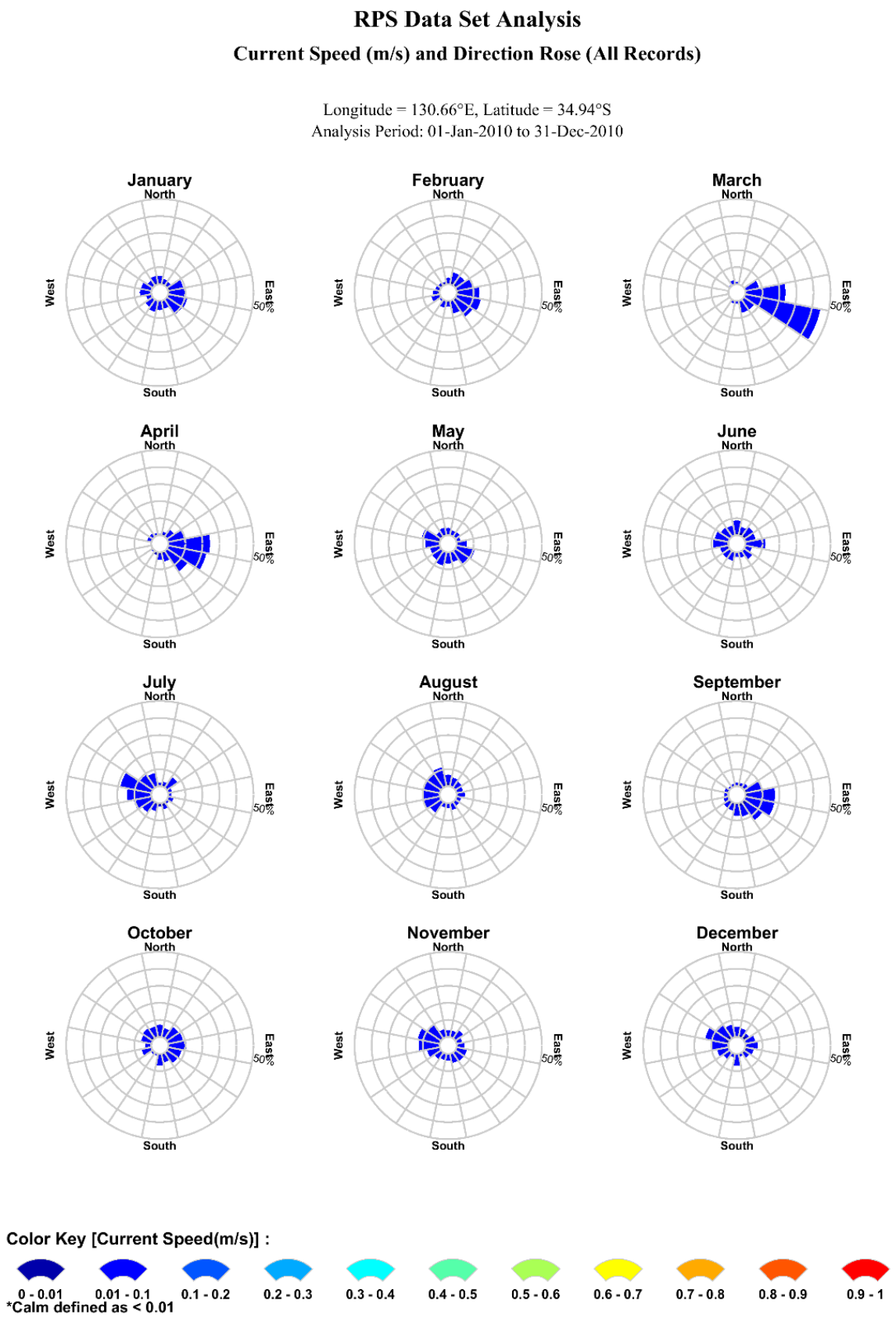

Figure 13: Monthly bottom waters current rose plots adjacent to Stromlo-1-well during 2010. The current roses were generated by combining the tidal currents and HYCOM ocean currents. The colour key shows the current speed (m/s), the compass shows the direction and the length of the wedge gives the percentage of the record for a particular speed and direction combination

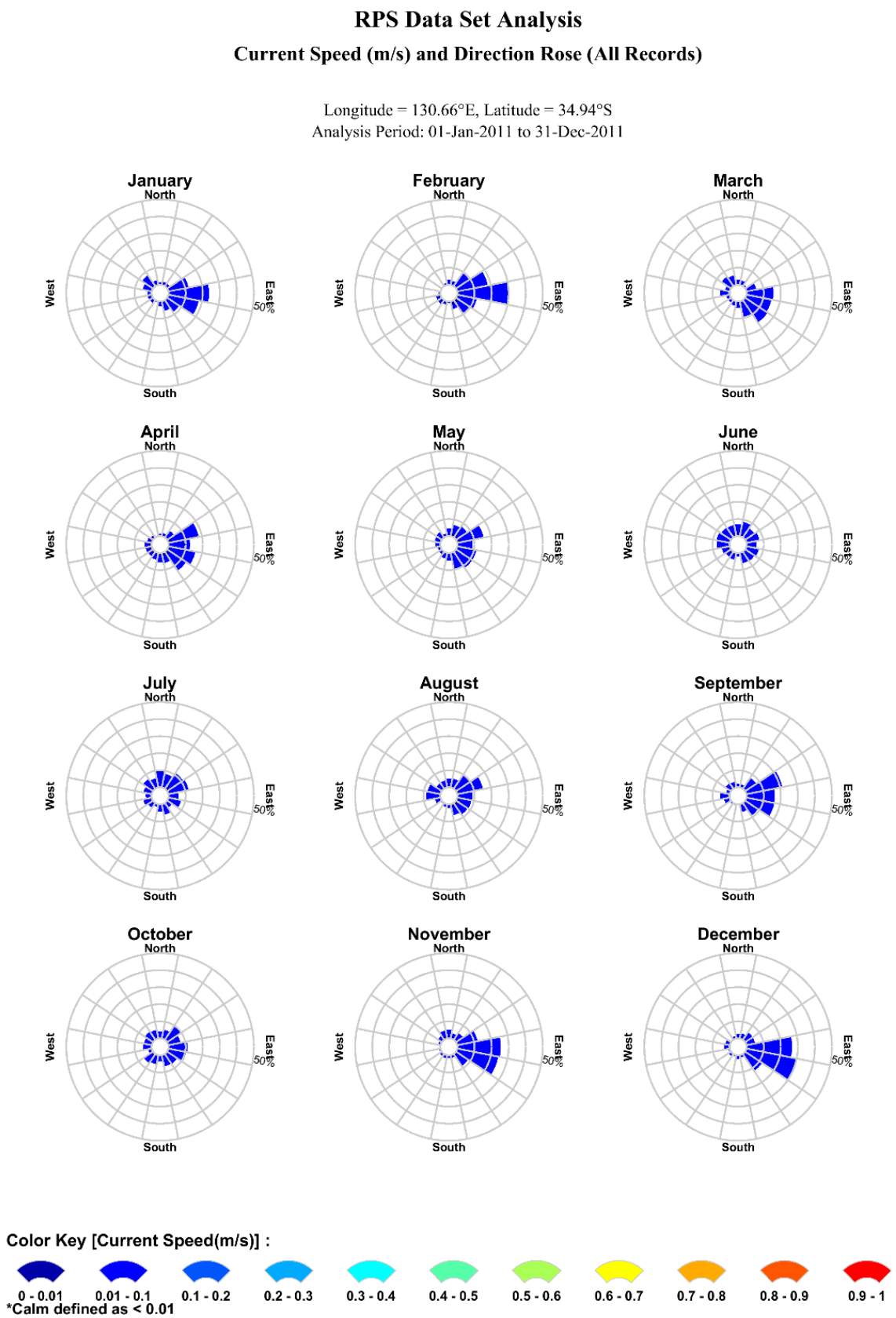

Figure 14: Monthly bottom waters current rose plots adjacent to Stromlo-1 during 2011. The current roses were generated by combining the tidal currents and HYCOM ocean currents. The colour key shows the current speed (m/s), the compass shows the direction and the length of the wedge gives the percentage of the record for a particular speed and direction combination

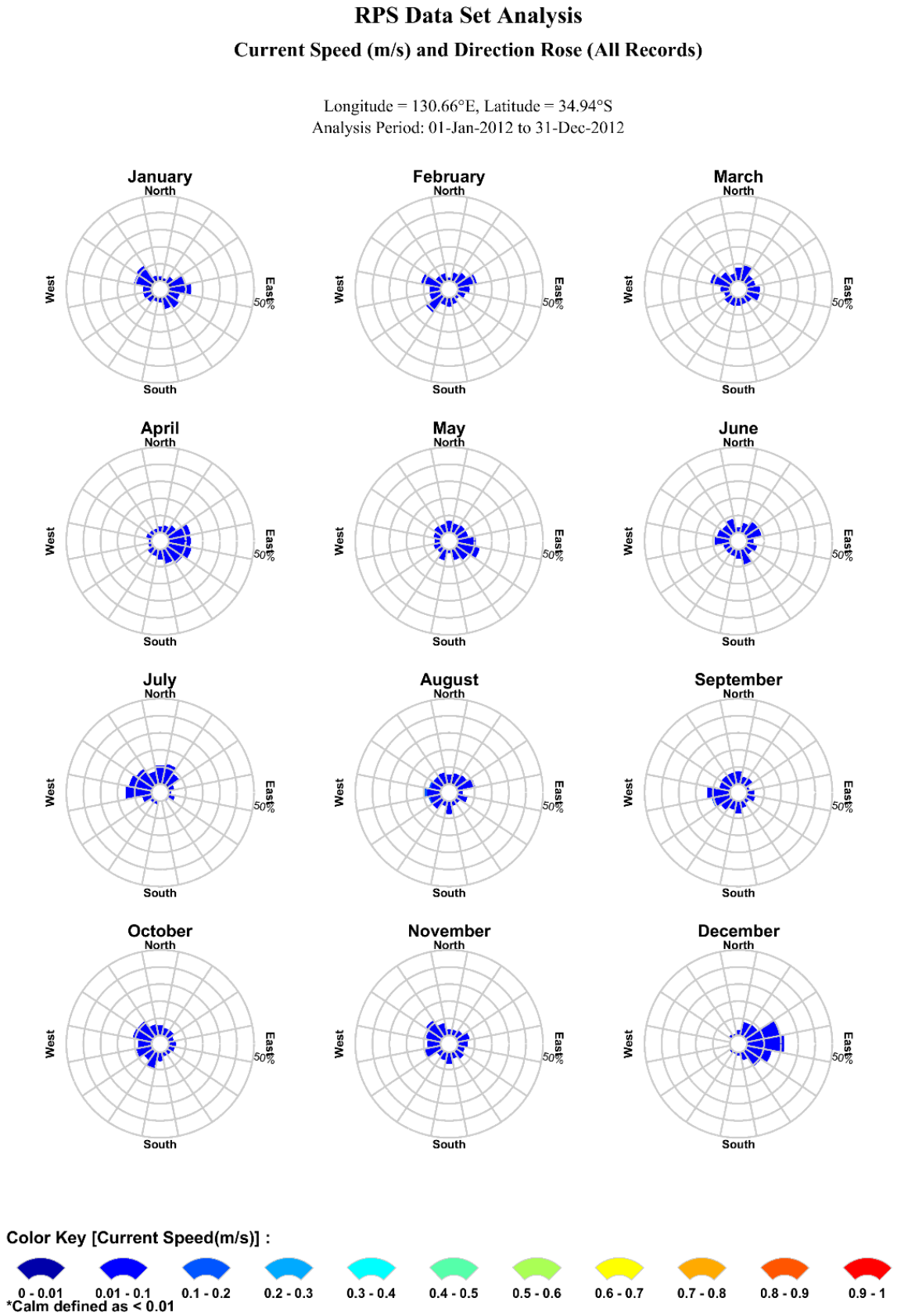

Figure 15: Monthly bottom waters current rose plots adjacent to Stromlo-1 during 2012. The current roses were generated by combining the tidal currents and HYCOM ocean currents. The colour key shows the current speed (m/s), the compass shows the direction and the length of the wedge gives the percentage of the record for a particular speed and direction combination

3.7 Net water current comparison

To ensure that the combined current calculations were suitably accurate, the calculated data (tidal current + ocean currents) were visually compared to measured data available from a location approximately 50 km north of the Stromlo-1 well site (34o 28’ 30’’ S, 130o 42’ 5’’ E; Figure 16) that was previously measured by RPS MetOcean (2013). Rose plots that illustrate the distribution of the speed and direction of current flows were generated from the calculated net-current data and compared to those produced from the measured current data that were extracted directly from the RPS MetOcean (2013) report. Comparisons between the calculated and measured datasets were made at 6 different depths across 2 different periods (see Table 6).

The current roses show the frequency at which the current flows towards a given direction at a given speed. Each sector of the rose represents currents flowing toward that direction e.g. currents flowing towards the north are represented by the sector extending towards the top of the rose. Sixteen directions are used, representing the cardinal directions. Each sector is divided into segments that are colour-coded, representing intervals in current speed. The length of each segment within a sector indicates the frequency that currents flowed toward that direction at the given speed.

A comparison of the current roses (Figure 17 to Figure 22) indicates good agreement between the calculated net-currents and the measured currents at surface over time. The calculated current captures spatial trends in the distribution of current data that was represented in the measured data. Both data sets indicate reduction in current speed with increasing depth, speeds of up to 0.6 m/s are indicated for 30 m, reducing to 0.2 m/s in the deepest layer (1000 m). Furthermore, both data sets indicate a shift in the current direction, with flows more frequently towards the eastern and southern sectors in the upper water column and more frequently towards the southern and south-western sector in the deeper layers. The rose plots also reveal that current might flow toward any direction at each of the depth’s levels.

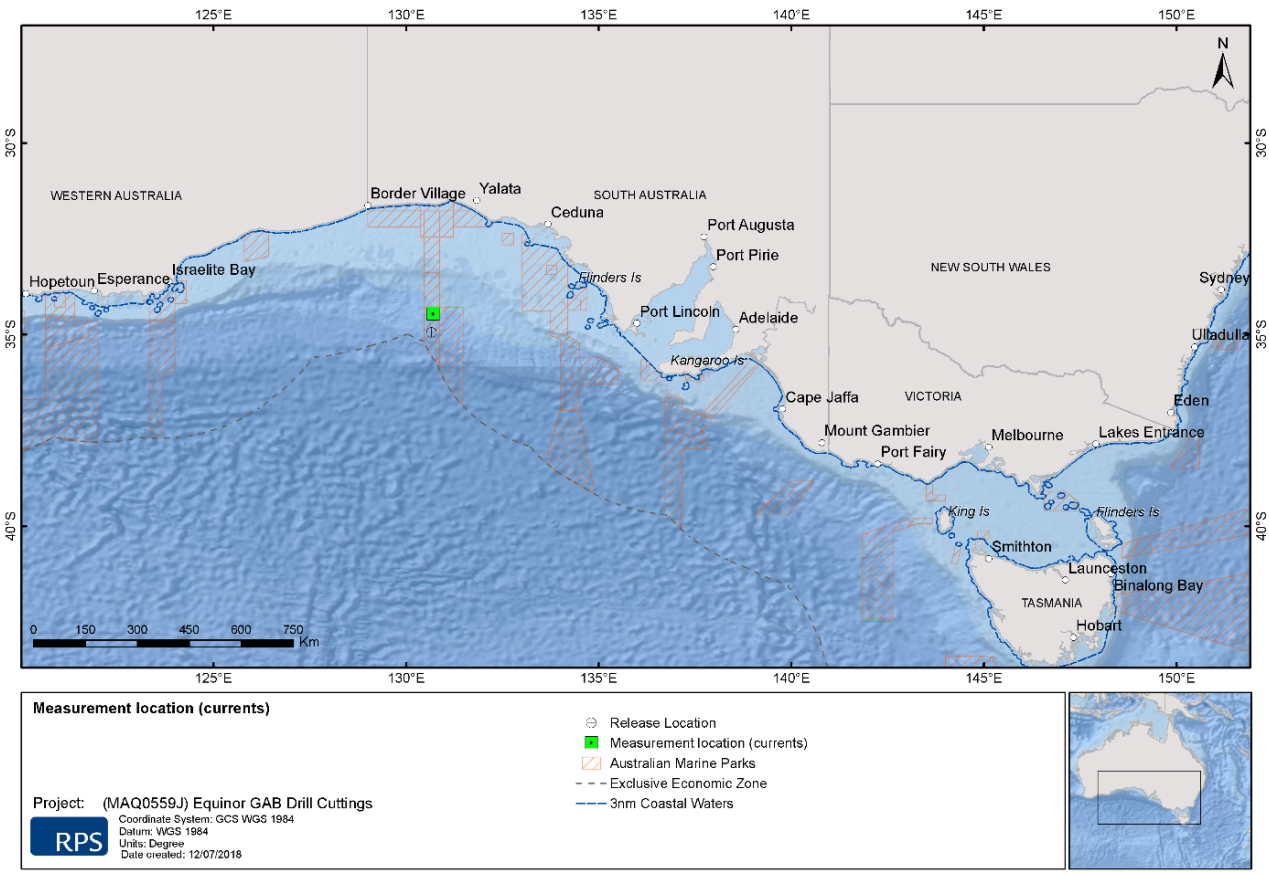

Figure 16: Current measurement location in relation to the Stromlo-1 well site

Table 6: Measured and calculated current data information

Depth (m)	Period	Measured data	Modelled data
30	03-11-2011 to 22-10-2012	ADCP	Tidal + ocean currents
50	03-11-2011 to 22-10-2012	ADCP	Tidal + ocean currents
70	03-11-2011 to 22-10-2012	ADCP	Tidal + ocean currents
200	03-11-2011 to 12-12-2012	CM04 - Current meter	Tidal + ocean currents
1000	03-11-2011 to 12-12-2012	CM04 - Current meter	Tidal + ocean currents
1000	03-11-2011 to 12-12-2012	CM04 - Current meter	Tidal + ocean currents

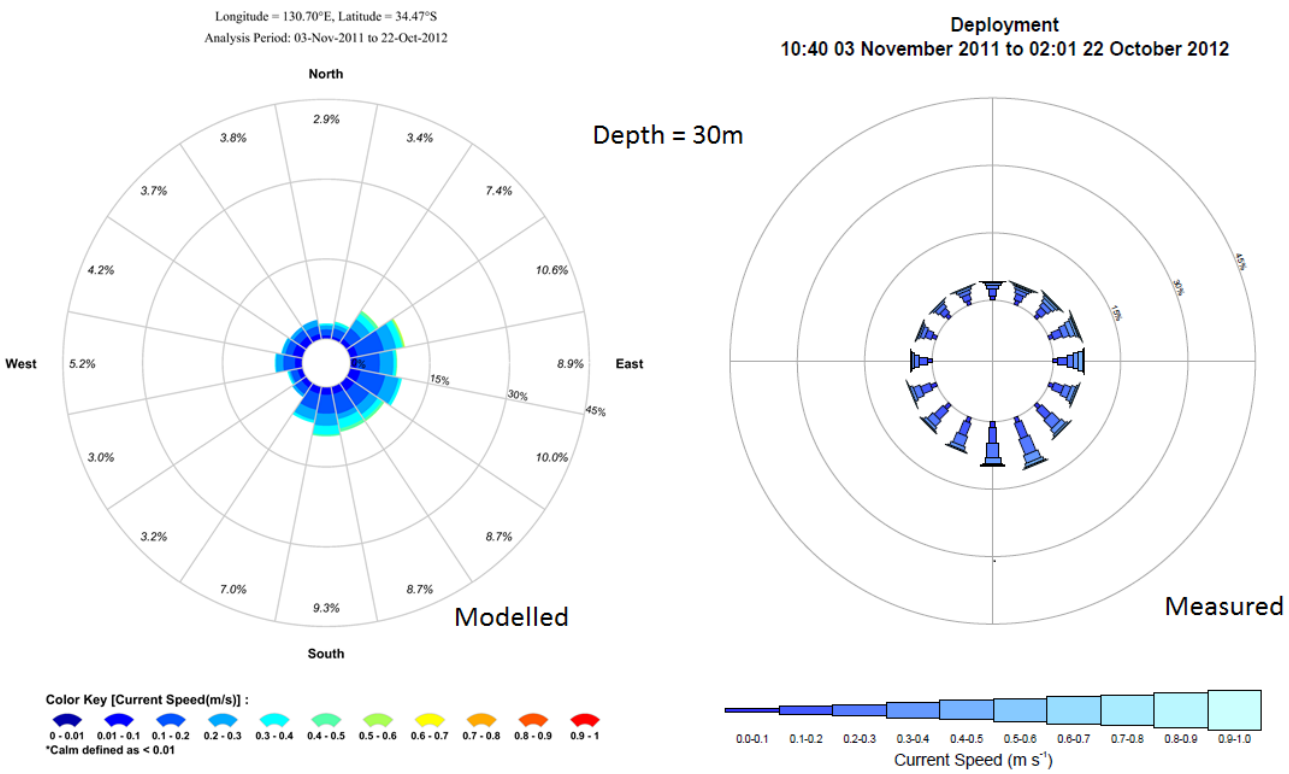

Figure 17: Modelled (left) and measured (right) current roses for depth layer of 30 m at 340 28' 30''S, 1300 42' 5''E. Source of measured data: RPS MetOcean (2013)

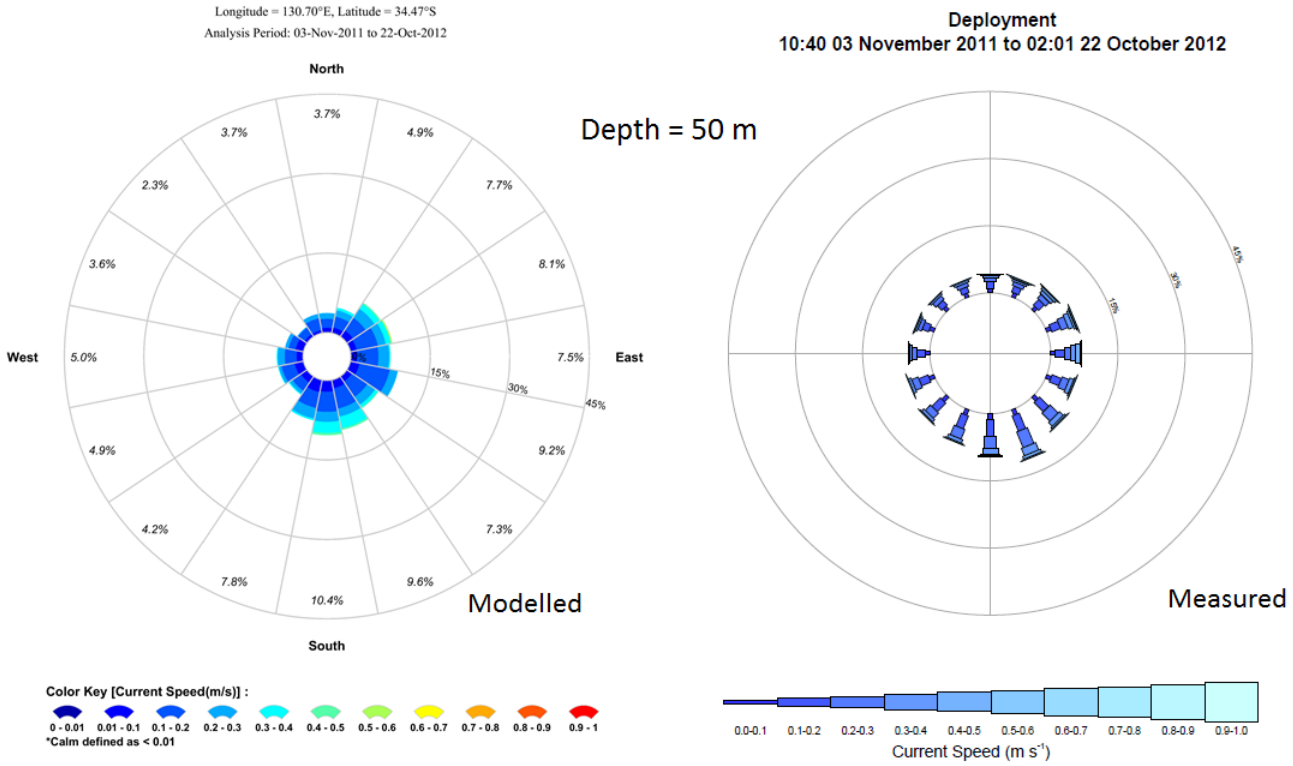

Figure 18: Modelled (left) and measured (right) current roses for depth layer of 50 m at 340 28' 30'' S, 1300 42' 5'' E. Source of measured data: RPS MetOcean (2013)

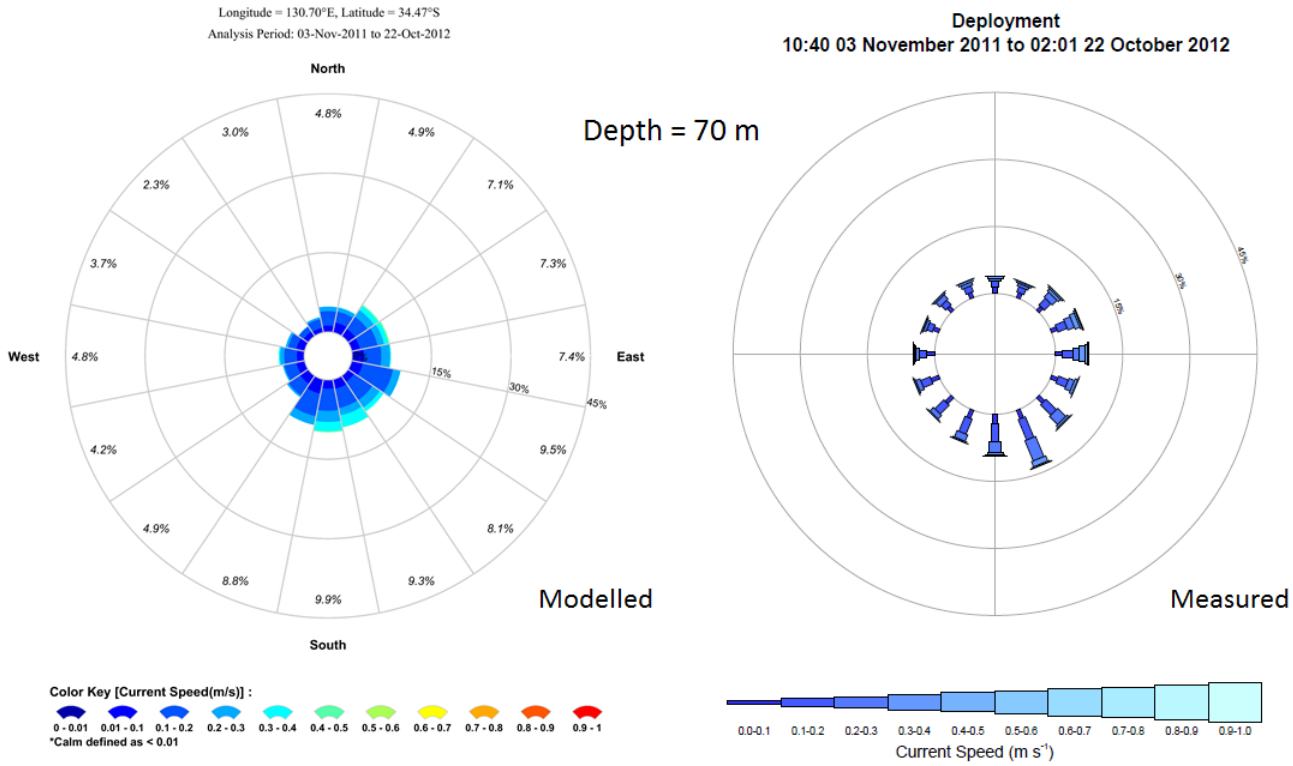

Figure 19: Modelled (left) and measured (right) current roses for depth layer of 70 m at 340 28' 30'' S, 1300 42' 5'' E. Source of measured data: RPS MetOcean (2013)

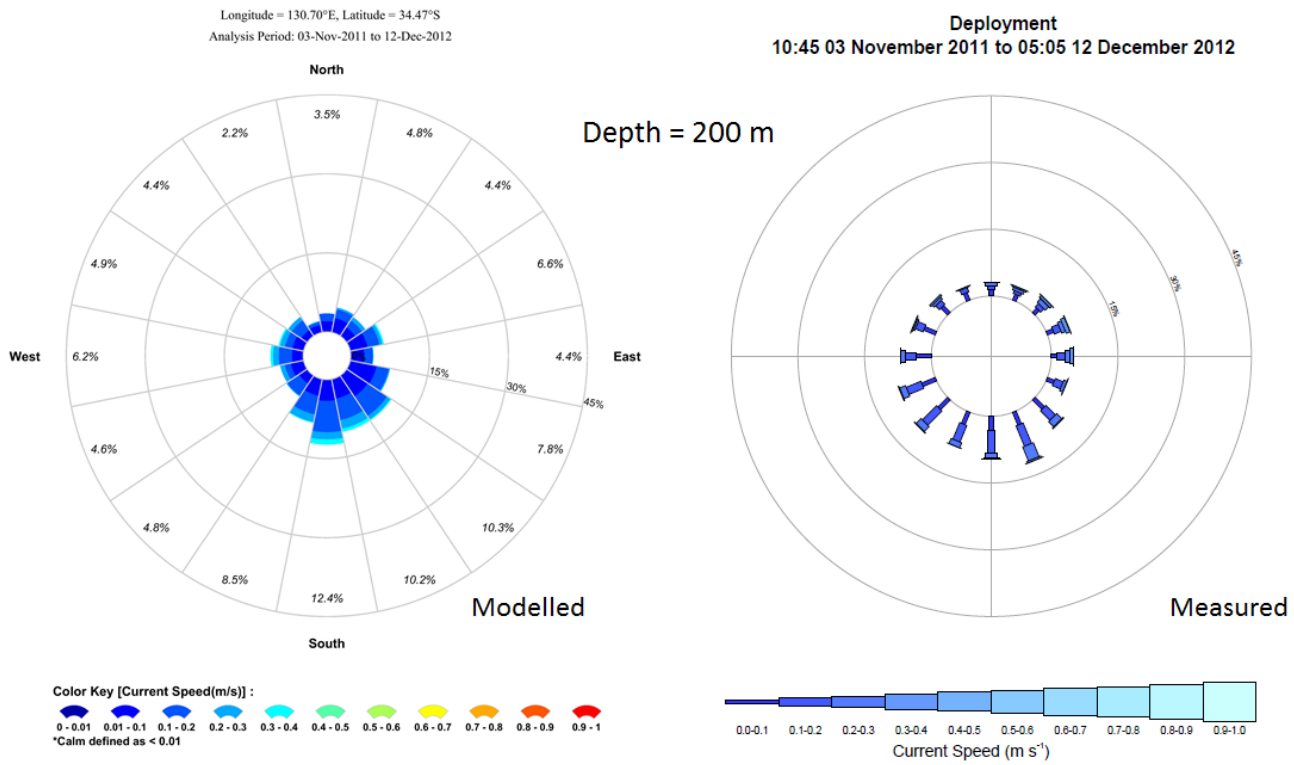

Figure 20: Modelled (left) and measured (right) current roses for depth layer of 200 m at 340 28' 30'' S, 1300 42' 5'' E. Source of measured data: RPS MetOcean (2013)

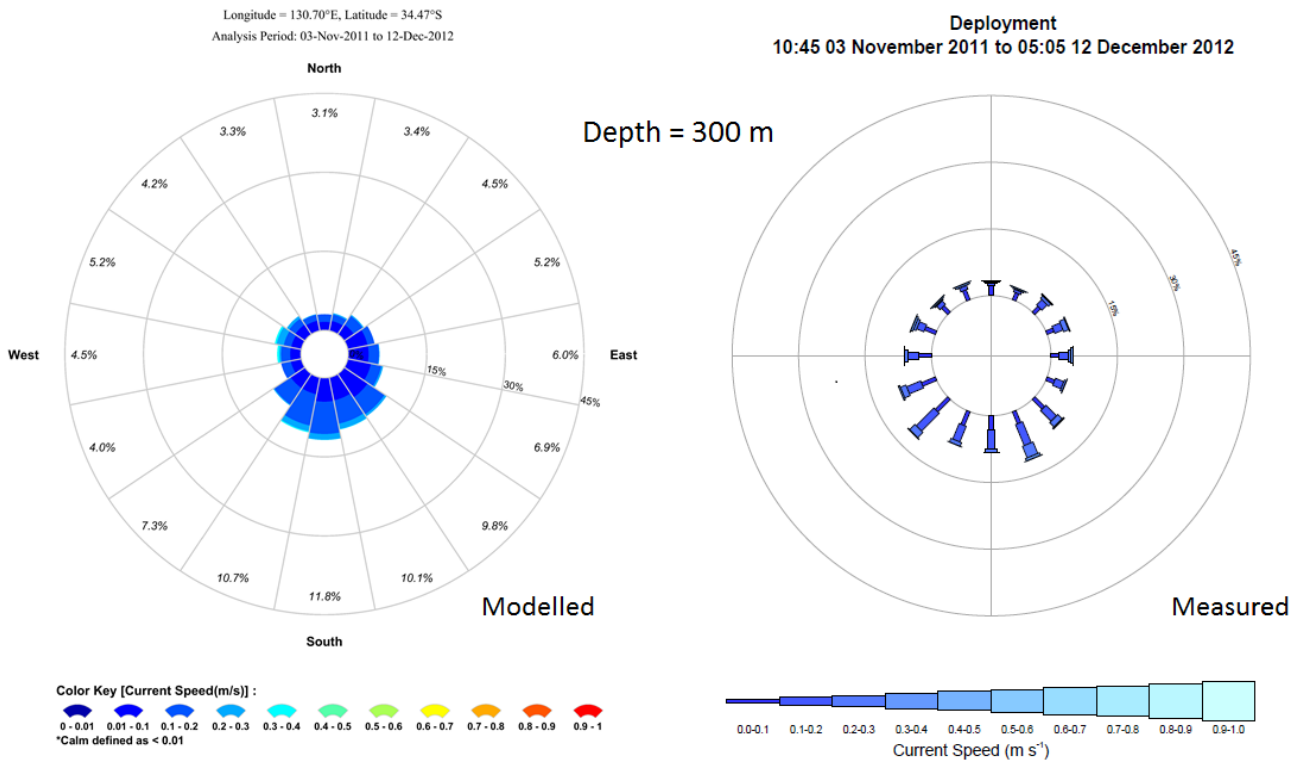

Figure 21: Modelled (left) and measured (right) current roses for depth layer of 300 m at 340 28' 30'' S, 1300 42' 5'' E. Source of measured data: RPS MetOcean (2013)

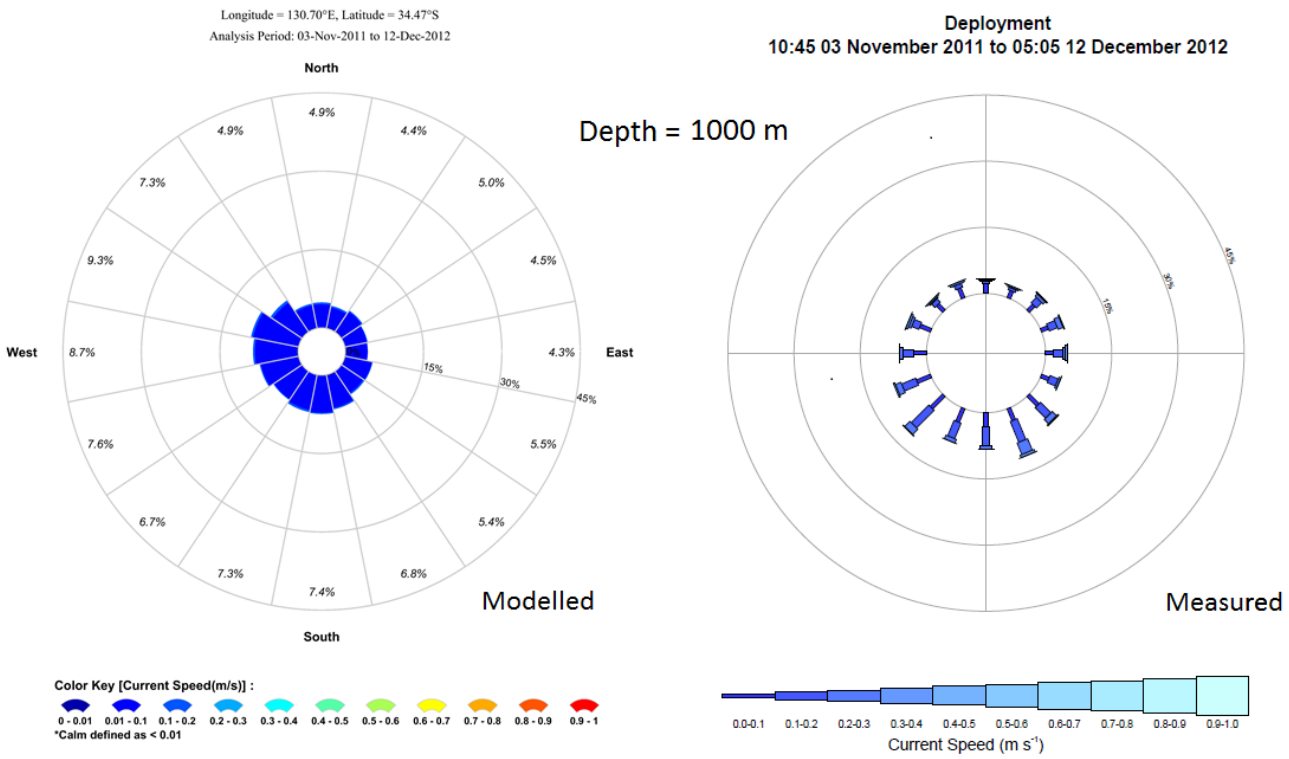

Figure 22: Modelled (left) and measured (right) current roses for depth layer of 1000 m at 340 28’ 30’’ S, 1300 42’ 5’’ E. Source of measured data: RPS MetOcean (2013)

4 WATER TEMPERATURE AND SALINITY

To accurately represent the water column temperature and salinity at the well, the monthly temperature and salinity values was obtained from the World Ocean Atlas 2013 database produced by the National Oceanographic Data Centre (National Oceanic and Atmospheric Administration) and its co-located World Data Centre for Oceanography (see Levitus et al., 2013).

The World Ocean Atlas 2013 is a set of objectively analysed (1° grid) fields of in situ parameters (e.g. temperature, salinity and dissolved oxygen) at standard depth levels for annual, seasonal, and monthly periods for the global oceans. The dataset represents the largest collection of restriction-free ocean profile data available internationally. Locarnini et al. (2013) and Zweng et al. (2013) discuss the temperature and salinity data as part of the World Ocean Atlas 2013 database.

Figure 23 shows the mean monthly temperature and salinity profiles from the adjacent data node (World Ocean Atlas 2013) to the model release location, which was used as input in the dispersion model.

Table 7 presents the annual temperature and salinity values adjacent to the release location as a function of depth.

Table 7: Annual water temperature and salinity profiles from the closest World Ocean Atlas 2013 data point closest to the release location. Source: World Ocean Atlas (2013)

Depth (m)	Annual mean water temperature (°C)	Annual mean salinity
0	16.96	35.49
10	16.91	35.49
50	16.27	35.47
75	15.23	35.41
100	14.38	35.38
250	12.34	35.13
500	9.21	34.67
1000	4.49	34.39
1250	3.17	34.47
1500	2.72	34.58

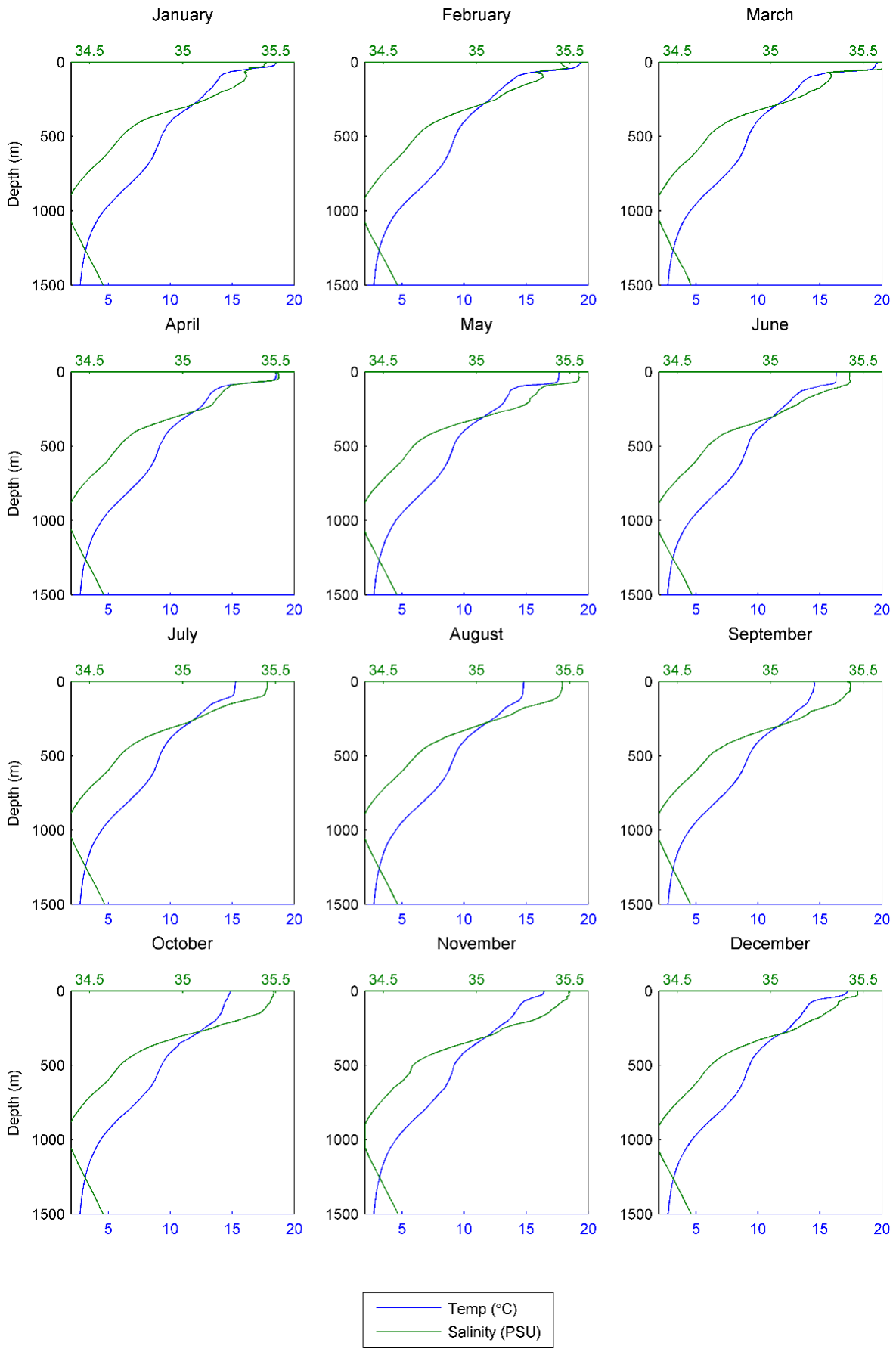

Figure 23: Monthly temperature (blue) and salinity (green) profiles from the closest World Ocean Atlas 2013 data point closest to the release location. Source: World Ocean Atlas (2013)

5 DISPERSION MODELLING METHODS

5.1 Sediment dispersion model description – MUDMAP

The MUDMAP model is a highly advanced three-dimensional plume model used by industry and regulators to aid in assessing the potential environmental effects from operational discharges such as drill cuttings, drilling muds and produced water. The MUDMAP model has been extensively validated and applied for discharge operations in coastal waters (e.g. Spaulding, 1994; King & McAllister, 1998; Burns et al., 1999). A document titled “A review of models in support of oil and gas exploration off the North Coast of British Columbia”, by the Institute of Ocean Sciences Fisheries and Oceans Canada (Foreman et al. 2005) stated that “for a drilling mud model, we feel that MUDMAP seems to be the best choice”.

The model itself is an enhancement of the Offshore Operators Committee (OOC) model and calculates the fates of discharges through three distinct stages (see Figure 24) as defined by laboratory and field studies (Koh & Chang, 1973; Khondaker, 2000):

- Stage 1: Convective descent - free fall of the combined mass of fluids and cuttings.
- Stage 2: Dynamic collapse stage - the collapse of the combined mass as it loses the initial jet related momentum and turbulence.
- Stage 3: Dispersion stage - the transport and dispersion of the discharged fluids and cuttings by the local currents. Dispersion of the discharged material will be enhanced with increased current speeds and water depth and with greater variation in current direction over time and depth.

Each stage plays an integral role at different temporal and spatial scales. The governing equations and solutions were built on the formulas originally developed by Koh & Chang (1973) and are extended by the work of Brands & Sauer (1983), known as the OOC model, for Stages 1 and 2 of plume motion.

The far-field calculation (passive dispersion stage), however, employs a particle-based, random walk procedure. The model predicts the dynamics of the discharge material and resulting sea floor concentrations and sediment thicknesses over the near field (i.e. the immediate area of the discharge) and the far-field (the wider region. Figure 24 shows a conceptual diagram of the dispersion and fates of cuttings and muds discharge to the ocean and the idealised representation of the three discharge phases.

Along with the advanced analyses tools, MUDMAP can simulate six classes of substances, each with its own density and particle size distribution. This means that the muds, cuttings, water and chemicals can be included in the near-field and far-field computations. The discharged material is represented by a large sample of Lagrangian particles (32,000). During the dispersion stage, the particles are transported in three-dimensions according to the current data and horizontal and vertical mixing coefficients at each time step according to the governing equations.

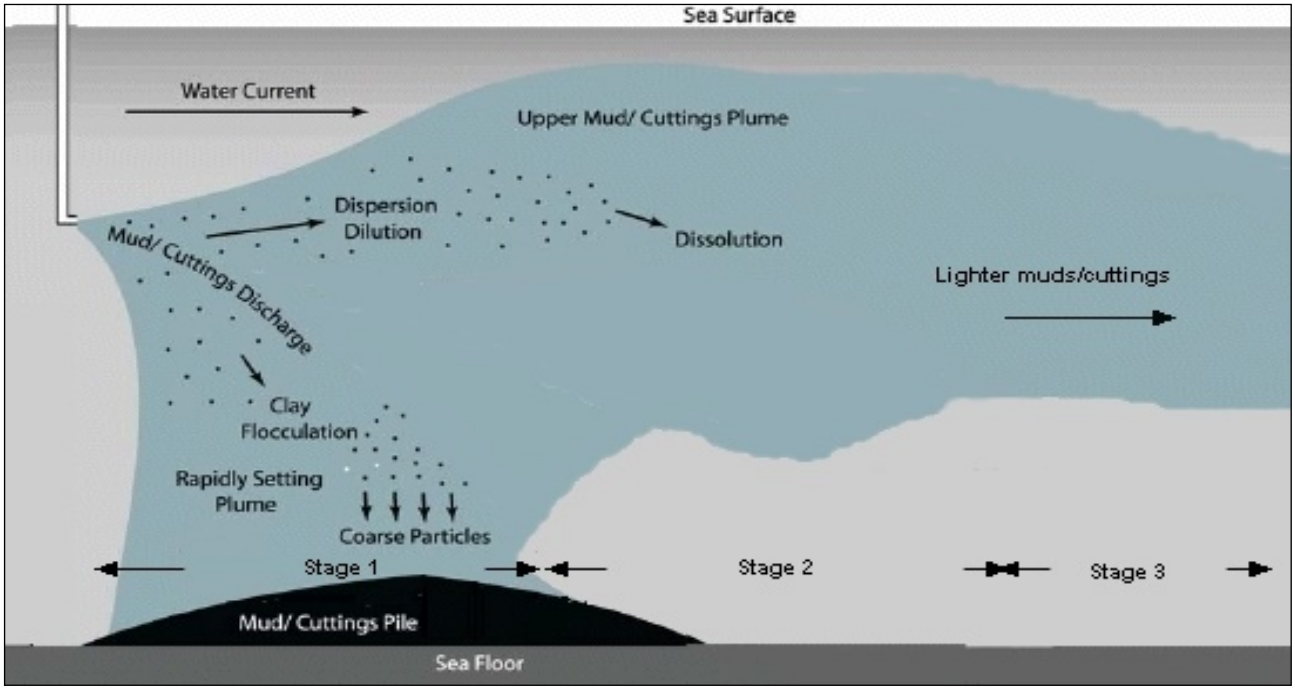

Figure 24: Conceptual diagram showing the general behaviour of cuttings and muds following the discharge to the ocean (Neff, 2005) and the idealised representation of the three discharge phases

5.2 Discharge program

The 42” conductor hole and the 26” surface hole intervals will be drilled using seawater and sweeps, while the two intermediate and bottom hole intervals (17.5”, 12.25” and 8.5”) will be drilled using synthetic based muds (SBM). Cuttings and adhered muds from the conductor and surface hole intervals will be returned directly to the sea floor. Cuttings and drilling muds from the two intermediate and bottom hole intervals will be brought to the platform through the riser, before being treated by solids control equipment to separate the drilling fluid from the cuttings. The cuttings and unrecoverable muds adhering to the cuttings will be discharged from a vertically orientated pipe 1 m below the sea surface.

Table 8 provides a summary of the estimated volumes of drill cuttings discharged for each well interval.

Table 8: Summary of the estimated volume of extracted drill cuttings and unrecoverable muds to be discharged

Bore diameter (inches)	Well interval	Discharge method	Cuttings		Muds		
			Volume discharged (m^3)	Type	Volume liquids and solids discharged (m^3)	Volume of solids discharged	
						%	m^3
42	Conductor	Returned directly to the sea floor	91.9	Sea water and sweeps	263.91	3.6	9.54
26	Surface hole	Returned directly to the sea floor	266.5	Sea water and sweeps	1193.96	3.1	37.04
17.5	Intermediate hole	Cuttings and SBM brought to drilling rig, then discharged to surface	203.4	SBM	12.72	17.5	2.23

Bore diameter (inches)	Well interval	Discharge method	Cuttings		Muds		
			Volume discharged (m^3)	Type	Volume liquids and solids discharged (m^3)	Volume of solids discharged	
						%	m^3
12.25	Intermediate hole	S Cuttings and SBM brought to drilling rig, then discharged to surface	69.0	SBM	3.02	7.9	0.24
8.5	Bottom hole	Cuttings and SBM brought to drilling rig, then discharged to surface	17.1	SBM	0.32	50	0.16
Total			**647.9**				**49.2**

SBM – synthetic based muds

5.2.1 Discharge input data

The input data used to setup the dispersion model included:

- Volume and discharge duration of the cuttings and unrecovered muds
- Particle size distribution and settling velocities of discharged cuttings and unrecoverable muds
- Bulk density of the discharged cuttings and unrecoverable muds
- Temperature and salinity profiles of the receiving waters
- Diameter and orientation of the discharge pipe
- Height/depth of the discharge point relative to mean sea level
- Depth-varying current data to represent local physical forcing.

Table 9 provides a summary of the discharge characteristics and the estimated volume of cuttings and muds used as input into the discharge model. The near-seabed discharges incorporated 358.4 m^3 of cuttings and 46.4 m^3 of muds. The model was run for an additional 1 day to allow the finer sediments to deposit on the sea floor. The sea surface discharges incorporated 289.5 m^3 of cuttings and 2.6 m^3 of adhered drilling muds. The model was run for long enough to allow finer cuttings and muds to settle out of suspension for surface discharges.

Table 9: Input data used for the drill cuttings and muds dispersion modelling

Parameter/description	Detail
Volume of cuttings discharged near the seabed (m^3)	358.4
Volume of drilling muds discharged near the seabed (m^3)	46.6
Volume of cuttings discharged near the sea surface (m^3)	289.5
Volume of drilling muds discharged near the sea surface (m^3)	2.6
Total volume of cuttings discharged (m^3)	647.9
Total volume of drilling muds discharged (m^3)	49.2
Density of cuttings (kg/ m^3)	2600
Density of drilling muds (kg/ m^3)	4200
Height of near-seabed discharge above seabed (m)	2

Parameter/description	Detail
Depth of sea surface discharges below sea surface (m)	1
Sea surface discharge pipe orientation	Vertically downward

It is proposed that conventional drilling methods will be used, so the particle size distributions for cuttings and drilling muds were represented by literature data for conventional drilling which suggest particle sizes would be expected to vary between 0.016 mm and 6 mm in diameter. The model was set up with four main particle classes to represent large, medium and light cuttings, and drilling fluid solids (i.e. mud particles). The proportion of each size class was adjusted for each well interval according to the proposed proportion of muds and cuttings, as shown in Table 10.

It is worth noting that particle size has a greater influence on the rate of settling than density (Neff, 2005). Therefore, when setting up the material for discharge in the model, each particle size class was distributed across up to six sub-categories with specific settling velocities. The settling velocities for the various size sub-categories were derived from empirical data provided by Dyer (1986), as summarised in Table 10.

Table 10: Grain sizes, settling velocities and percentage distributions for the cuttings and muds

Class	Grain size (mm)	Settling velocity (cm/s)	Drilling with sea water and sweeps Distribution (%)	Drilling with SBM Distribution (%)
Large cuttings	**6**	**53.62**	**8.6**	**8.2**
	5	49.46	8.6	8.2
	2	28.55	8.6	8.3
	1	12.73	5.8	5.5
	0.5	7.5	5.8	5.5
	0.45	6.6	2.9	2.8
Medium cuttings	0.4	6	2.9	2.8
	0.35	5	2.8	2.8
	0.3	4	2.8	2.8
	0.25	3.1	2.8	2.8
	0.2	2.3	2.8	2.8
	0.15	1.6	2.8	2.7
Small cuttings	0.1	0.8	2.8	2.7
	0.05	0.22	2.8	2.7
	0.04	0.15	2.9	2.7
	0.03	0.08	2.9	5.5
	0.02	0.04	2.9	0.0
Drilling fluid solids	0.063	0.34	0.4	0.0
	0.05	0.22	1.6	1.8
	0.035	0.11	3.7	4.1
	0.026	0.06	6.0	25.3
	0.02	0.038	7.4	0.0
	0.016	0.026	9.4	0.0

5.3 Grid configuration

A uniform sized rectangular grid covering a 10 km (longitude, x-direction) by 10 km (latitude, y-direction) region around the well location was employed to calculate the concentration of drill cuttings and muds in the water column and on the sea floor. The resolution of each grid cell was approximately 10 m (x) x 10 m (y) x 1 m (z).

5.4 Mixing parameters

The horizontal and vertical dispersion coefficients are used in dispersion modelling to represent the mixing and diffusion processes caused by turbulence, which are sub-grid processes at the scale of the hydrodynamic model drivers. The dispersion coefficients are expressed in units of rate of area change (m^2/s). Increasing the horizontal dispersion coefficient will increase the horizontal spread of the discharge plume and decrease the centreline concentrations. Increasing the vertical dispersion coefficient spreads the discharge further across the vertical layers.

The horizontal turbulent diffusion of the plume is dependent on the hydrodynamic conditions (i.e. wind, wave and current) and the physical scale of the plume compared to the scales of the oceanic processes that disperse the plume. For a plume of approximately 10-100 m width, dispersion occurs primarily through small-scale horizontal swirling motions and vertical mixing, with a horizontal dispersion rate of the order of 0.1 m^2/s. As the plume grows to a scale of 1-10 km, it begins to be subject to mesoscale eddies and horizontal dispersion rate becomes of the order of a few to tens of m^2/s. At even larger scales, the plume would be larger than the mesoscale eddies and eddy mixing becomes the dominant mechanism, with a rate of horizontal dispersion of 100-1000 m^2/s.

For this project, with an open ocean environment and length scales of 10 m to 1 km, a horizontal diffusion rate of 0.25 m^2/s was applied. A value of 0.10 cm^2/s was set for the vertical dispersion coefficient to account for the influence of turbulence within the water column, as well as wave-induced.

5.5 Minimum reporting thresholds

The MUDMAP model can track and predict sediment concentrations and thickness to very low levels that may not be of ecological significance; therefore, biologically-relevant thresholds were selected for reporting the modelling outcomes.

A study by Rogers (1990) reported that a sedimentation rate of 1 $mg/cm^2/day$ resulted in no effect or minimal effect to benthic communities. Based on the combined cuttings and muds density of approximately 2700 kg/m^3, this sedimentation rate is equivalent to 1.35 mm/year. Therefore, as a conservative measure, a thickness of 0.05 mm was employed as a minimum reporting threshold.

Based on available literature, thresholds of 1-10 mm and above 10 mm were used to define low and high exposure, respectively, in this study. In addition, Trannum et al. (2009) reported a significant decrease in species count, abundance of individuals, Shannon-Wiener diversity, and biomass of marine animals with increasing depth of deposited cuttings (3-24 mm). Furthermore, a study by Kjeilen-Eilertsen et al. (2004) reports that depositional thicknesses greater than 9.6 mm are likely to cause smothering impacts on benthic ecosystems, including corals. It is also worth noting that a study by Smit et al. (2008) established that a thickness threshold of greater than 6.5 mm would be needed before potential harm to benthic macrofauna occur. Assuming newly settled cuttings and drilling muds will be less compact due to incorporation of water between grains of sediment deposits a bulking factor of 2.5 was applied to the reported thicknesses to account for inter-particle voids.

In addition, the minimum reporting threshold for TSS concentrations used for this study is 5 mg/L. Nelson et al. (2016) reports <10 mg/L as a minimal or no effect, whilst concentrations above 10 mg/L have a sublethal effect to pelagic biota. Furthermore, IOGP (2016) cite that very high concentrations (>1830 mg/L) of TSS has been shown to result in mortality of pelagic biota. Hence, threshold ranges of 10-1830 mg/L and above 1830 mg/L were used to define low and high exposure, respectively.

Table 11: Reporting thresholds for sediment thickness and TSS concentrations for the drill cuttings and muds discharge modelling

Reporting criteria	Sediment thickness (mm)	Total suspended solids concentration (mg/L)
Minimum reporting threshold	0.05	5
Low exposure	1–10	10 – 1830
High exposure	Above 10	Above 1830

6 RESULTS

Predicted sediment thickness results are presented in Section 6.2. Section 6.2.1 presents the predicted sediment thickness based on the monthly results for 2010, 2011 and 2012 modelled years. Section 6.2.2 presents the integration of all model results to assess the overall potential extent.

Section 6.3 presents the maximum TSS concentrations within the 0- 100 m water depth layer. Section 6.3.1 presents the integration of all model results to assess the overall potential extent of maximum TSS concentrations within the 0 – 100 m water depth layer.

6.1 Presentation of model results

Predicted sediment thickness results are presented in Section 6.2. Section 6.2.1 presents the predicted sediment thickness based on the monthly results for 2010, 2011 and 2012 modelled years. Section 6.2.2 presents the integration of all model results to assess the overall potential extent.

Section 6.3 presents the maximum TSS concentrations within the 0- 100 m water depth layer. Section 6.3.1 presents the integration of all model results to assess the overall potential extent of maximum TSS concentrations within the 0 – 100 m water depth layer.

6.2 Sediment thickness

6.2.1 Combined discharges for each month

Figure 25 to Figure 60 shows the coverage and sediment thickness of cuttings and unrecoverable drilling muds on the sea floor if the operation commenced on the 1st of each calendar month during 2010, 2011 and 2012, respectively.

Table 12 presents the predicted maximum sediment thickness, total area of coverage of deposited cuttings and muds above the minimum reporting threshold and low exposure thresholds. In addition, Table 13 presents the minimum distance from the deposited material above the minimum reporting threshold to Anna's Pimple and Murray's Mount.

The maximum sediment thickness (or height of mound) on the sea floor, for any month modelled, ranged between 1690 mm (September 2010) and 4036 mm (May 2012). The maximum heights were predicted to generally occur within 50 m from the release location.

The predicted area of coverage above the minimum reporting threshold varied from 3.13 km^2 to 3.87 km^2 under December and February 2011 current conditions, respectively. The maximum total area above the low threshold was 0.21 km^2 (May 2011).

No cuttings and muds were predicted to deposit on, or in the vicinity of, Anna's Pimple or Murray's Mount under any month modelled during the 2010, 2011 and 2012 current conditions. The minimum distance from the deposited material above the minimum reporting threshold to Anna's Pimple and Murray's Mount was 16.0 km and 19.9 km, respectively, during July 2011 conditions.

Table 12: Predicted maximum sediment thickness and total area of coverage of deposited cuttings and muds above the minimum reporting threshold (0.05 mm) and low exposure thresholds (1 mm). Results are based on the combined near-seabed and sea surface discharges initiated at the start of each month during 2010, 2011 and 2012

Month	Maximum thickness (mm)			Area (km^2) above minimum reporting threshold of 0.05 mm			Area (km^2) above low threshold of 1 mm		
	2010	2011	2012	2010	2011	2012	2010	2011	2012
January	3088	2344	2503	3.26	3.44	3.58	0.08	0.11	0.13
February	1897	1741	2770	3.74	3.87	3.81	0.14	0.14	0.11
March	2861	2423	1762	3.62	3.40	3.74	0.16	0.11	0.11

Month	Maximum thickness (mm)			Area (km^2) above minimum reporting threshold of 0.05 mm			Area (km^2) above low threshold of 1 mm		
	2010	2011	2012	2010	2011	2012	2010	2011	2012
April	1814	2838	3059	3.37	3.35	3.74	0.17	0.12	0.11
May	2300	3865	4036	3.41	3.38	3.32	0.17	0.21	0.12
June	3052	3787	2271	3.25	3.27	3.15	0.14	0.15	0.14
July	3374	2597	2679	3.17	3.79	3.19	0.18	0.13	0.16
August	3461	2064	2981	3.29	3.82	3.79	0.16	0.12	0.12
September	1690	2444	2017	3.29	3.82	3.79	0.09	0.14	0.09
October	2686	2158	2000	3.83	3.64	3.75	0.11	0.12	0.10
November	3952	2623	1745	3.21	3.41	3.41	0.15	0.14	0.17
December	3580	1727	1947	3.47	3.13	3.21	0.13	0.15	0.17
Minimum	**1690**	**1727**	**1745**	**3.17**	**3.13**	**3.15**	**0.08**	**0.11**	**0.09**
Maximum	**3952**	**3865**	**4036**	**3.83**	**3.87**	**3.81**	**0.18**	**0.21**	**0.17**

Table 13: Predicted minimum distance from deposited material above the minimum reporting threshold (0.05 mm) to Anna's Pimple and Murray's Mount resulting from the combined discharge of cuttings and muds from the combined near-seabed and sea surface discharges. Results are presented for model simulations initiated at the start of each month 2010, 2011 and 2012

Month	Minimum distance (km) from Anna's Pimple to deposited material above the minimum reporting threshold			Minimum distance (km) from Murray's Mount to deposited material above the minimum reporting threshold		
	2010	2011	2012	2010	2011	2012
January	18.9	19.3	18.8	22.3	22.7	23.4
February	18.6	19.8	18.8	22.2	23.5	22.7
March	17.4	17.4	18.8	20.9	21.1	22.7
April	18.5	18.6	18.1	22.7	22.5	22.0
May	19.9	17.0	17.9	23.8	20.9	21.9
June	18.3	18.1	18.0	22.1	22.0	21.8
July	18.1	16.0	17.7	22.0	19.9	21.6
August	18.9	19.7	17.9	22.7	23.8	21.7
September	19.2	19.7	18.8	22.7	22.9	22.5
October	17.8	16.5	18.9	22.1	19.9	22.6
November	16.4	19.9	18.9	20.2	23.7	22.7
December	19.1	20.8	18.3	22.8	24.5	22.0
Minimum	**16.4**	**16.0**	**17.7**	**20.2**	**19.9**	**21.6**
Maximum	**19.9**	**20.8**	**18.9**	**23.8**	**24.5**	**23.4**

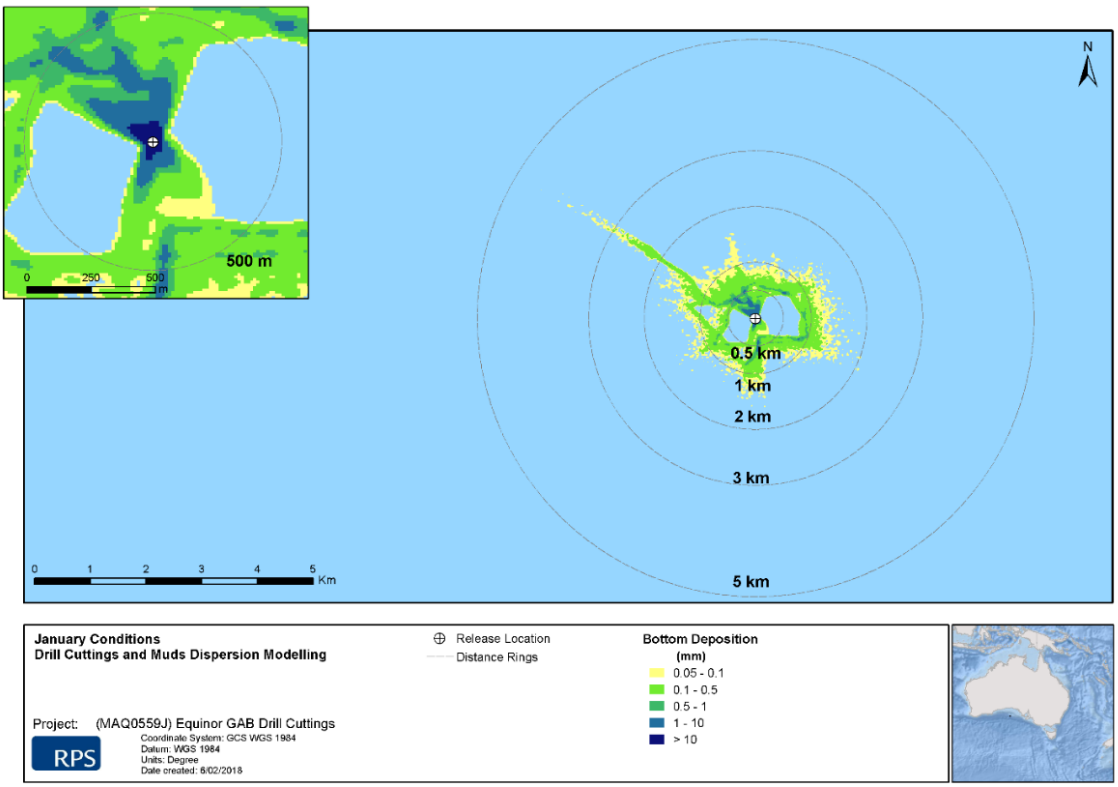

Figure 25: Predicted coverage and sediment thickness from the discharge of drill cuttings and unrecoverable drilling muds on the sea floor if the operation commenced 1st January 2010

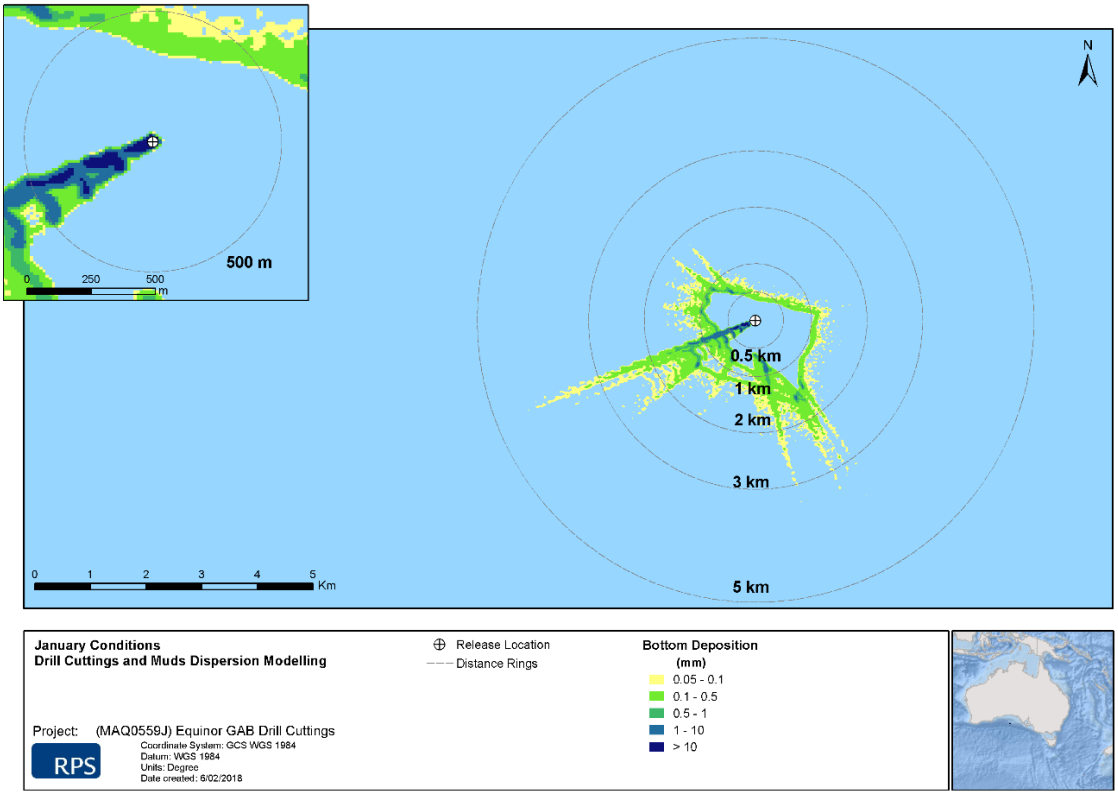

Figure 26: Predicted coverage and sediment thickness from the discharge of drill cuttings and unrecoverable drilling muds on the sea floor if the operation commenced 1st January 2011

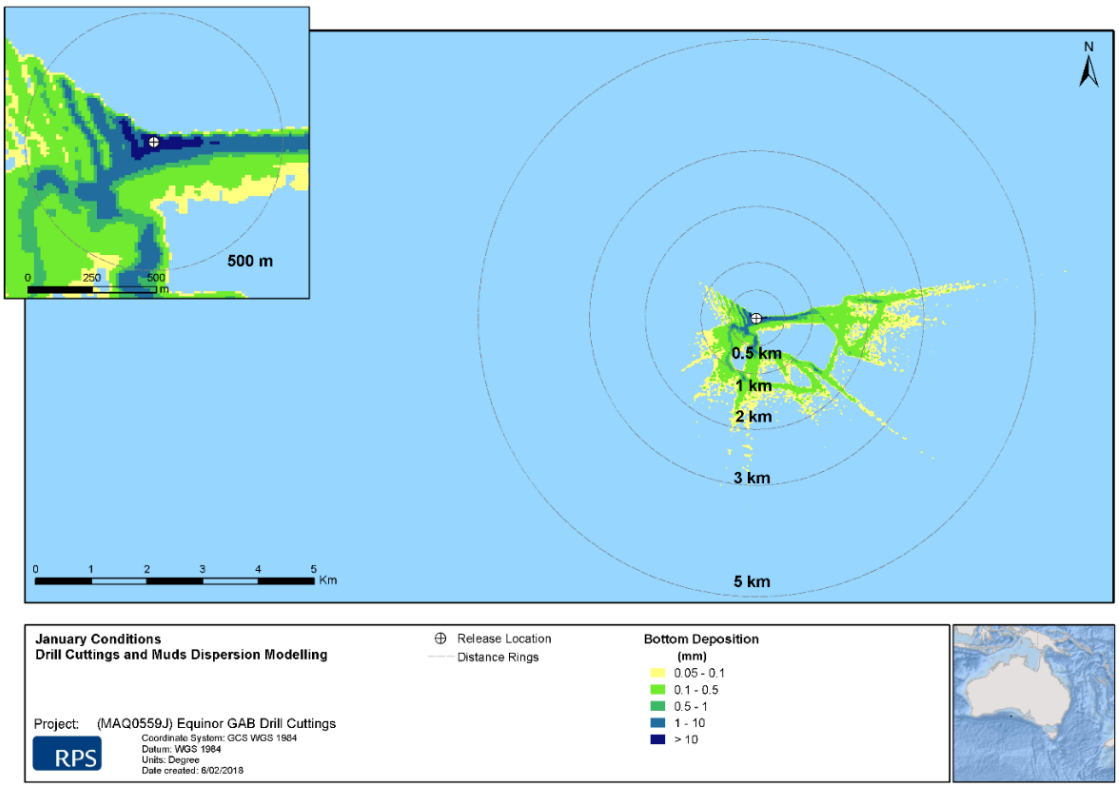

Figure 27: Predicted coverage and sediment thickness from the discharge of drill cuttings and unrecoverable drilling muds on the sea floor if the operation commenced 1st January 2012

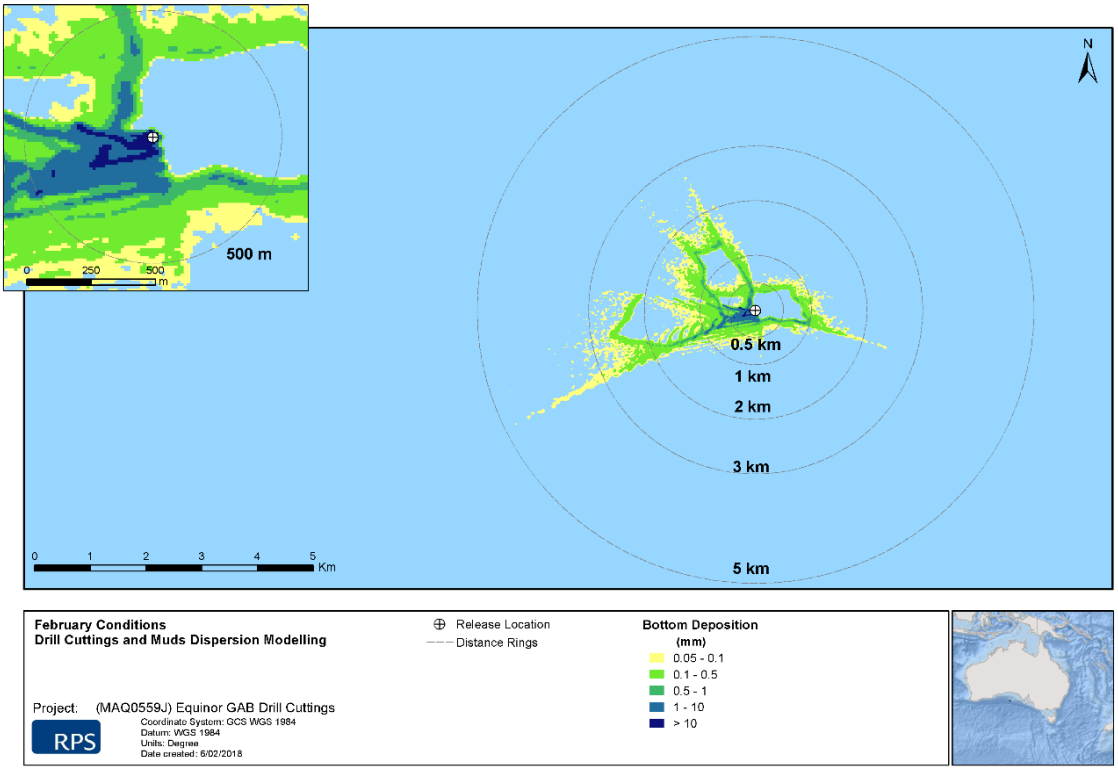

Figure 28: Predicted coverage and sediment thickness from the discharge of drill cuttings and unrecoverable drilling muds on the sea floor if the operation commenced 1st February 2010

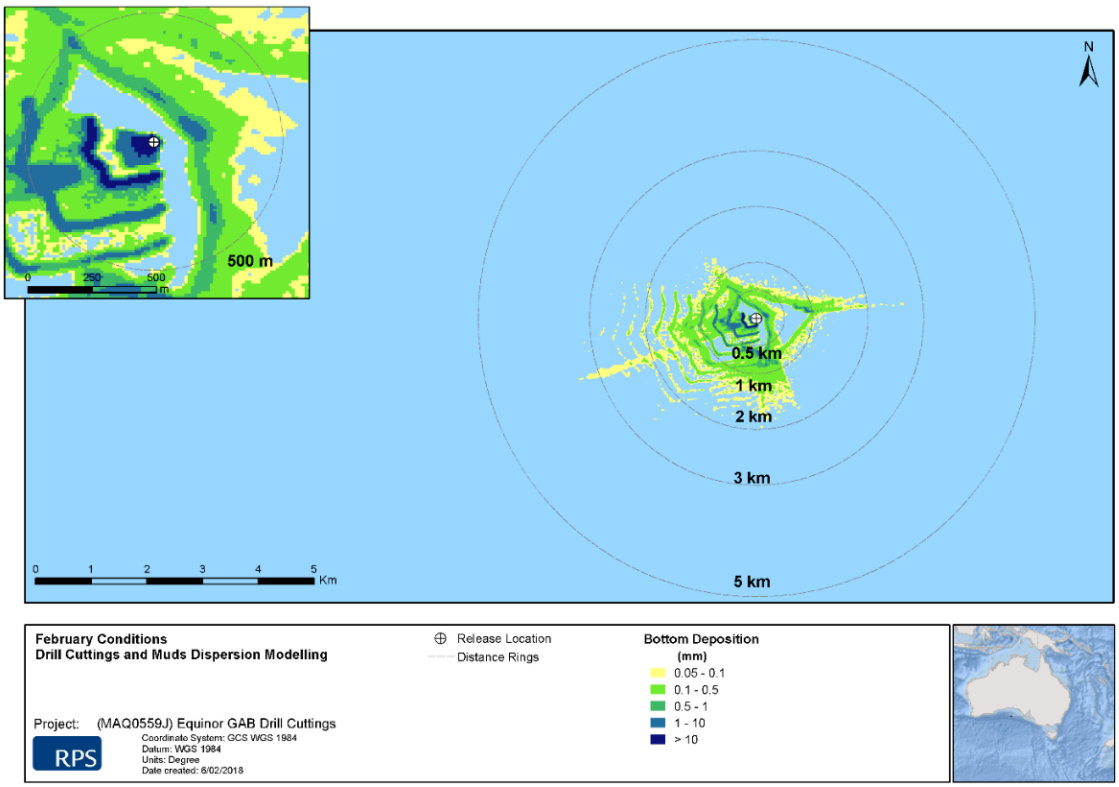

Figure 29: Predicted coverage and sediment thickness from the discharge of drill cuttings and unrecoverable drilling muds on the sea floor if the operation commenced 1st February 2011

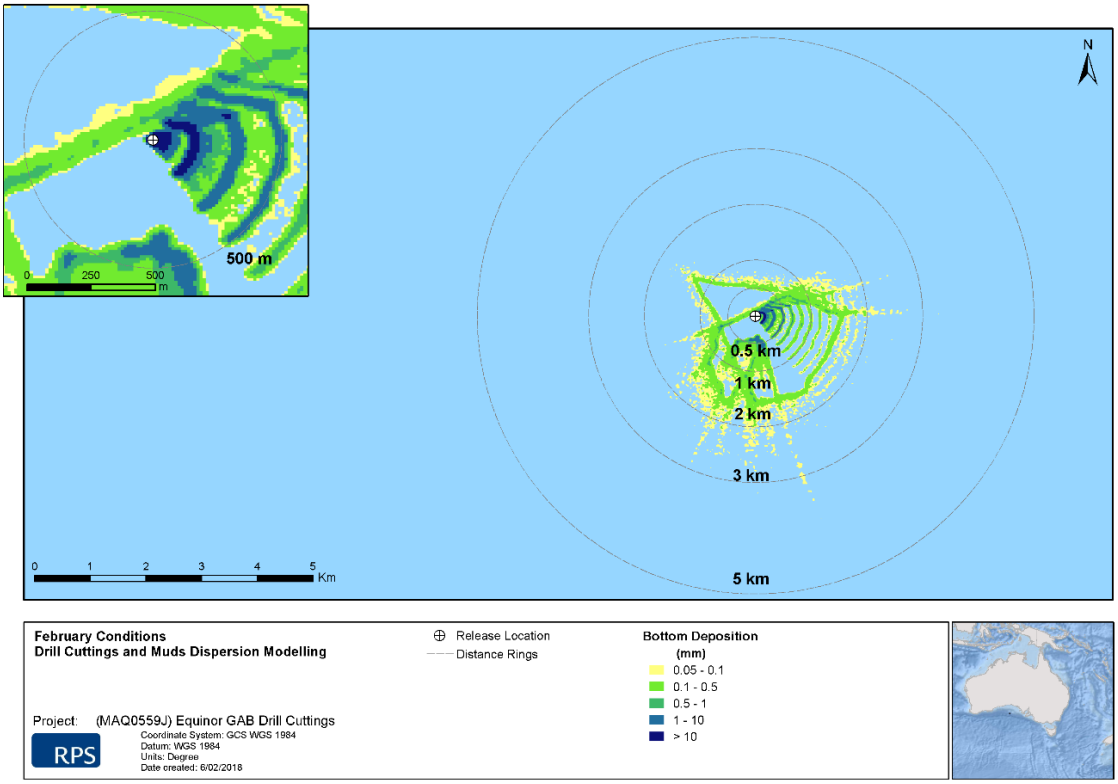

Figure 30: Predicted coverage and sediment thickness from the discharge of drill cuttings and unrecoverable drilling muds on the sea floor if the operation commenced 1st February 2012

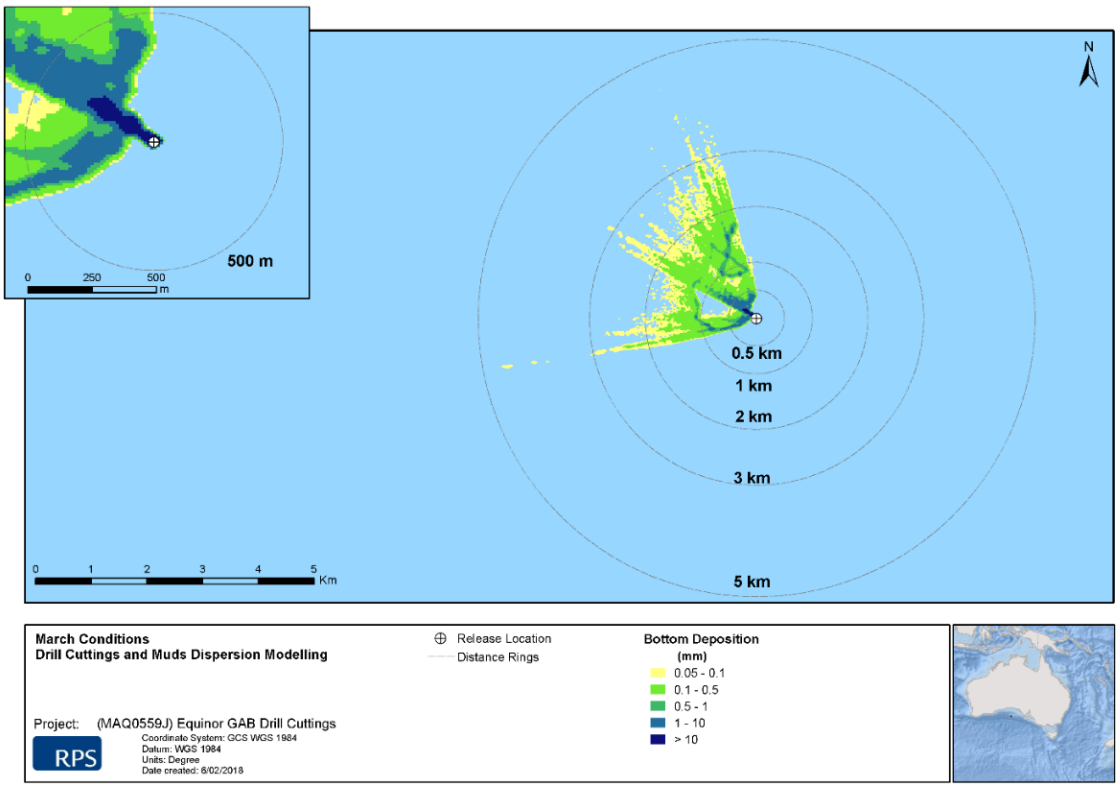

Figure 31: Predicted coverage and sediment thickness from the discharge of drill cuttings and unrecoverable drilling muds on the sea floor if the operation commenced 1st March 2010

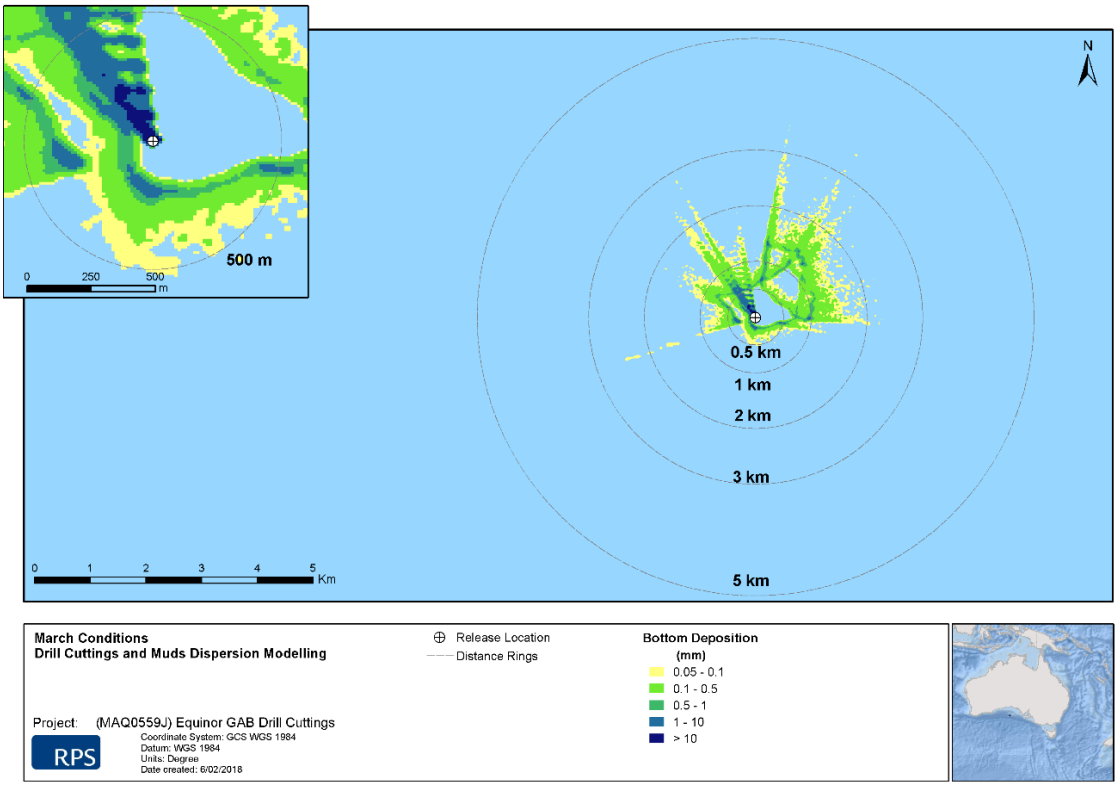

Figure 32: Predicted coverage and sediment thickness from the discharge of drill cuttings and unrecoverable drilling muds on the sea floor if the operation commenced 1st March 2011

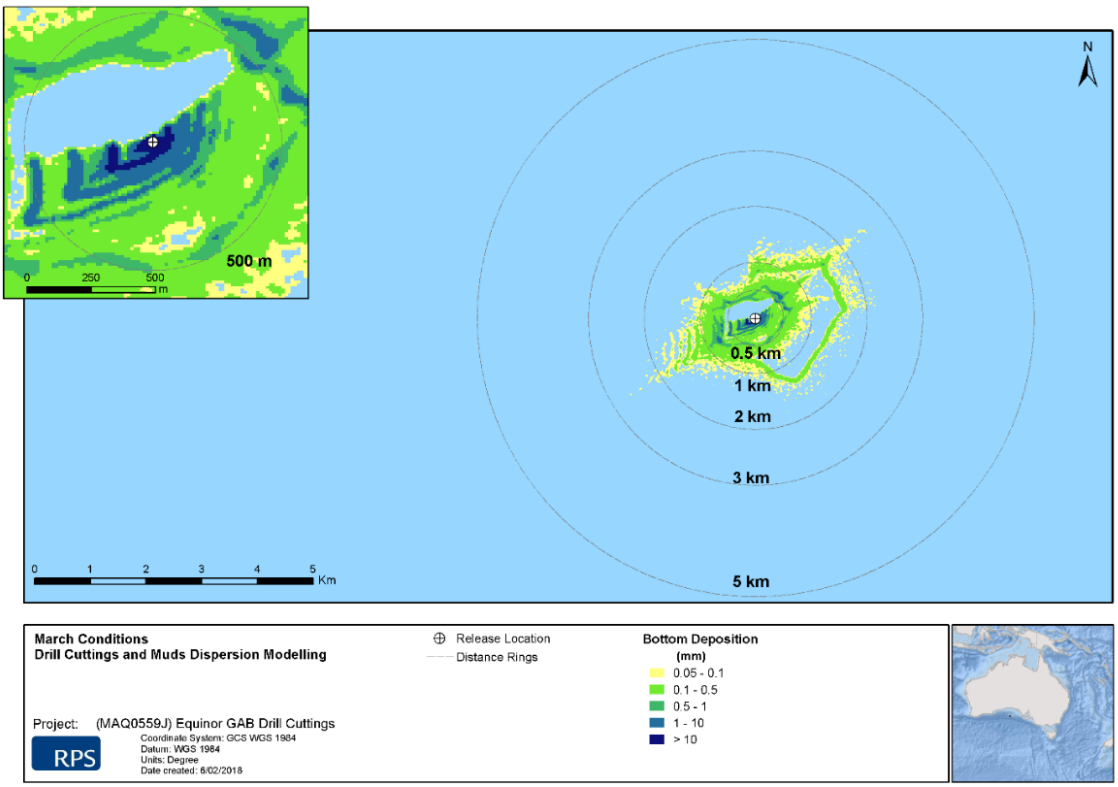

Figure 33: Predicted coverage and sediment thickness from the discharge of drill cuttings and unrecoverable drilling muds on the sea floor if the operation commenced 1st March 2012

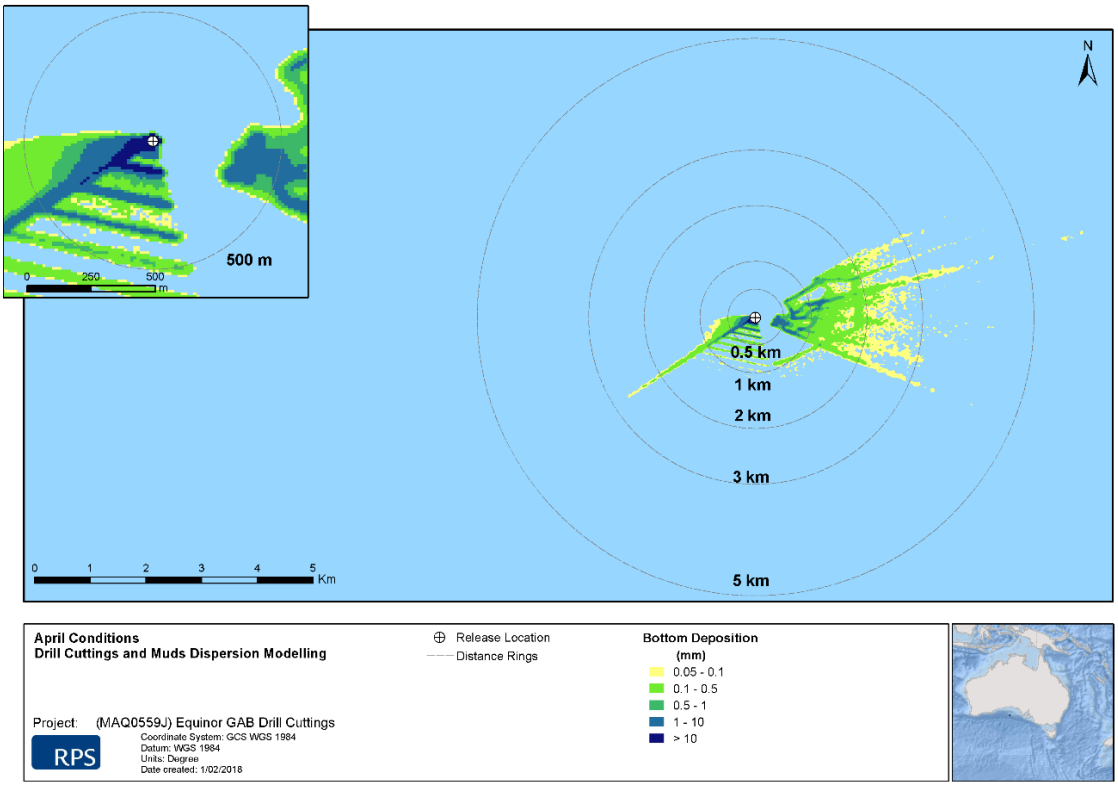

Figure 34: Predicted coverage and sediment thickness from the discharge of drill cuttings and unrecoverable drilling muds on the sea floor if the operation commenced 1st April 2010

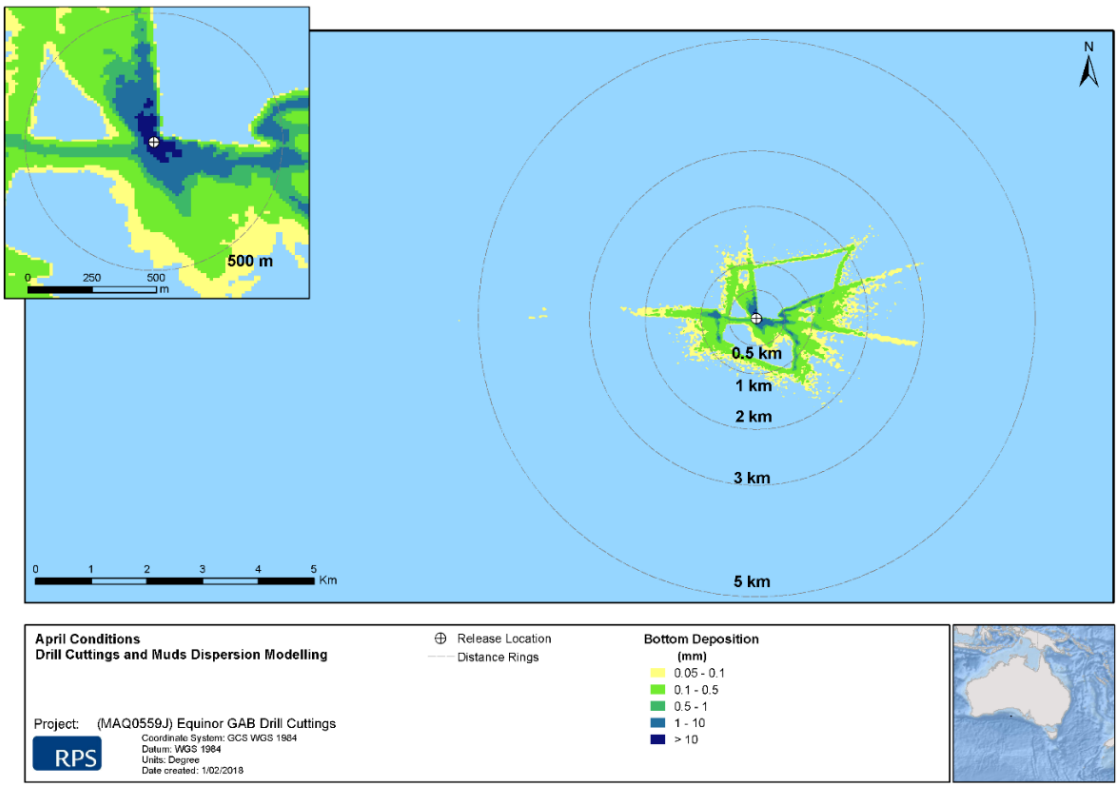

Figure 35: Predicted coverage and sediment thickness from the discharge of drill cuttings and unrecoverable drilling muds on the sea floor if the operation commenced 1st April 2011

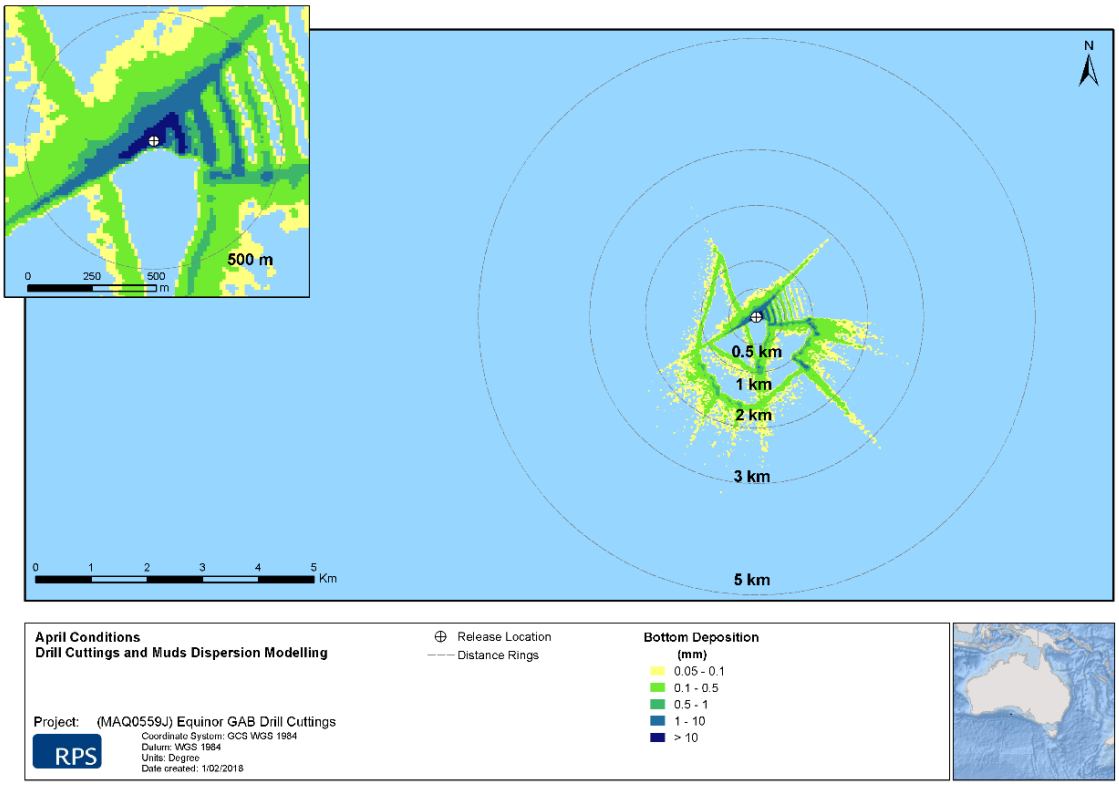

Figure 36: Predicted coverage and sediment thickness from the discharge of drill cuttings and unrecoverable drilling muds on the sea floor if the operation commenced 1st April 2012

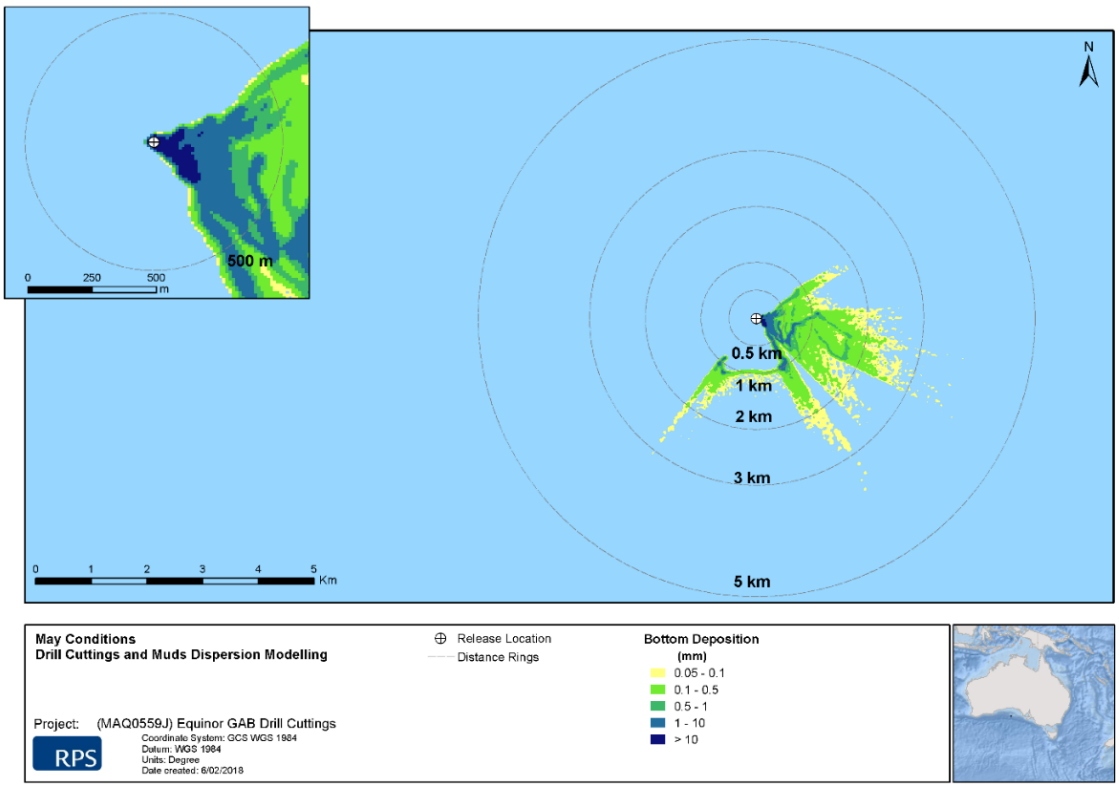

Figure 37: Predicted coverage and sediment thickness from the discharge of drill cuttings and unrecoverable drilling muds on the sea floor if the operation commenced 1st May 2010

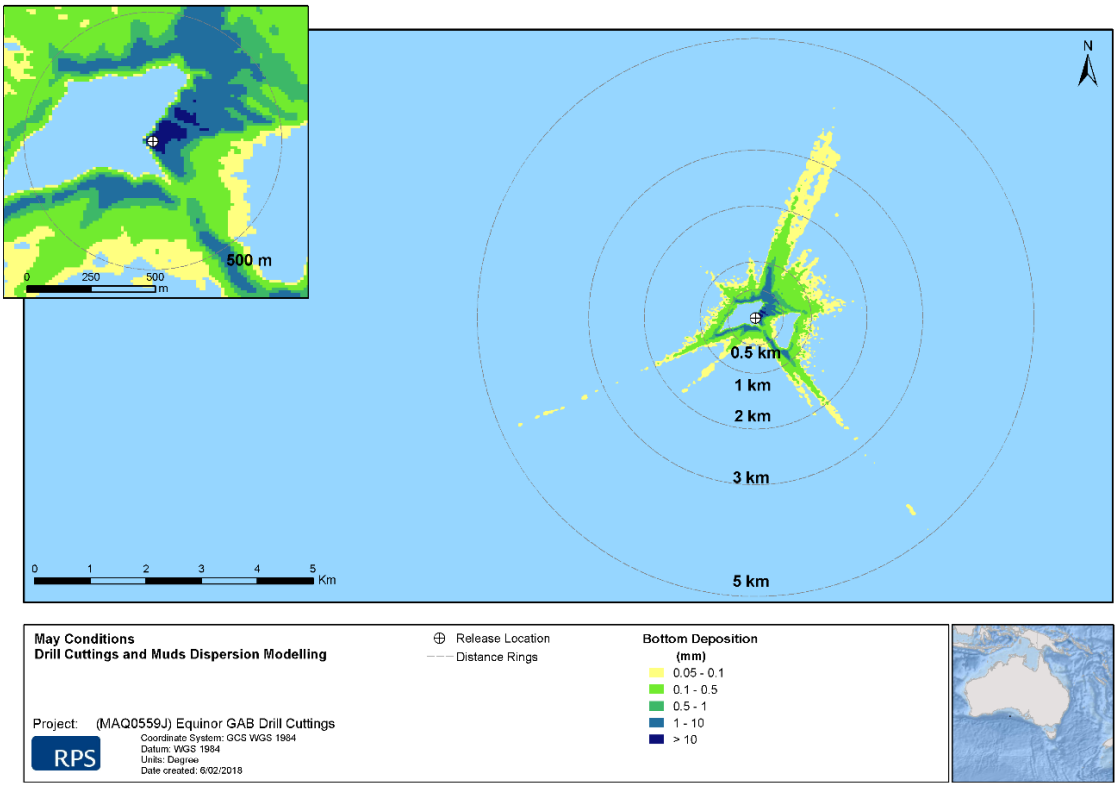

Figure 38: Predicted coverage and sediment thickness from the discharge of drill cuttings and unrecoverable drilling muds on the sea floor if the operation commenced 1st May 2011

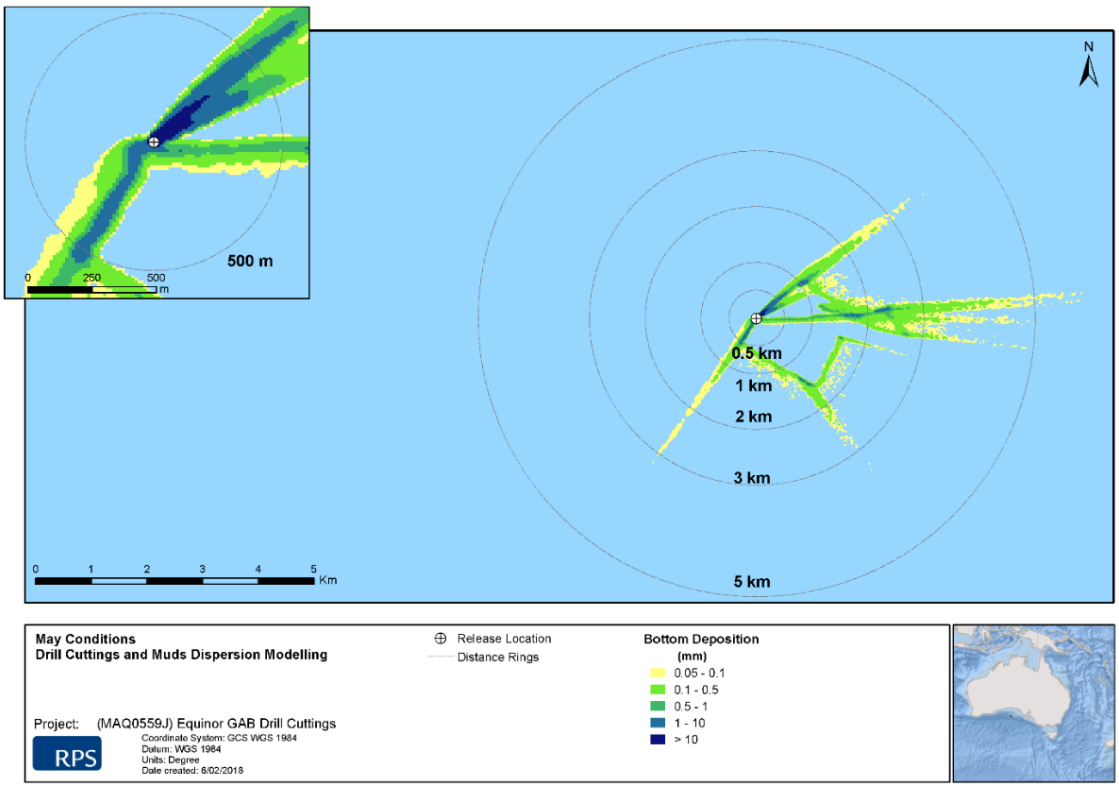

Figure 39: Predicted coverage and sediment thickness from the discharge of drill cuttings and unrecoverable drilling muds on the sea floor if the operation commenced 1st May 2012

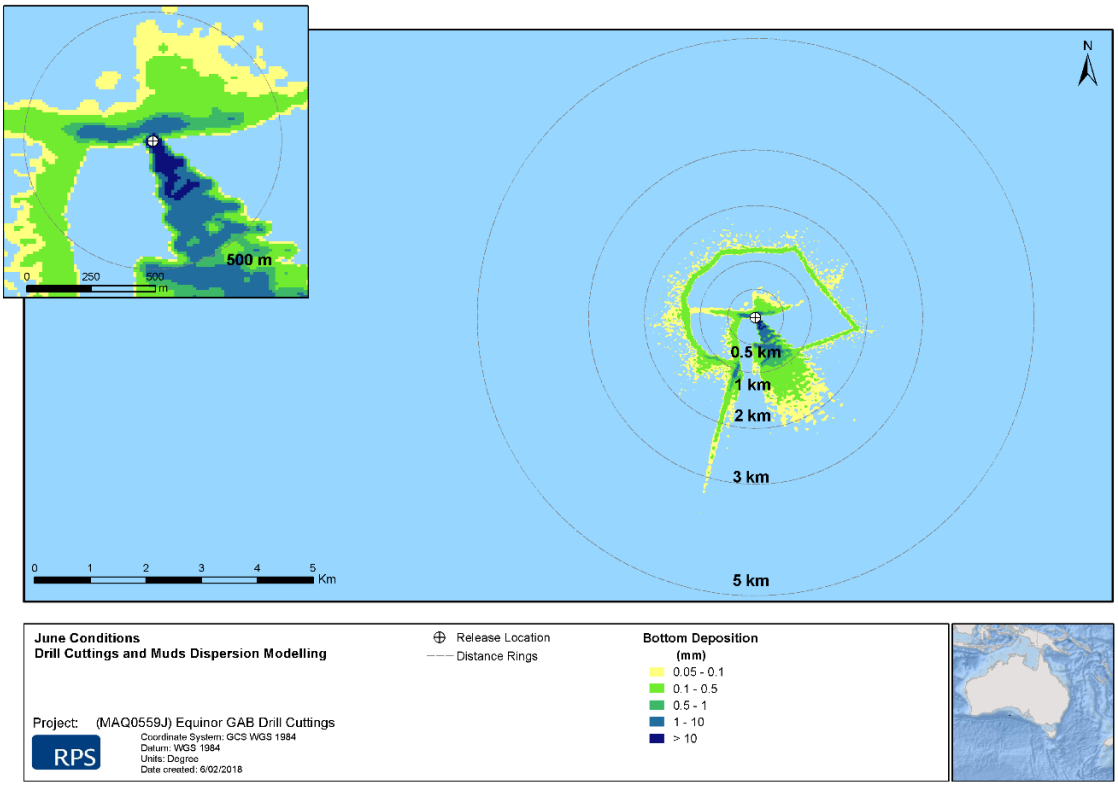

Figure 40: Predicted coverage and sediment thickness from the discharge of drill cuttings and unrecoverable drilling muds on the sea floor if the operation commenced 1st June 2010

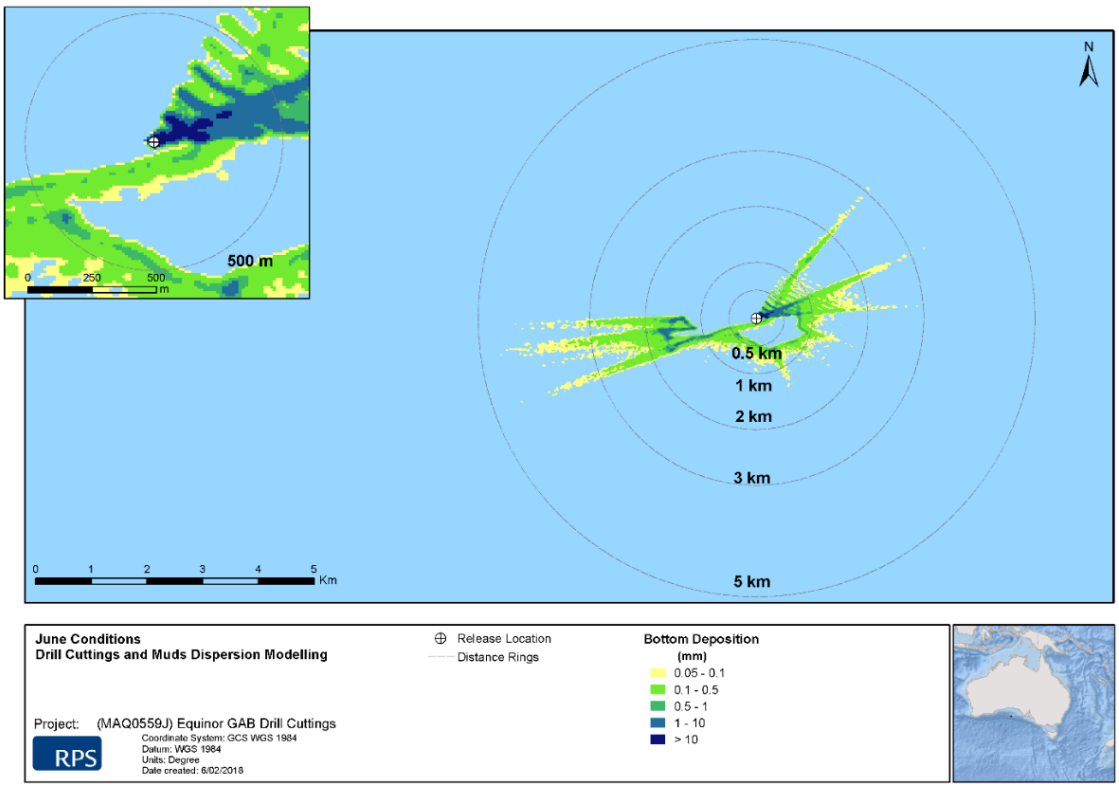

Figure 41: Predicted coverage and sediment thickness from the discharge of drill cuttings and unrecoverable drilling muds on the sea floor if the operation commenced 1st June 2011

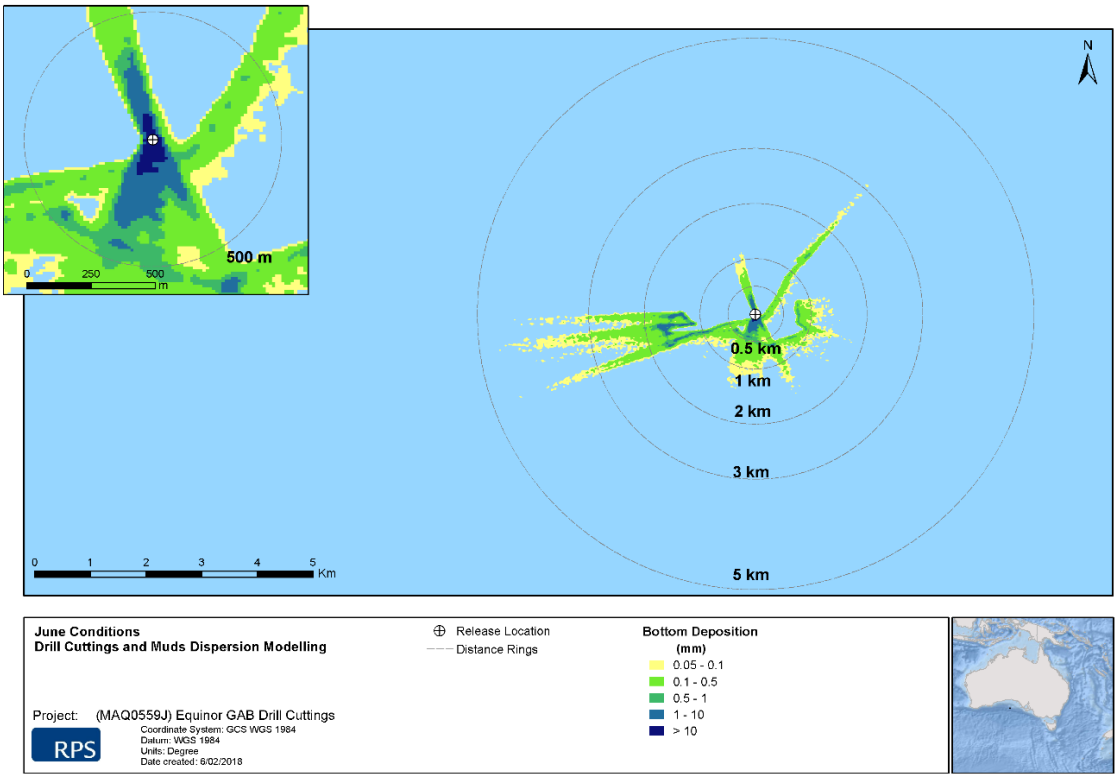

Figure 42: Predicted coverage and sediment thickness from the discharge of drill cuttings and unrecoverable drilling muds on the sea floor if the operation commenced 1st June 2012

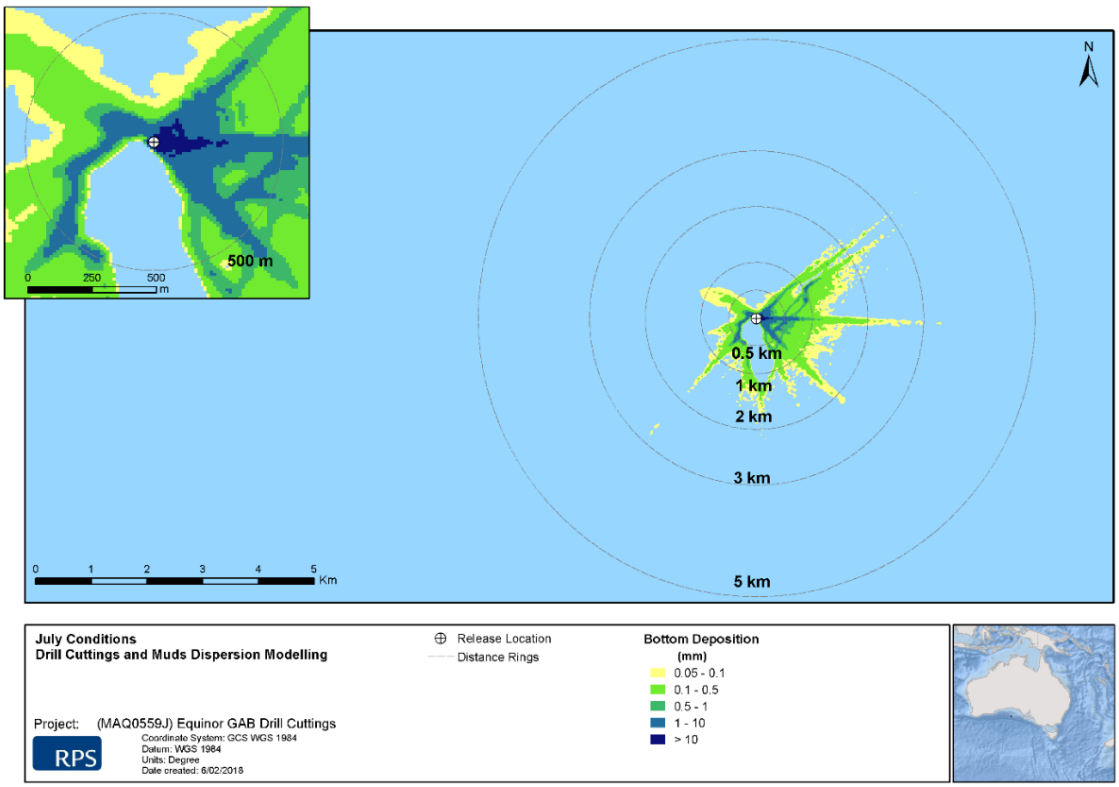

Figure 43: Predicted coverage and sediment thickness from the discharge of drill cuttings and unrecoverable drilling muds on the sea floor if the operation commenced 1st July 2010

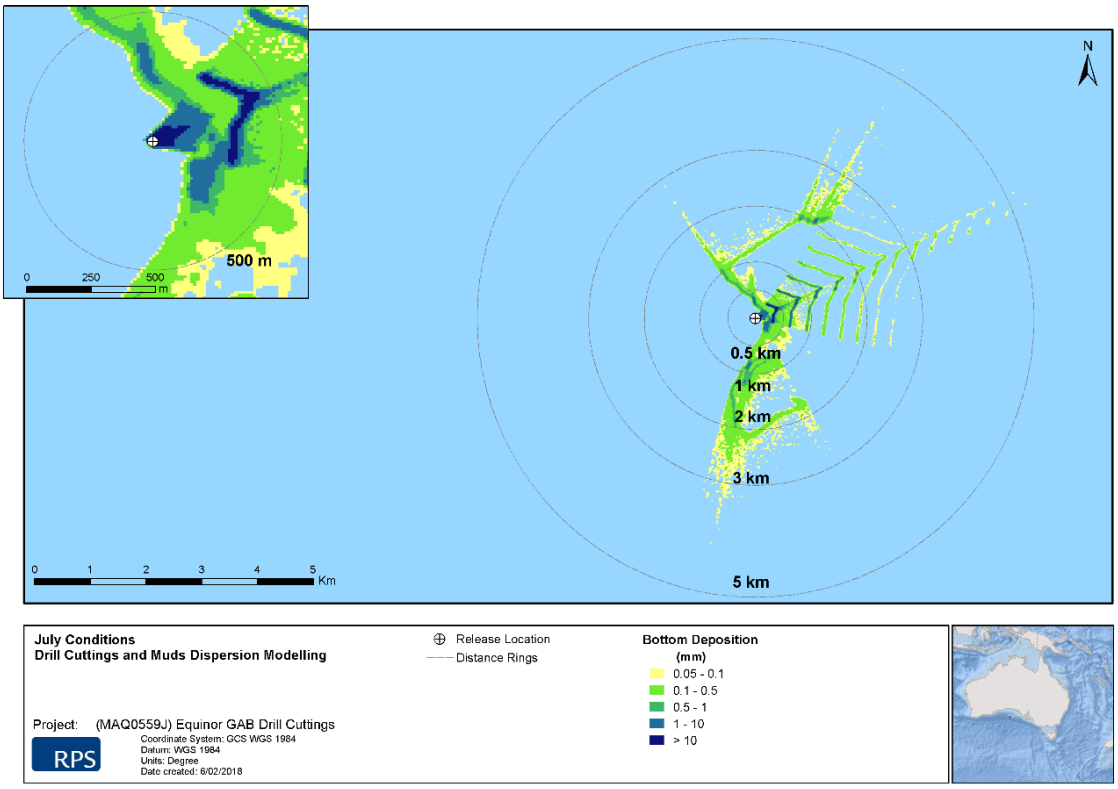

Figure 44: Predicted coverage and sediment thickness from the discharge of drill cuttings and unrecoverable drilling muds on the sea floor if the operation commenced 1st July 2011

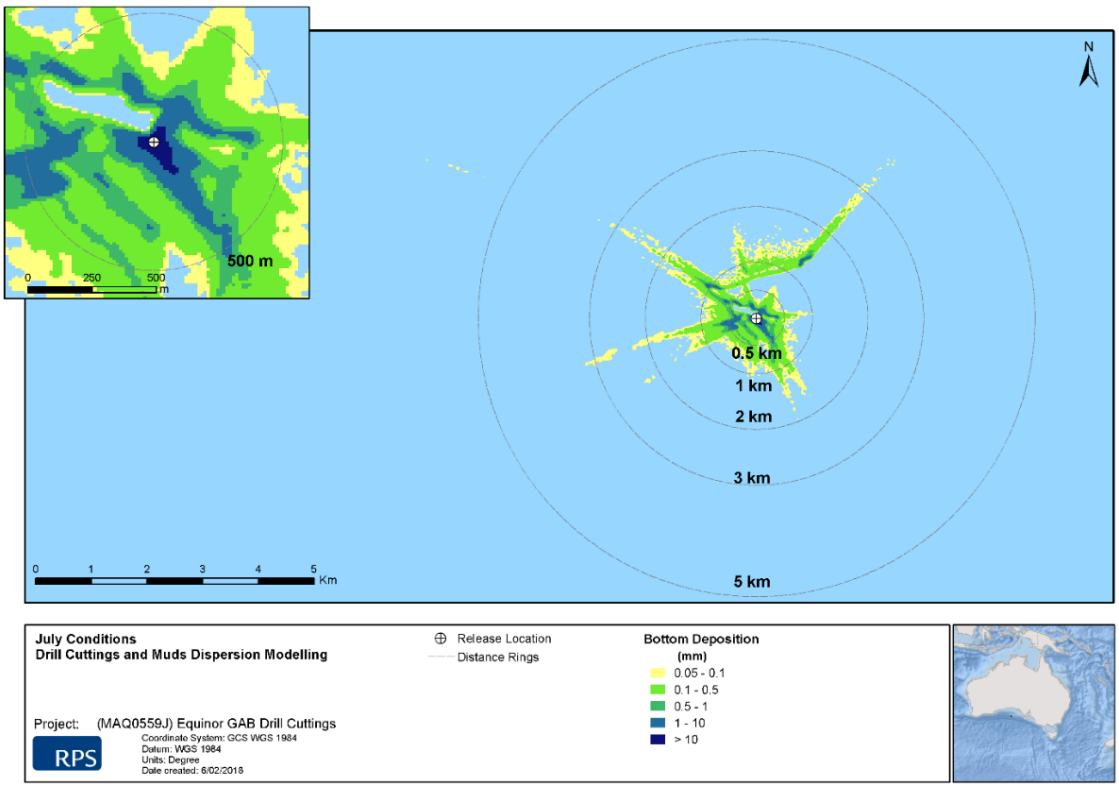

Figure 45: Predicted coverage and sediment thickness from the discharge of drill cuttings and unrecoverable drilling muds on the sea floor if the operation commenced 1st July 2012

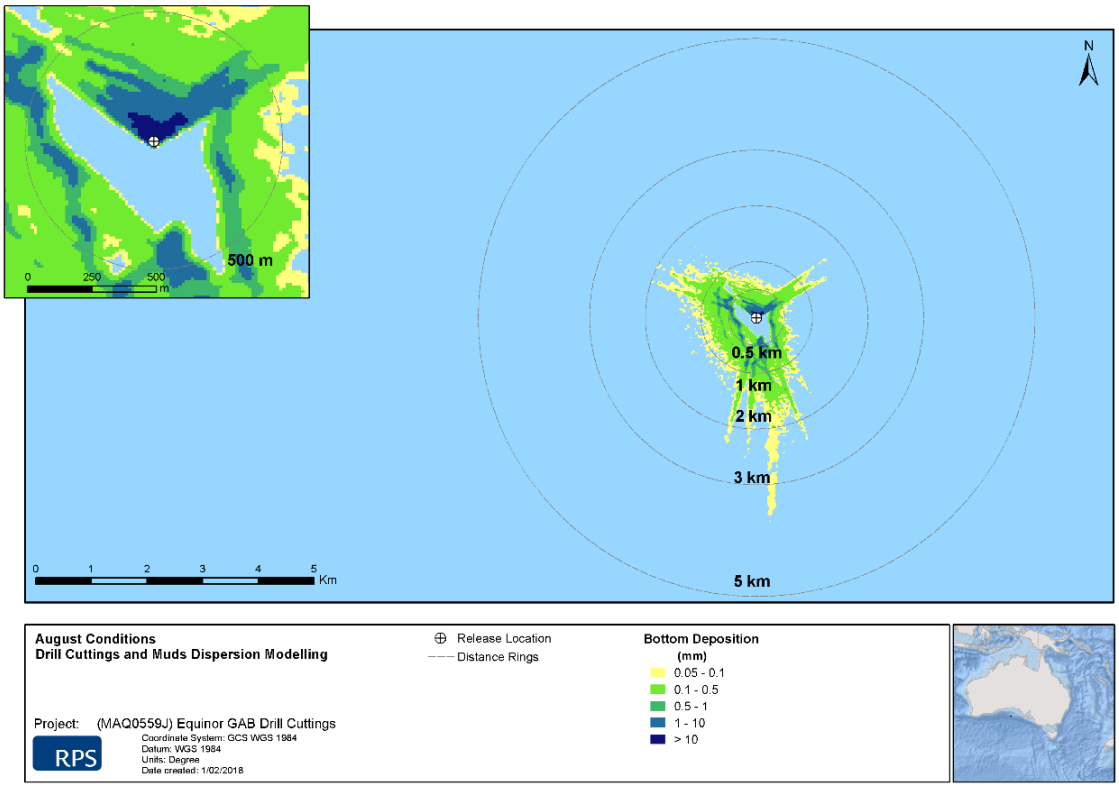

Figure 46: Predicted coverage and sediment thickness from the discharge of drill cuttings and unrecoverable drilling muds on the sea floor if the operation commenced 1st August 2010

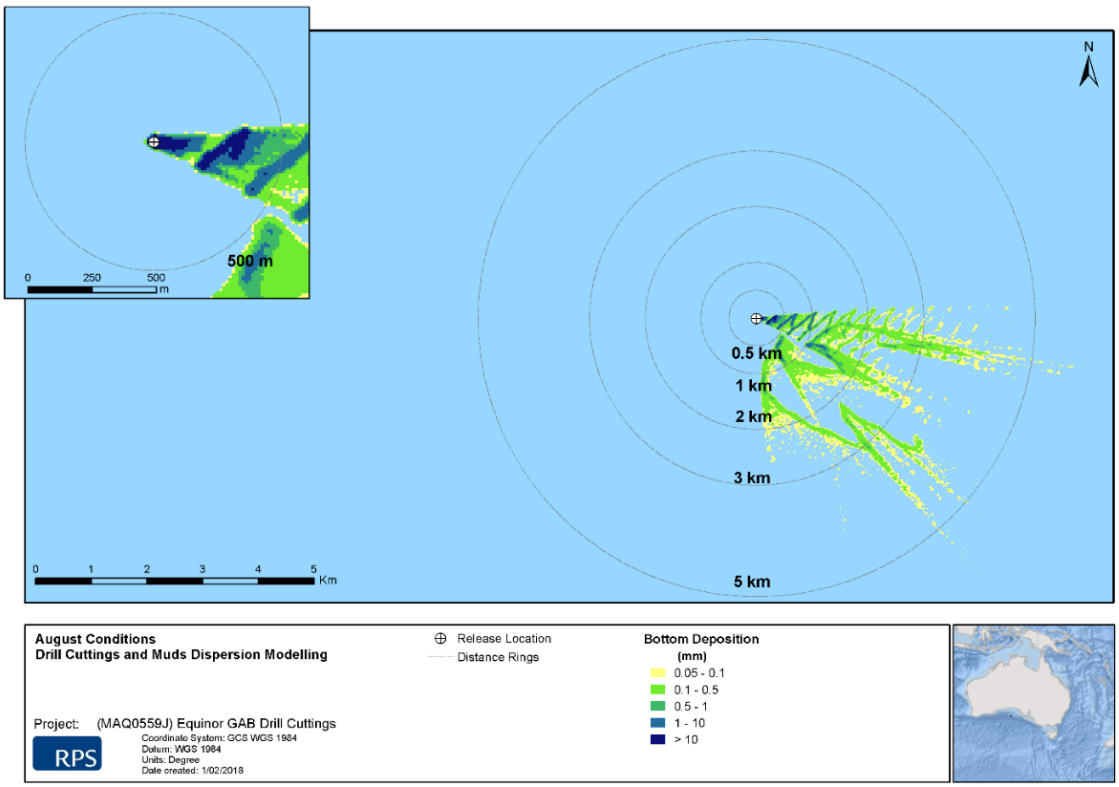

Figure 47: Predicted coverage and sediment thickness from the discharge of drill cuttings and unrecoverable drilling muds on the sea floor if the operation commenced 1st August 2011

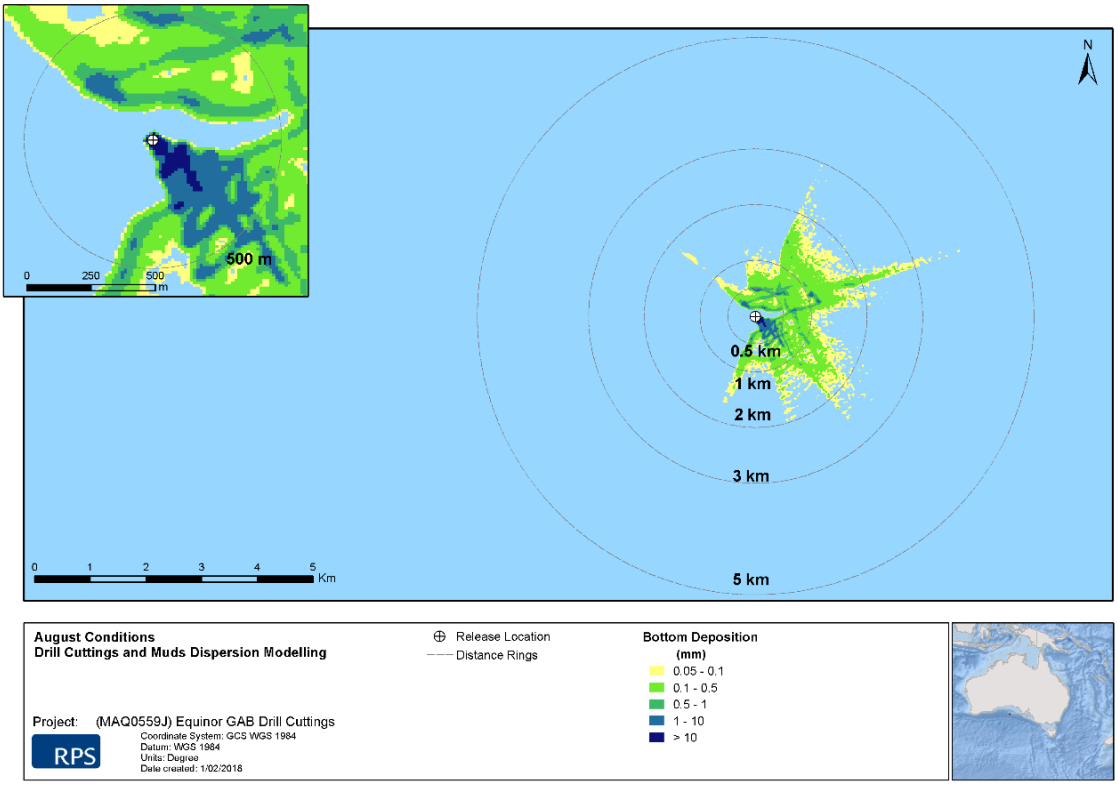

Figure 48: Predicted coverage and sediment thickness from the discharge of drill cuttings and unrecoverable drilling muds on the sea floor if the operation commenced 1st August 2012

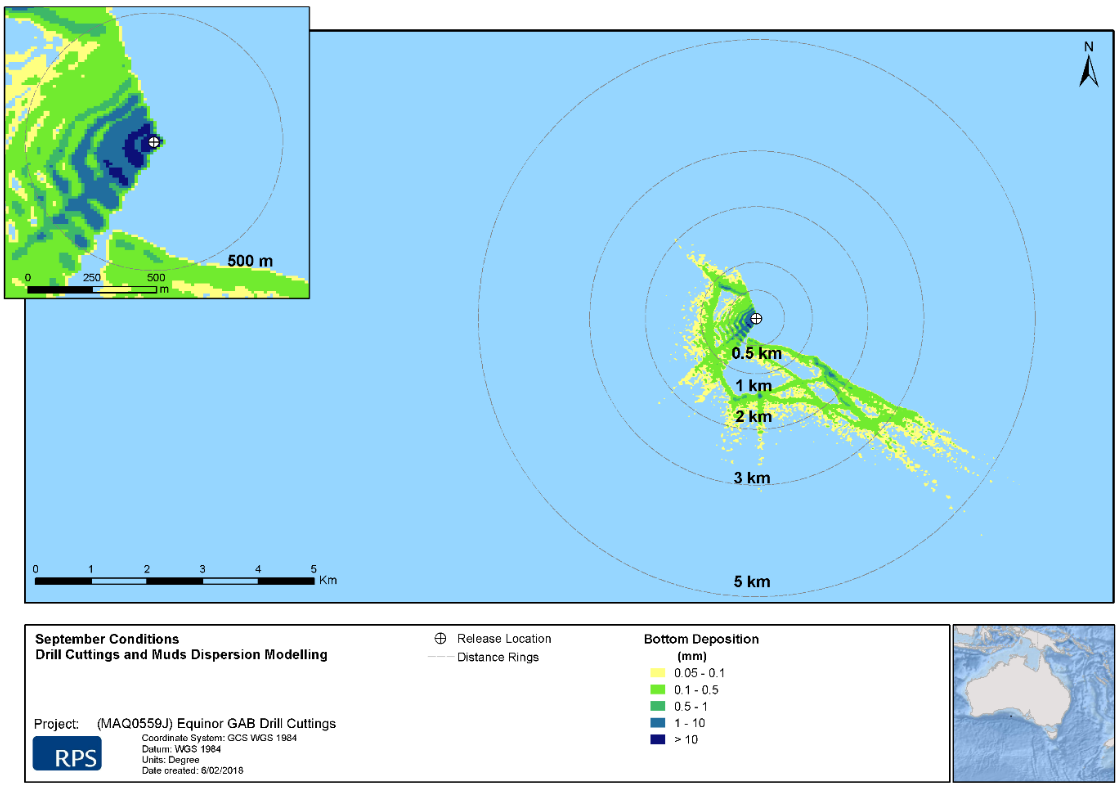

Figure 49: Predicted coverage and sediment thickness from the discharge of drill cuttings and unrecoverable drilling muds on the sea floor if the operation commenced 1st September 2010

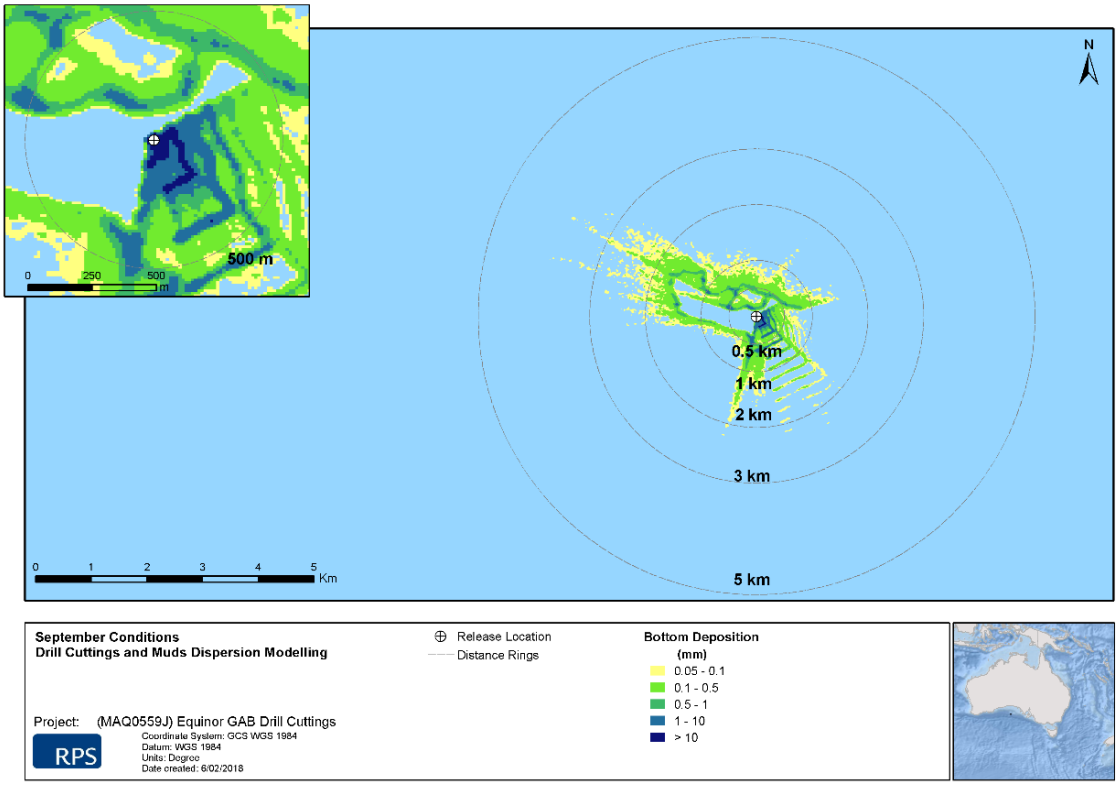

Figure 50: Predicted coverage and sediment thickness from the discharge of drill cuttings and unrecoverable drilling muds on the sea floor if the operation commenced 1st September 2011

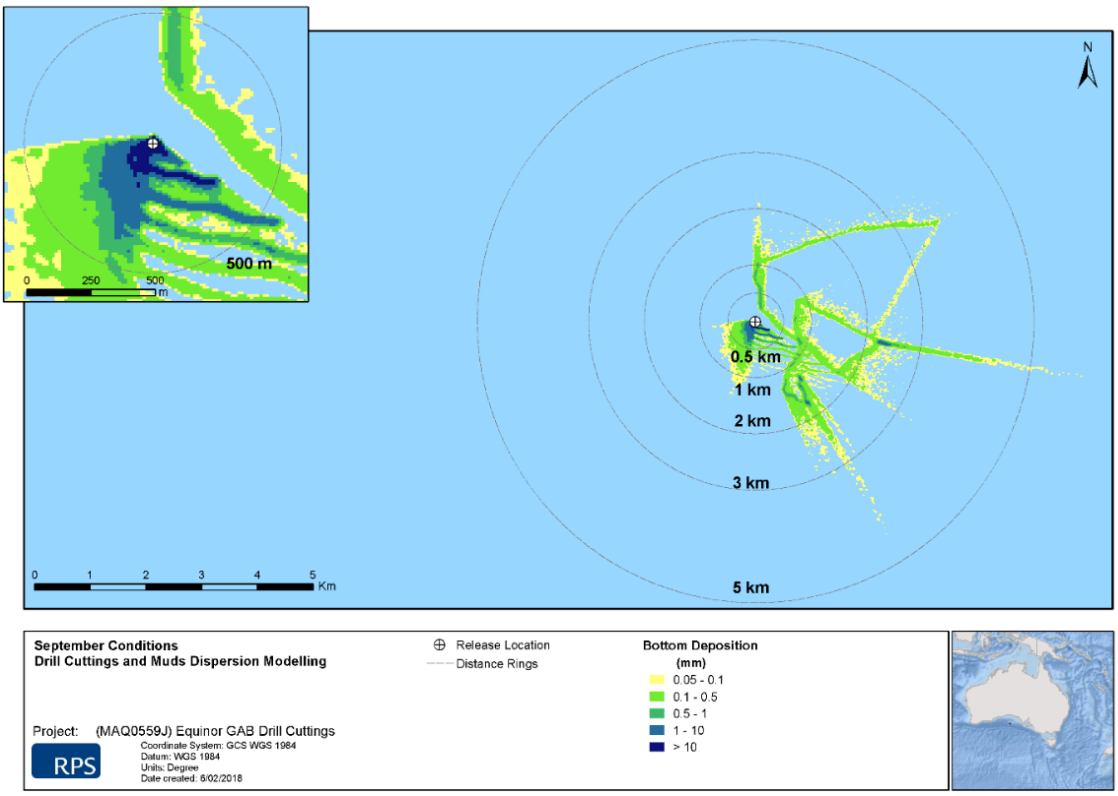

Figure 51: Predicted coverage and sediment thickness from the discharge of drill cuttings and unrecoverable drilling muds on the sea floor if the operation commenced 1st September 2012

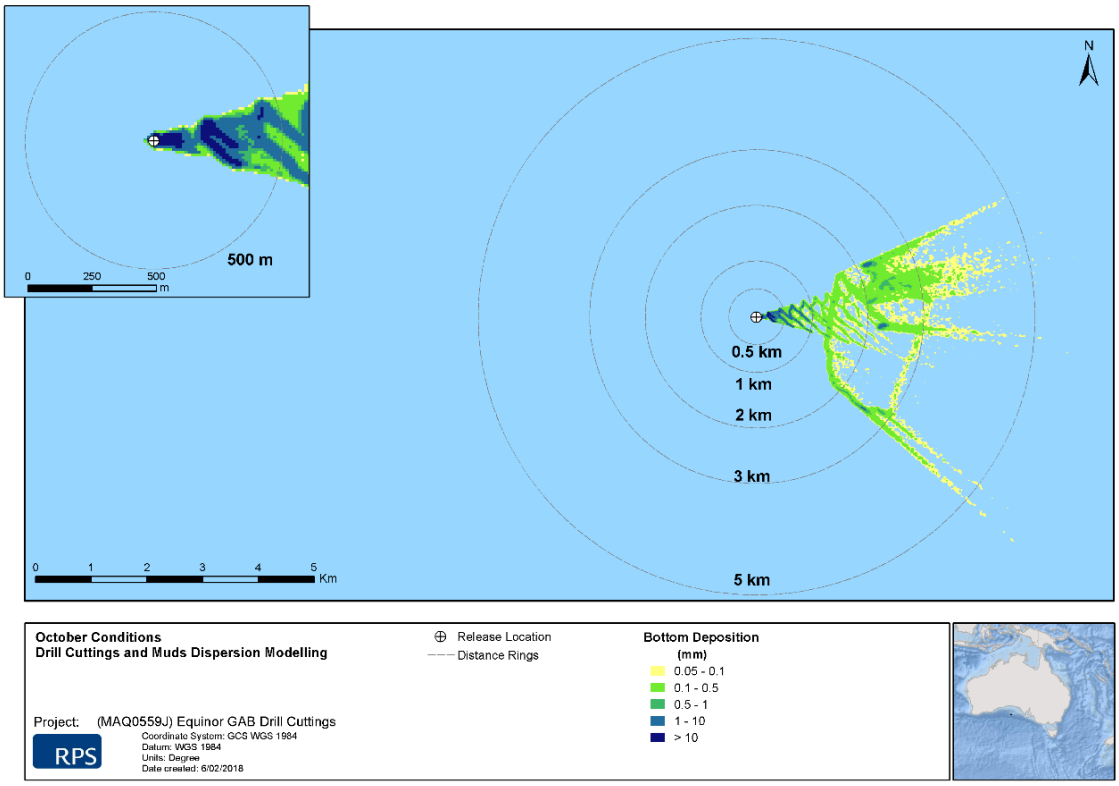

Figure 52: Predicted coverage and sediment thickness from the discharge of drill cuttings and unrecoverable drilling muds on the sea floor if the operation commenced 1st October 2010

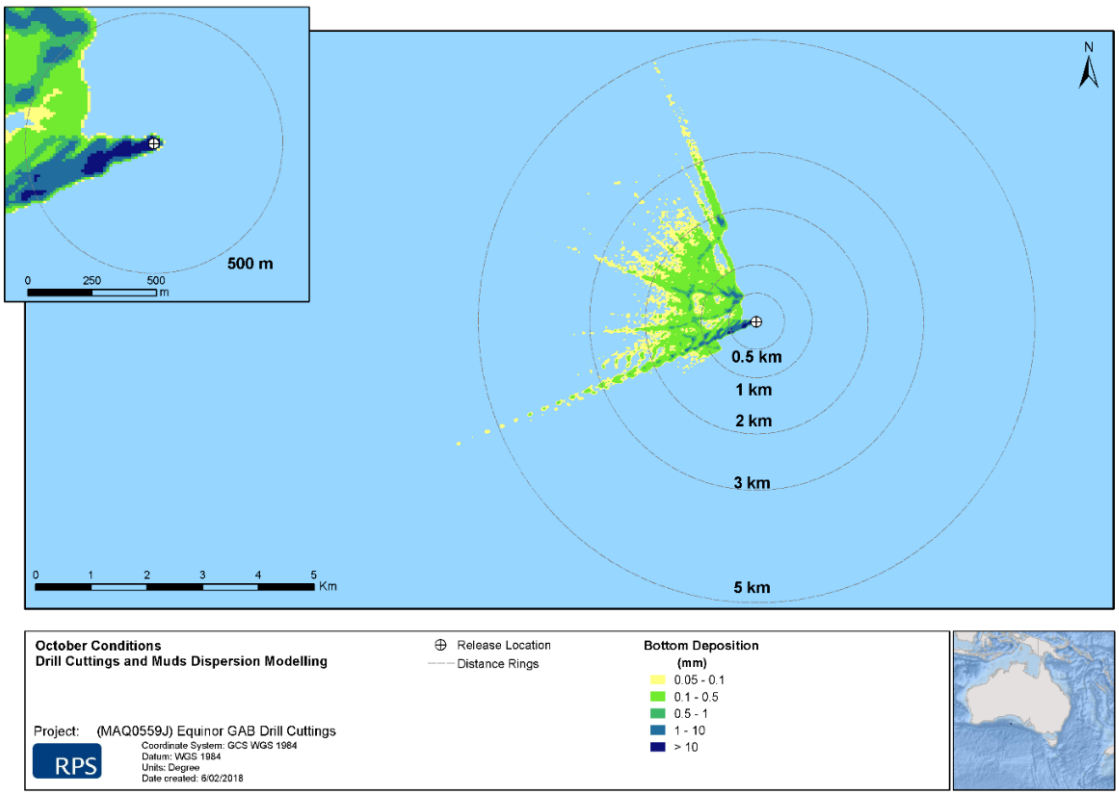

Figure 53: Predicted coverage and sediment thickness from the discharge of drill cuttings and unrecoverable drilling muds on the sea floor if the operation commenced 1st October 2011

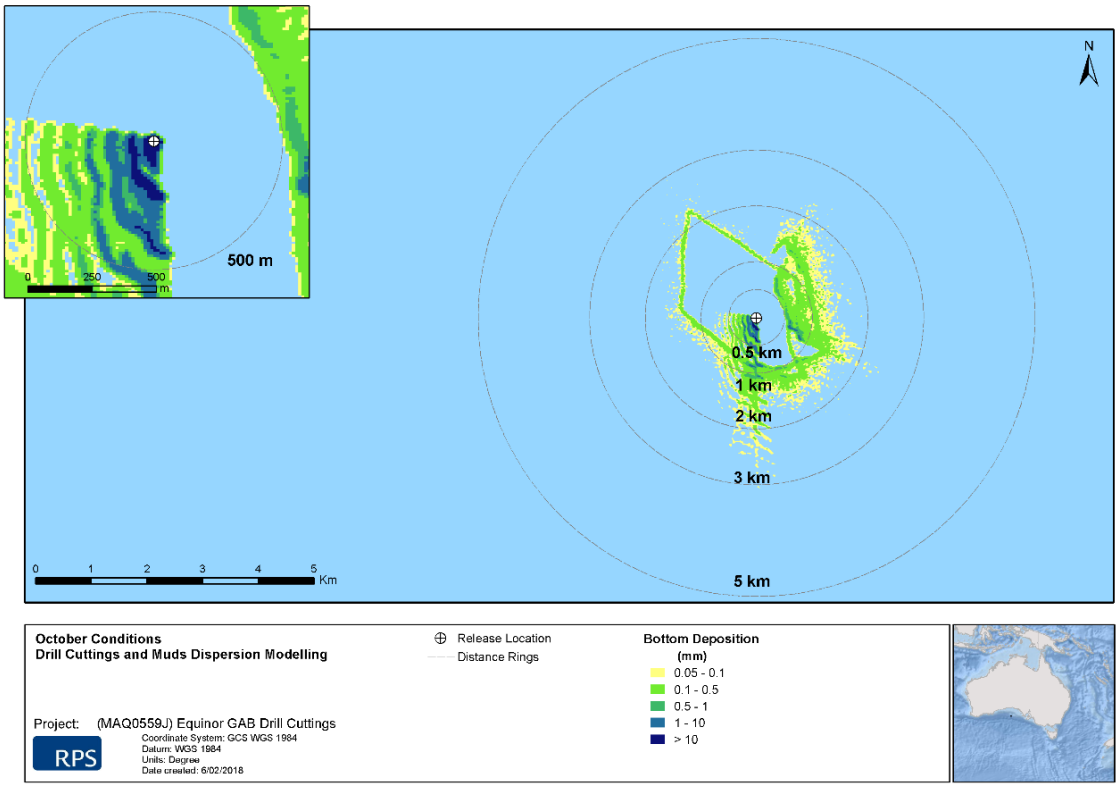

Figure 54: Predicted coverage and sediment thickness from the discharge of drill cuttings and unrecoverable drilling muds on the sea floor if the operation commenced 1st October 2012

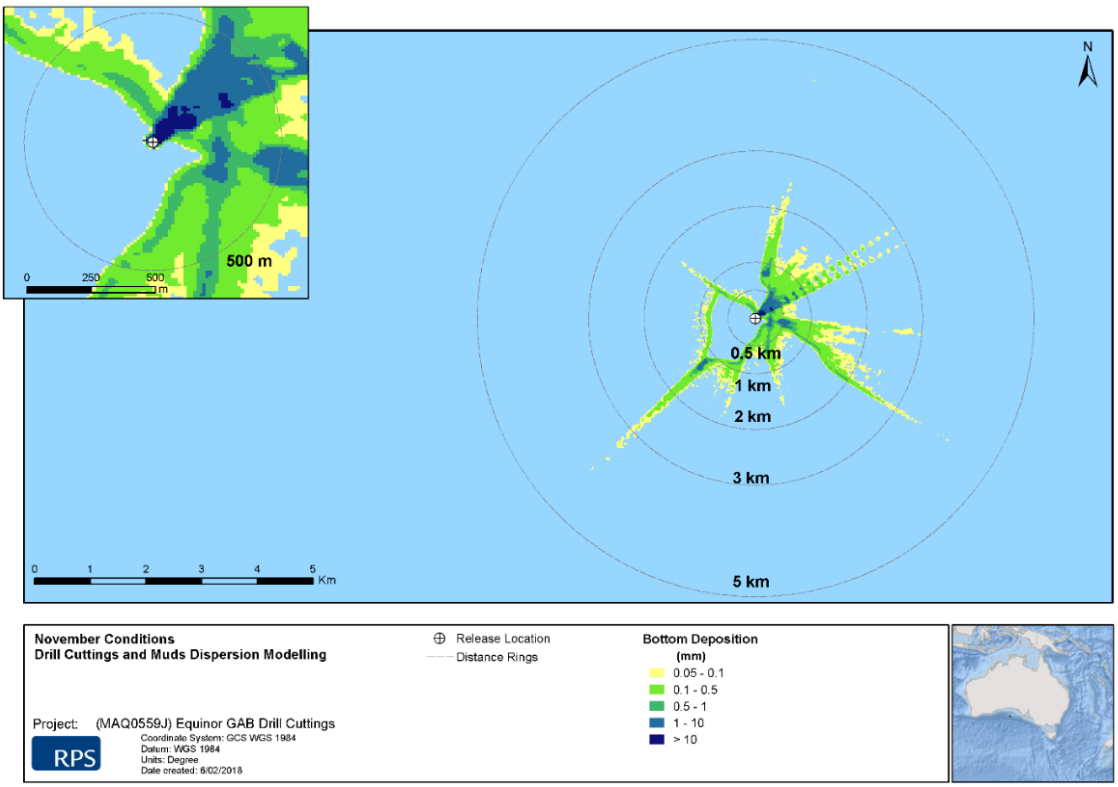

Figure 55: Predicted coverage and sediment thickness from the discharge of drill cuttings and unrecoverable drilling muds on the sea floor if the operation commenced 1st November 2010

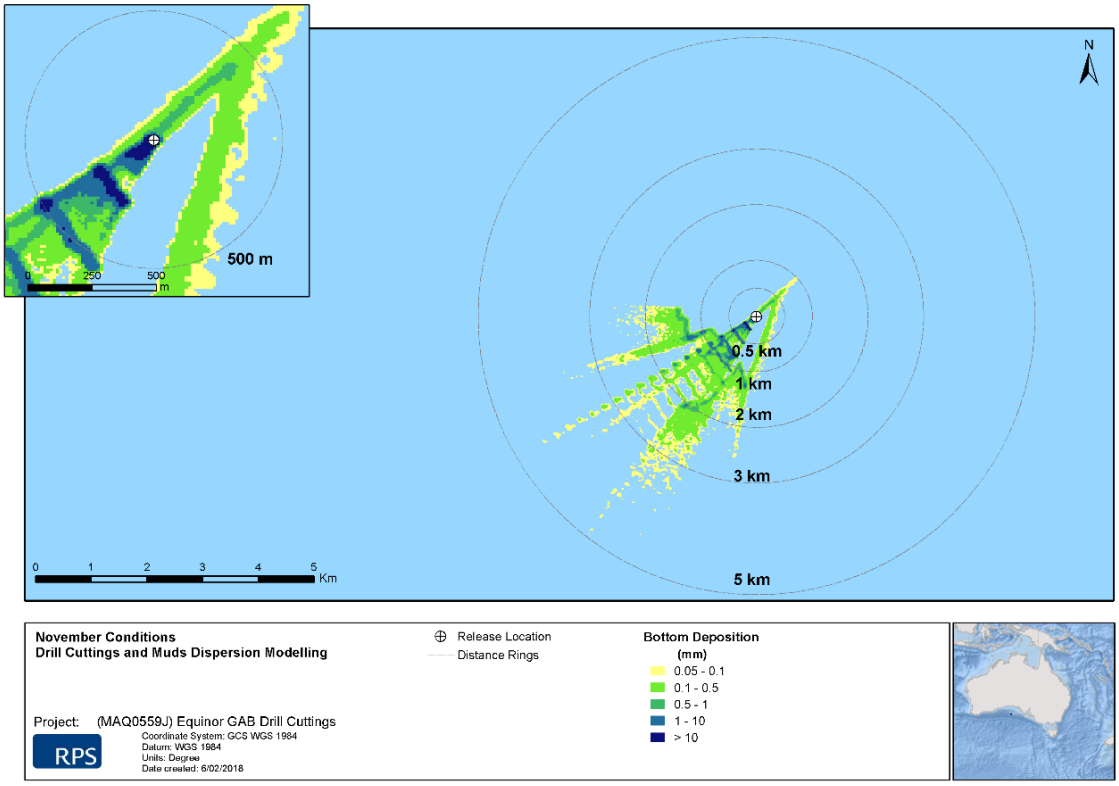

Figure 56: Predicted coverage and sediment thickness from the discharge of drill cuttings and unrecoverable drilling muds on the sea floor if the operation commenced 1st November 2011

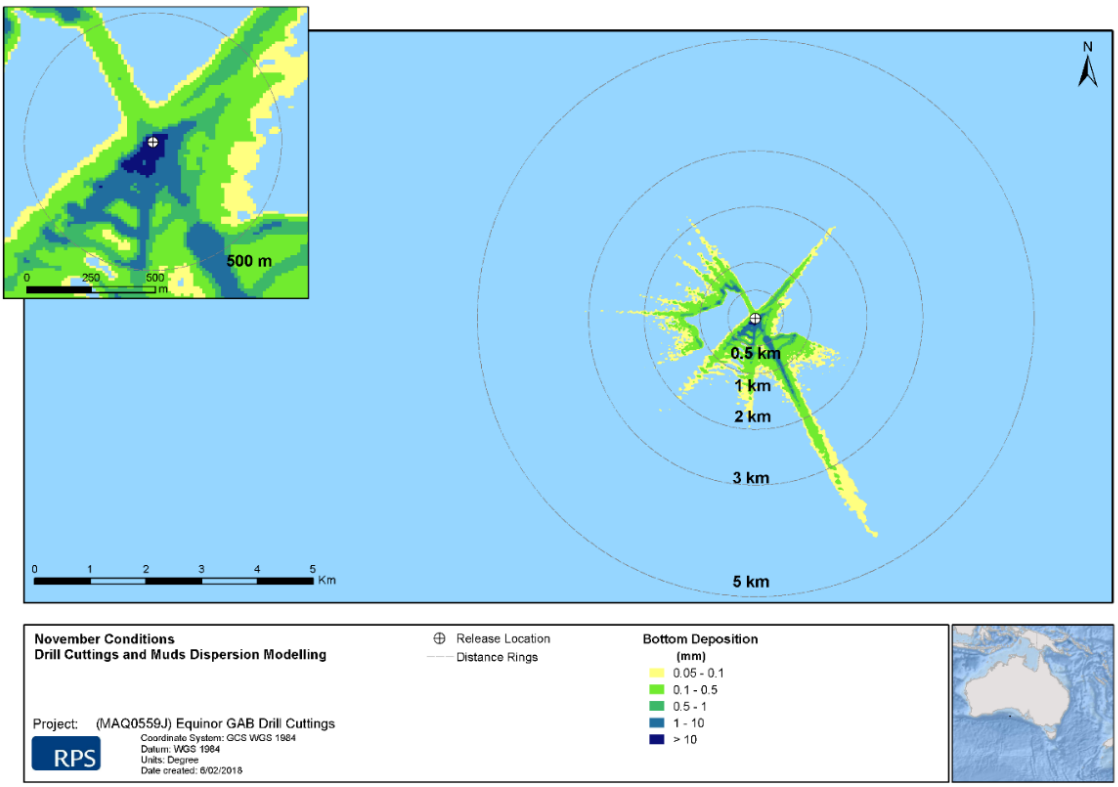

Figure 57: Predicted coverage and sediment thickness from the discharge of drill cuttings and unrecoverable drilling muds on the sea floor if the operation commenced 1st November 2012

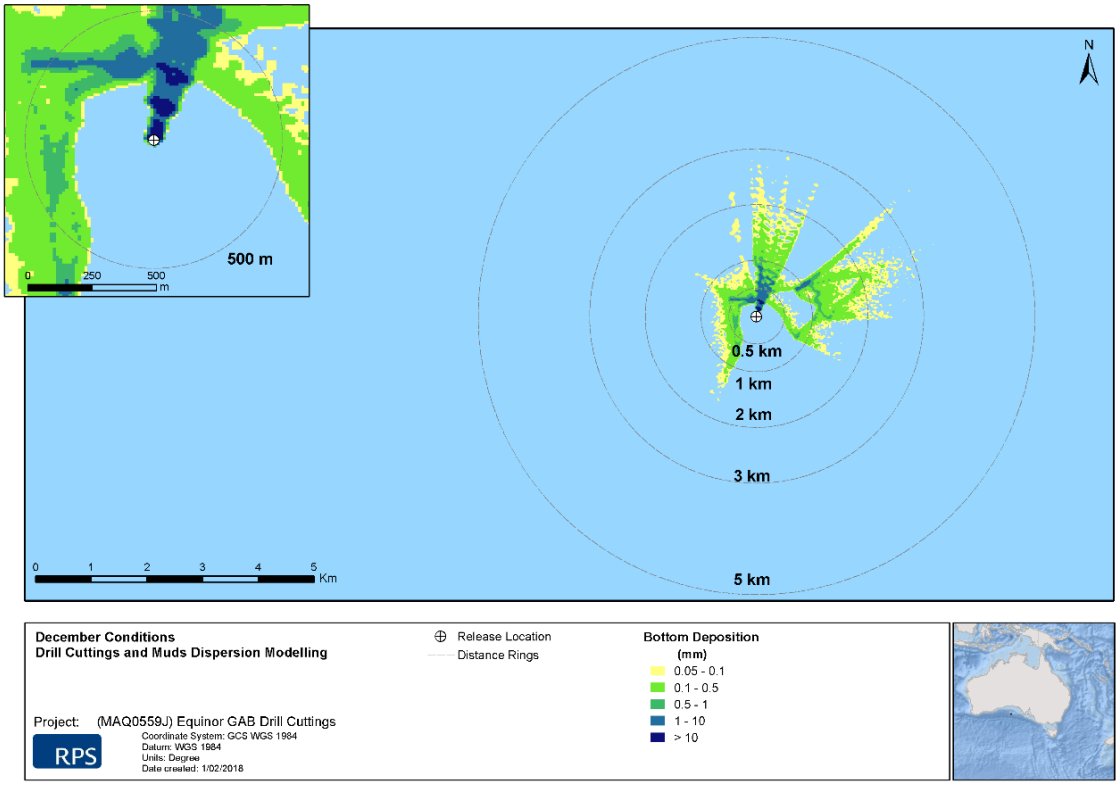

Figure 58: Predicted coverage and sediment thickness from the discharge of drill cuttings and unrecoverable drilling muds on the sea floor if the operation commenced 1st December 2010

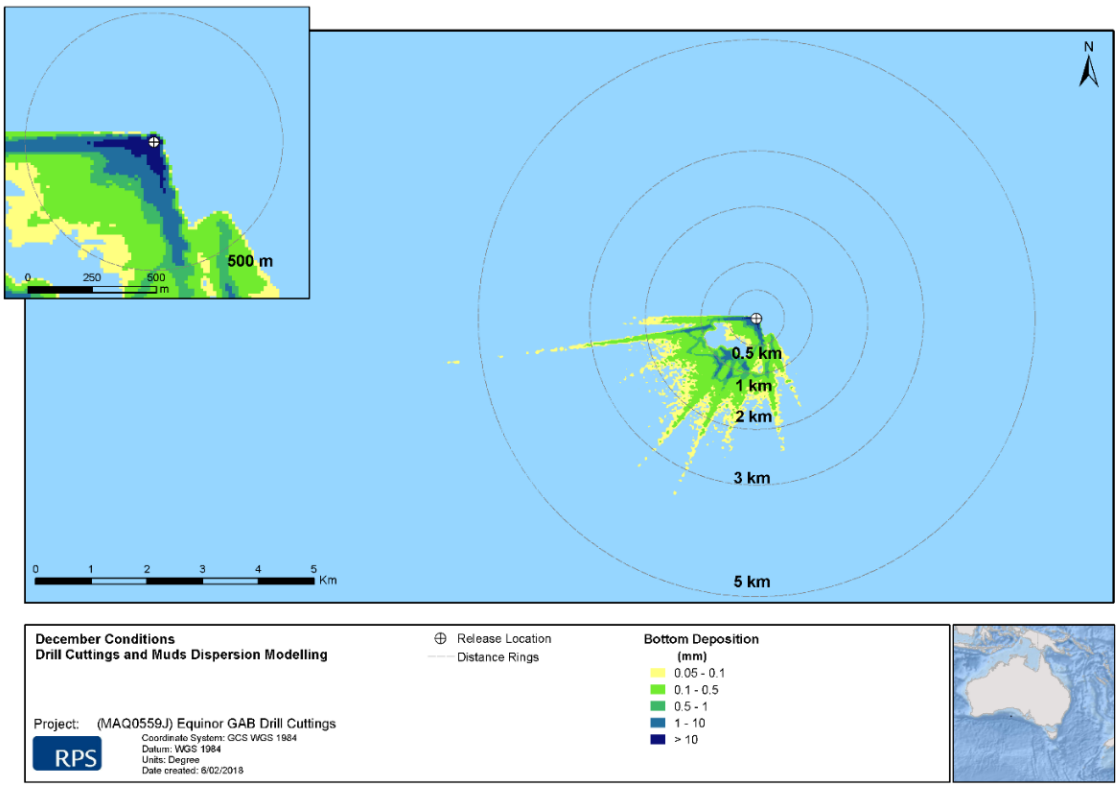

Figure 59: Predicted coverage and sediment thickness from the discharge of drill cuttings and unrecoverable drilling muds on the sea floor if the operation commenced 1st December 2011

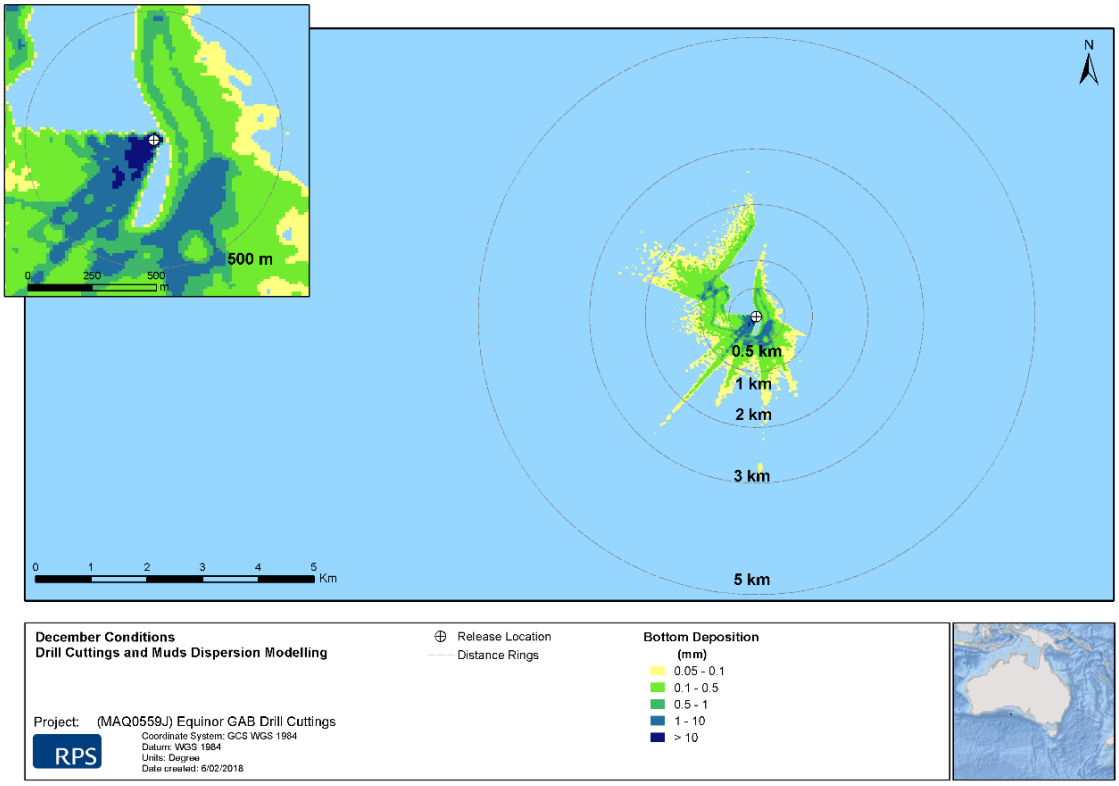

Figure 60: Predicted coverage and sediment thickness from the discharge of drill cuttings and unrecoverable drilling muds on the sea floor if the operation commenced 1st December 2012

Figure 61 shows a cross-sectional view of the predicted deposition as a function of distance by commencing the discharge under May 2012 current conditions, during which the maximum deposition of 4036 mm was predicted (see Table 12). The figure highlights the cuttings and muds pile adjacent to the release location and the rapid decline with distance. Note the vertical axis in Figure 61 is greatly exaggerated.

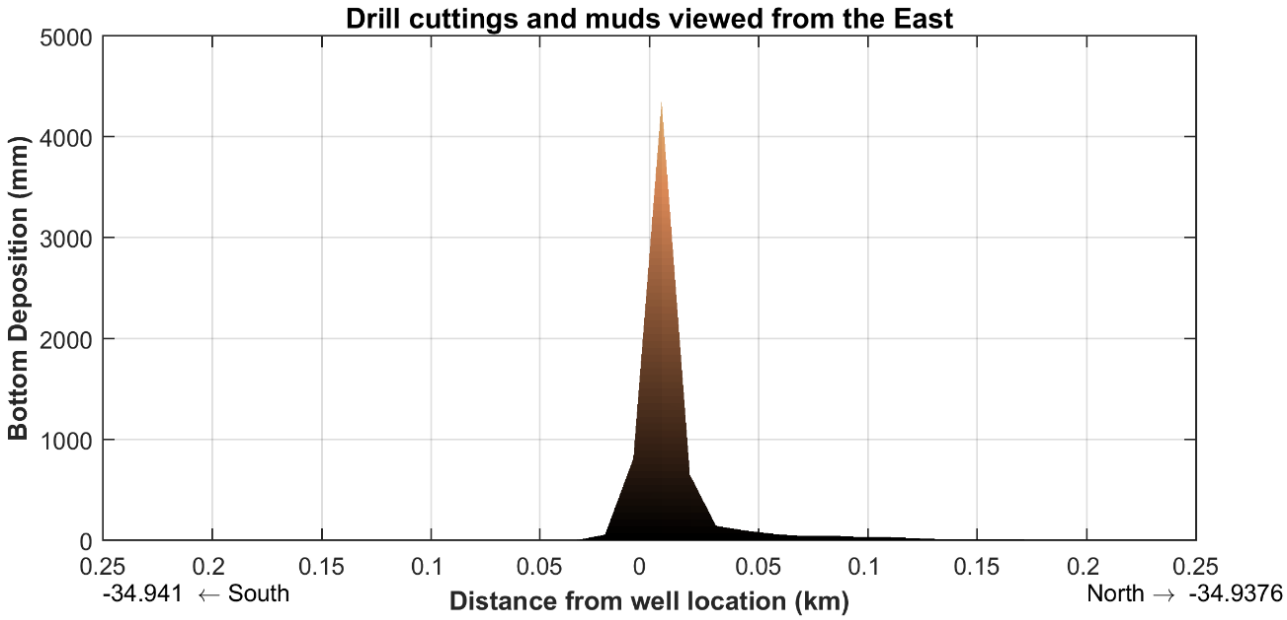

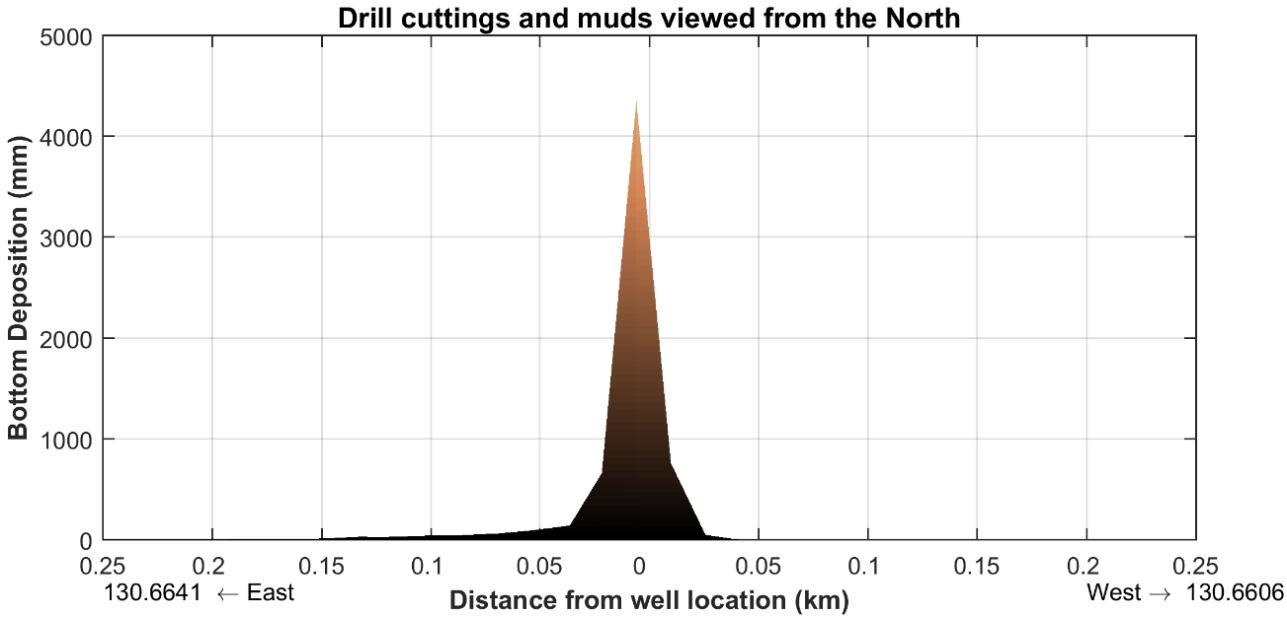

Figure 61: Cross-sectional view of the predicted sediment thickness on the sea floor along the north-south axis (upper image) and east-west axis (lower image). Results are based on the combined near-seabed and sea surface discharge of drill cuttings and unrecoverable muds commencing May 2012. Note the vertical scale is exaggerated

6.2.2 Integration of model results: sediment thickness

Figure 62 shows the maximum thickness at each grid cell from all monthly simulations (combined near-seabed and surface discharges) used to define the area of greatest extent from the discharge of cuttings and unrecoverable muds.

The total area of coverage on the sea floor above the minimum reporting threshold was 24.62 km^2, which was predicted to occur up to a maximum distance of 5.65 km from the well. In comparison, the area of coverage based on the low (1-10 mm) and high (>10 mm) exposure thresholds was 1.78 km^2 and 0.17 km^2, respectively equating to 7% and 1% of the total area of coverage, respectively. The maximum distance from the well to low (1-10 mm) and high (>10 mm) exposure thresholds was 2.34 km and 0.7 km, respectively.

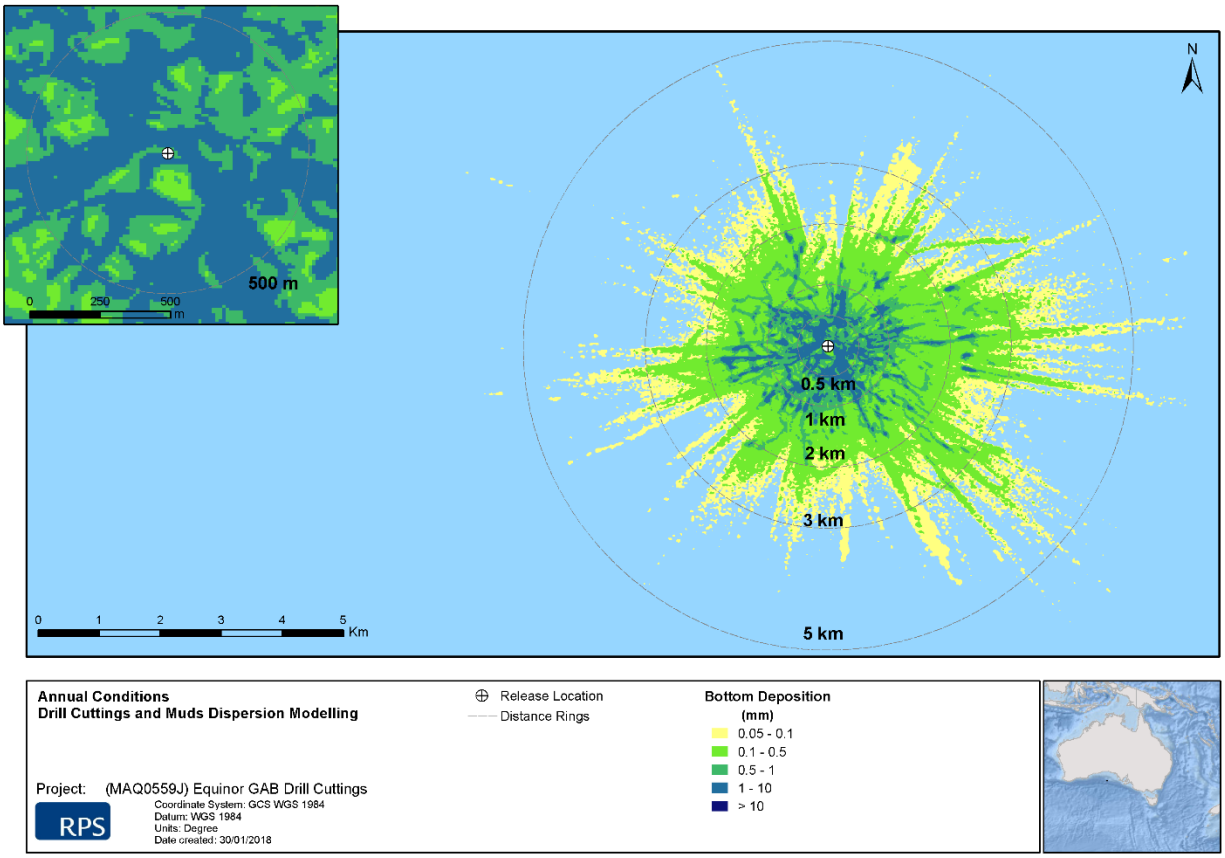

Figure 62: Predicted maximum thickness at each grid cell from all 36 monthly simulations (combined near-seabed and surface discharges) used to define the area of greatest extent from the discharge of cuttings and unrecoverable muds

Table 14: Predicted area of coverage on the sea floor and distance as a function of sediment thickness. Results are based on the collective assessment of monthly simulations (near-seabed and surface discharges) modelled under January to December 2010 – 2012 conditions

Sediment thickness (mm)	Collective assessment of monthly combined (near-seabed and surface discharge) simulations		
	Area of coverage of discharged cuttings and muds (km^2)	Percentage of area covered	Maximum distance from well (km)
0.05 – 0.1	9.23	37%	5.65
0.1 – 0.5	10.82	44%	4.24
0.5 – 1	2.61	11%	2.93
1 – 10	1.78	7%	2.34
> 10	0.17	1%	0.7
Total	**24.62**	**100%**	

6.3 Total suspended solids concentrations

6.3.1 Integration of model results: in-water total suspended solids concentrations

Figure 63 provides a map of the maximum instantaneous TSS concentrations in each model grid cell for the upper surface waters (0-100 m) from the surface discharge of drill cuttings and unrecoverable muds from all surface discharge simulations initiated at the start of each month during 2010, 2011 and 2012 conditions. Note the presented results are not cumulative concentrations from all model outputs; rather they are the maximum concentration for each grid cell from any of the 36 monthly simulations.

Table 15 presents the maximum instantaneous TSS concentration, maximum area and distance above the minimum reporting threshold (5 mg/L) based on the collective assessment of all surface discharges in the upper surface waters (0–100 m).

The maximum instantaneous TSS concentration of 1857 mg/L occurred in the immediate vicinity of the discharge outlet (< 10 m). The predicted area exposed to TSS concentrations above the minimum reporting threshold was 4.32 km^2, while the maximum distance of distance was 3.92 km northeast of the release location.

Table 16 presents the area of exposure and maximum distances from well at each TSS interval for the upper surface waters (0–100 m). Results are based on the collective assessment of all surface discharge simulations initiated at the start of each month during 2010, 2011 and 2012 conditions. Sixty-six percent of the predicted area predominantly consisted of concentrations between 5 to 10 mg/L, equivalent to 2.86 km^2. Instantaneous concentrations above 10 mg/L was predicted to have an area of coverage of 1.2 km^2 (or 28% of total area of exposure) while concentrations greater than 25 mg/L were predicted to have an area of coverage of 0.23 km^2 (5% of total area of exposure). The maximum distance from the well to TSS concentrations above 5 mg/L was 3.92 km northeast. The extent of TSS concentrations greater than 10 mg/L, 25 mg/L, and 50 mg/L was 2.08 km, 0.87 km and 0.46 km from release location, respectively. Predicted TSS concentrations greater than 100 mg/L were restricted to within 0.03 km (30 m) from the release location.

Table 15: Predicted maximum TSS concentration, maximum area and distance above the minimum reporting threshold (above 5 mg/L) in the upper surface waters (0–100 m). Results are based on the collective assessment of all surface discharges initiated at the start of each month during 2010, 2011 and 2012 conditions

Maximum TSS concentration (mg/l)	Area (km^2) exposed to tss concentrations above minimum reporting threshold of 5 mg/l	Maximum distance (km) from the well to the minimum reporting threshold of 5 mg/l
1857	4.32	3.92

Table 16: Predicted areas of exposure and maximum distances from the well to each TSS interval in the upper surface waters (0–100 m). Results are based on the collective assessment of all surface discharges initiated at the start of each month during 2010, 2011 and 2012 conditions

TSS concentrations (mg/l)	Area exposed to TSS concentration (km^2)	Maximum distance (km) from well to the TSS concentration			
		North-east quadrant	South-east quadrant	South-west quadrant	North-west quadrant
>5	4.32	3.92	3.65	3.01	2.41
>10	1.20	2.08	1.88	1.34	1.19
>25	0.23	0.87	0.76	0.59	0.50
>50	0.03	0.44	0.46	0.29	0.26
>100	<0.01	0.02	0.02	0.03	0.03
Total	**4.32**				

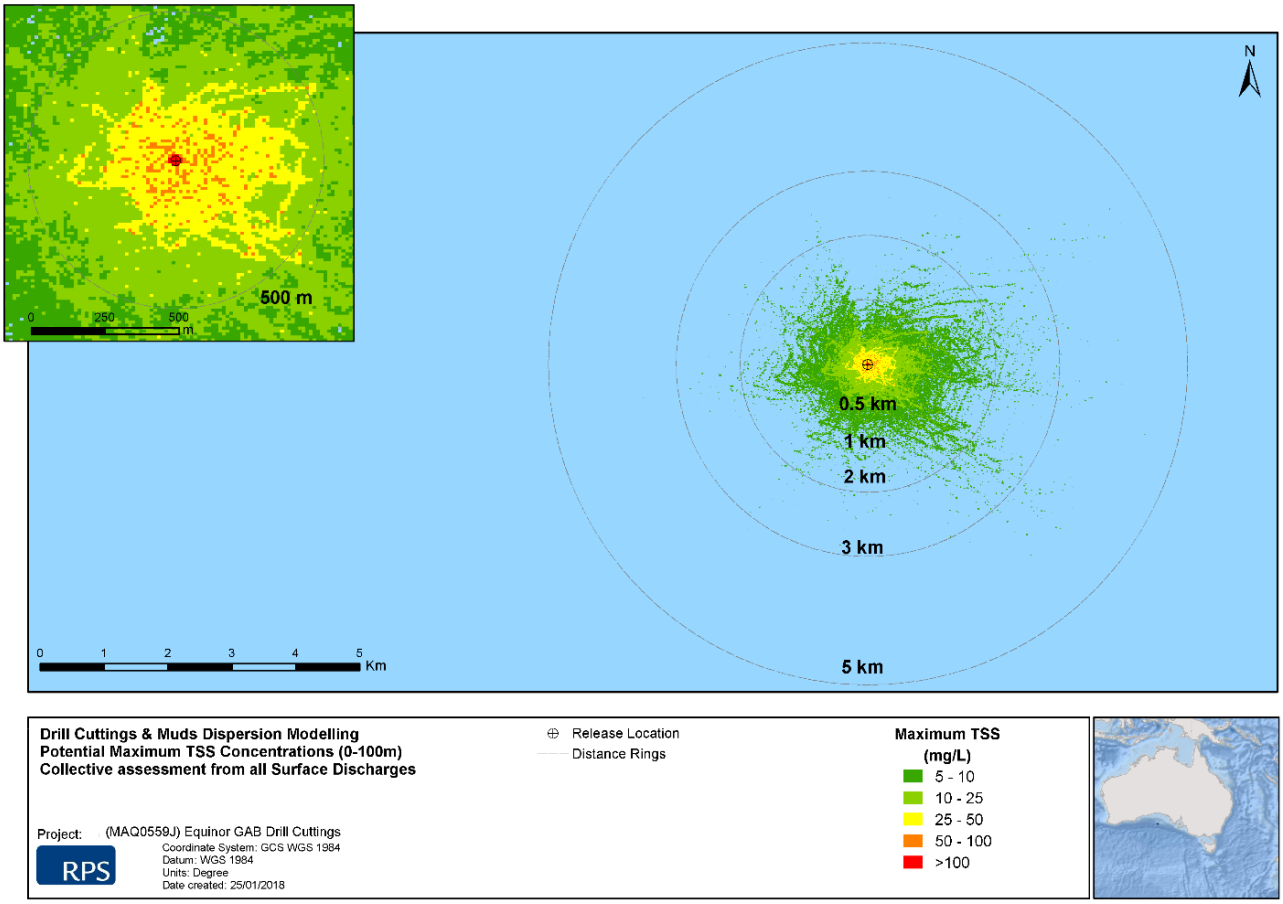

Figure 63: Predicted maximum instantaneous TSS concentrations in each grid cell based on the collective assessment of all monthly surface discharges in the upper surface waters (0–100 m). Results are presented for model simulations initiated at the start of each month during 2010, 2011 and 2012 conditions

6.3.2 Example time-series snapshot: in-water total suspended solids concentrations

Figure 64 presents an example time-series snapshots of the maximum predicted TSS concentrations, based on 3 hourly intervals, resulting from the surface discharge of drill cuttings and unrecoverable drilling muds commencing on the 12th April 2010. The figures demonstrate the dynamic nature of the plume, with TSS concentrations decreasing with increasing distance from the source of suspended solids (i.e. release location).

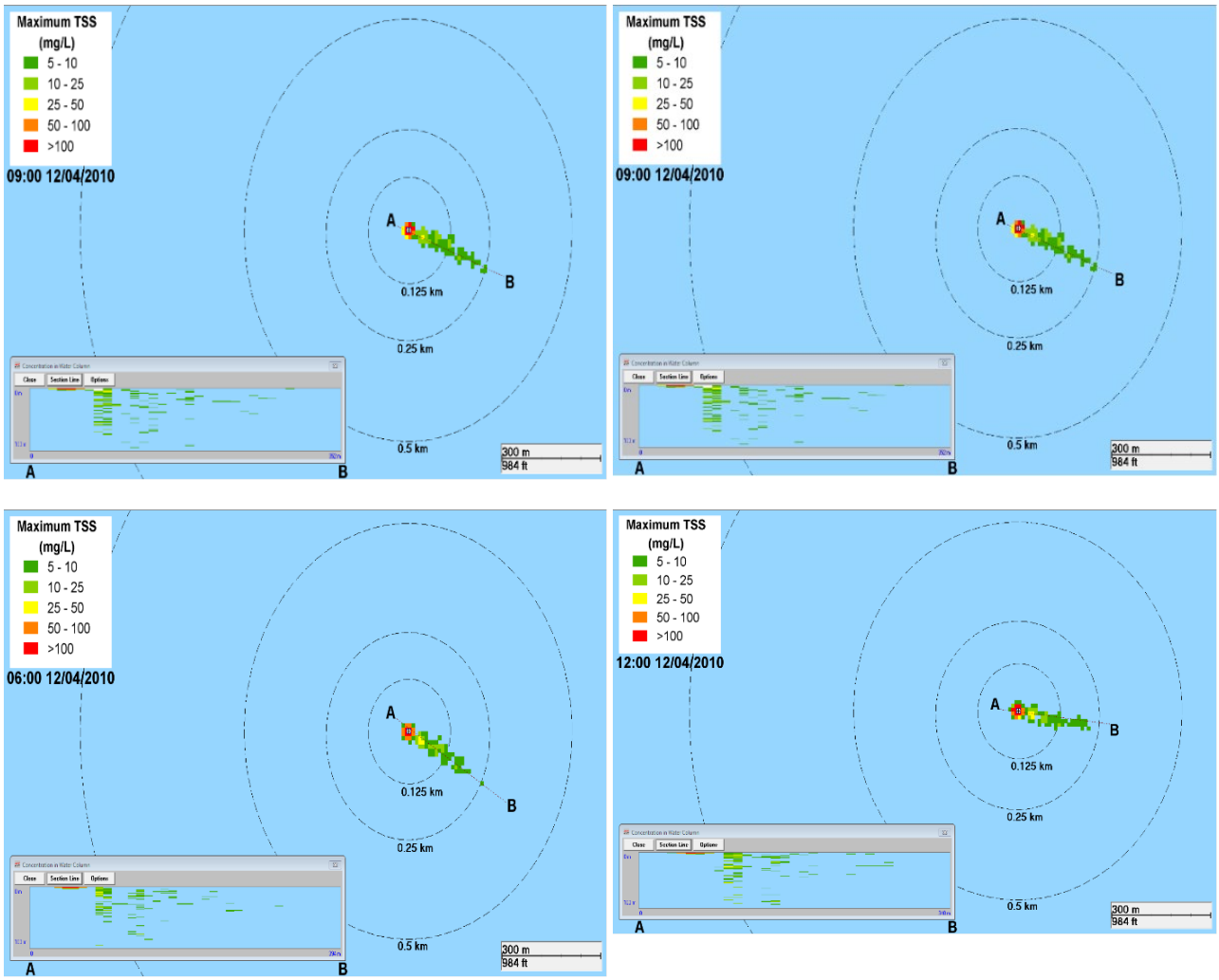

Figure 64: Example time-series snapshots of the maximum predicted TSS concentrations, at 3 hourly intervals, resulting from the surface discharge of drill cuttings and drilling muds commencing on the 12th April 2010. Note figure insets displays depth profiles through the water column across transect A to B in each figure

7 REFERENCES

Andersen, OB 1995, 'Global ocean tides from ERS 1 and TOPEX/POSEIDON altimetry', Journal of Geophysical Research: Oceans, vol. 100, no. C12, pp. 25249–25259.

Becker, JJ, Sandwell, DT, Smith, WHF, Braud, J, Binder, B, Depner, J, Fabre, D, Factor, J, Ingalls, S, Kim, S-H, Ladner, R, Marks, K, Nelson, S, Pharaoh, A, Trimmer, R, Von Rosenberg, J, Wallace, G & Weatherall, P 2009, 'Global bathymetry and evaluation data at 30 arc seconds resolution: SRTM30_PLUS', Marine Geodesy, vol. 32, no. 4, pp. 355–371.

Burns, K, Codi, S, Furnas, M, Heggie, D, Holdway, D, King, B, & McAllister, F 1999, 'Dispersion and Fate of Produced Formation Water Constituents in an Australian Northwest Shelf Shallow Water Ecosystem', Marine Pollution Bulletin, vol. 38, no. 7, pp. 593–603.

Brandsma, M.G. and Sauer, T.C. Jr., 1983. The OOC model: prediction of short term fate of drilling mud in the ocean, Part I model description and Part II model results. Proceedings of Workshop on An Evaluation of Effluent Dispersion and Fate Models for OCS Platforms. Santa Barbara, California, 7th – 10th February, 1983.

Chassignet, EP, Hurlburt, HE, Smedstad, OM, Halliwell, GR, Hogan, PJ, Wallcraft, AJ, Bleck, R 2006, Ocean prediction with the hybrid coordinate ocean model (HYCOM), Springer, Netherlands.

Chassignet, EP, Hurlburt, HE, Smedstad, OM, Halliwell, GR, Hogan, PJ, Wallcraft, AJ, Baraille, R & Bleck. R 2007, 'The HYCOM (hybrid coordinate ocean model) data assimilative system', Journal of Marine Systems, vol. 65, no. 1, pp. 60–83.

Chassignet, EP, Hurlburt, HE, Metzger, EJ, Smedstad, OM, Cummings, JA, Halliwell, GR, Bleck, R, Baraille, R, Wallcraft, AJ, Lozano, C & Tolman, HL 2009, US GODAE: global ocean prediction with the HYbrid Coordinate Ocean Model (HYCOM) (No. NRL/JA/7304-08-8335), Naval Research Lab Stennis Space Centre MS Oceanography Division, Mississippi.

Copeland, G 1996, UK Seminar on current research on data rich models of tidal flow and effluent dispersion, University of Strathclyde, Glasgow.

Davies, AM 1977a, 'The numerical solutions of the three-dimensional hydrodynamic equations using a B-spline representation of the vertical current profile', in JC Nihoul (ed), Bottom Turbulence: Proceedings of the 8th Liège Colloquium on Ocean Hydrodynamics, Elsevier Scientific, Amsterdam, pp. 1–25.

Davies, AM 1977b, 'Three-dimensional model with depth-varying eddy viscosity', in JC Nihoul (ed), Bottom Turbulence: Proceedings of the 8th Liège Colloquium on Ocean Hydrodynamics, Elsevier Scientific, Amsterdam, pp. 27–48.

Dyer, KR 1986, Coastal and Estuarine Sediment Dynamics, John Wiley & Sons Ltd., Chichester.

Foreman, M, Beauchemin, L, Cherniawsky, J, Pena, M, Cummins, P, & Sutherland. G 2005, A review of models in support of oil and gas exploration off the North Coast of British Columbia, Institute of Ocean Sciences, Canada.

Fu, R, Del Genio, AD, & Rossow, WB 1994, 'Influence of ocean surface conditions on atmospheric vertical thermodynamic structure and deep convection', Journal of Climate, vol. 7, no. 7, pp. 1092–1108.

Gordon, R 1982, Wind driven circulation in Narragansett Bay, Doctor of philosophy thesis, University of Rhode Island, Kingston.

International Association of Oil and Gas Producers (IGOP) 2016, Environmental fates and effects of ocean discharge of drill cuttings and associated drilling fluids from offshore oil and gas operations, Report 543.

Isaji, T & Spaulding, M 1984, 'A model of the tidally induced residual circulation in the Gulf of Maine and Georges Bank', Journal of Physical Oceanography, vol. 14, no. 6, pp. 1119–1126.

Isaji, T, Howlett, E, Dalton C, & Anderson, E 2001, 'Stepwise-continuous-variable-rectangular grid hydrodynamics model', Proceedings of the 24th Arctic and Marine Oil spill Program (AMOP) Technical Seminar (including 18th TSOCS and 3rd PHYTO), Environment Canada, Edmonton, pp. 597–610.

Khondaker, AN 2000, 'Modeling the fate of drilling waste in marine environment – an overview', Journal of Computers and Geosciences, vol. 26, no. 5, pp. 531–540.

King, B & McAllister, FA 1998, 'Modelling the dispersion of produced water discharges', APPEA Journal, vol. 38, no. 1, pp.681–691.

Kjeilen-Eilertsen G, Trannum, H, Jak, RG, Smit, MGD, Neff, J and Durell, G 2004, Literature report on burial: derivation of PNEC as component in the MEMW model tool. Report AM 2004/024. ERMS report 9B.

Koh, RCY & Chang, YC 1973, Mathematical model for barged ocean disposal of waste, U.S. Army Engineer Waterways Experiment Station, Vicksburg.

Kostianoy, AG, Ginzburg, AI, Lebedev, SA, Frankignoulle, M & Delille, B 2003, 'Fronts and mesoscale variability in the southern Indian Ocean as inferred from the TOPEX/POSEIDON and ERS-2 Altimetry data', Oceanology, vol. 43, no. 5, pp. 632–642.

Levitus, S, Antonov, JI, Baranova, OK, Boyer, TP, Coleman, CL, Garcia, HE, Grodsky, AI, Johnson, DR, Locarnini, RA, Mishonov, AV, Reagan, JR, Sazama CL, Seidov, D, Smolyar, I, Tarosh, ES & Zweng, MM 2013, 'The World Ocean Database', Data Science Journal, vol. 12, no. 0, pp. WDS229–WDS234.

Locarnini, RA, Mishonov, AV, Antonov, JI, Boyer, TP, Garcia, HE, Baranova, OK, Zweng, MM, Paver, CR, Reagan, JR, Johnson, DR, Hamilton, M & Seidov, D 2013, 'Volume 1: Temperature', S Levitus & A Mishonov (eds), World Ocean Atlas 2013, National Oceanographic Data Centre – National Oceanographic and Atmospheric Administration, Washington.

Ludicone, D, Santoleri, R, Marullo, S & Gerosa, P 1998, 'Sea level variability and surface eddy statistics in the Mediterranean Sea from TOPEX/POSEIDON data', Journal of Geophysical Research I, vol. 103, no. C2, pp. 2995–3011.

Matsumoto, K, Takanezawa, T & Ooe, M 2000, 'Ocean tide models developed by assimilating TOPEX/POSEIDON altimeter data into hydrodynamical model: A global model and a regional model around Japan', Journal of Oceanography, vol. 56, no. 5, pp. 567–581.

Middleton, JF & Bye, JAT 2007, 'A review of the shelf-slope circulation along Australia's southern shelves: Cape Leeuwin to Portland', Progress in Oceanography, vol. 75, no. 1, pp. 1–41.

National Aeronautics and Space Administration (NASA) 2013a, National Aeronautics and Space Administration/Jet Propulsion Laboratory TOPEX/Poseidon Fact Sheet, NASA, viewed 23 November 2013, https://sealevel.jpl.nasa.gov/missions/topex/topexfactsheet

National Aeronautics and Space Administration (NASA) 2013b, National Aeronautics and Space Administration/Jet Propulsion Laboratory TOPEX/Poseidon, NASA, viewed 23 November 2013, https://sealevel.jpl.nasa.gov/missions/topex

Nedweed, T 2004, Best practices for drill cuttings and mud discharge modelling. SPE 86699. Paper presented at the 7th SPE International Conference on Health, Safety and Environment in Oil and Gas Exploration and Production, Calgary, Alberta, Canada. Society of Petroleum Engineers, P6.

Neff, J 2005, Composition, environment fates, and biological effect of water based drilling fluids and cuttings discharged to the marine environment: A synthesis and annotated bibliography, Battelle, Duxbury.

Nelson, DS, McManus, J, Richmond, RH, King Jr, DB, Gailani, JZ, Lackey, TC & Bryant, D 2016, 'Predicting dredging-associated effects to coral reefs in Apra Harbor, Guam – Part 2: Potential coral effects', Journal of Environmental Management, vol. 168, p. 111–122.

Owen, A., 1980, 'A three-dimensional model of the Bristol Channel', Journal of Physical Oceanography, vol. 10, no. 8, pp. 1290–1302.

Qiu, B & Chen, S 2010, 'Eddy-mean flow interaction in the decadally modulating Kuroshio Extension system', Deep-Sea Research II, vol. 57, no. 13, 1098–1110.

Rochford, DJ 1986, 'Seasonal changes in the distribution of Leeuwin Current waters of Southern Australia', Marine and Freshwater Research, vol. 37, no, 1, pp. 1–10.

Rogers, CS, 1990, 'Responses of coral reefs and reef organisms to sedimentation', Marine Ecology Progress Series, vol. 62, no. 1, pp. 185–202.

RPS MetOcean Pty Ltd, 2013. Ceduna Basin Current Measurements, November 2011 to December 2012, Final Data Report. Report No. R1592v0. Prepared for BP Developments Australia Pty Ltd, RPS MetOcean Pty Ltd, Perth, Western Australia.

Smit, MGD, Holthaus, KIE, Trannum, H, Neff, J, Kjeilen-Eilertsen, G, Jak, RG, Singsaas, I, Huijbregts, MAJ & Hendriks, AJ 2008, 'Species sensitivity distributions for suspended clays, sediment burial, and grain size change in the marine environment', Environmental Toxicology & Chemistry, vol. 27, no. 4, pp. 1006-1012.

Spaulding, ML 1994, 'Drilling, production fluids dispersion predicted by model', Offshore, vol. 54, no. 4, pp. 78–82.

Trannum, HC, Nilsson, HC, Schaanning, MT & Øxnevad, S 2009, 'Effects of sedimentation from water-based drill cuttings and natural sediment on benthic macrofaunal community structure and ecosystem processes', Journal of Experimental Marine Biology and Ecology, vol. 383, no. 2, pp.111–121.

Yaremchuk, M & Tangdong, Q 2004, 'Seasonal variability of the large-scale currents near the coast of the Philippines', Journal of Physical Oceanography, vol. 34, no. 4, pp. 844–855.

Zigic, S, Zapata, M, Isaji,T, King, B, & Lemckert, C 2003, 'Modelling of Moreton Bay using an ocean/coastal circulation model', Proceedings of the 16th Australasian Coastal and Ocean Engineering Conference, the 9th Australasian Port and Harbour Conference and the Annual New Zealand Coastal Society Conference, Institution of Engineers Australia, Auckland, paper 170.

Zweng, MM, Reagan, JR, Antonov, JI, Locarnini, RA, Mishonov, AV, Boyer, TP, Garcia, HE, Baranova, OK, Johnson, DR, Seidov, D & Biddle MM 2013, 'Volume 2: Salinity' S Levitus & A Mishonov (eds), World Ocean Atlas 2013, National Oceanographic Data Centre – National Oceanographic and Atmospheric Administration, Washington